



Michael Rubart and Douglas P. Zipes

ANATOMY OF THE CARDIAC CONDUCTION SYSTEM, 629

Sinoatrial Node, 629
 Atrioventricular Junctional Area and Intraventricular Conduction System, 632
 Innervation of the Atrioventricular Node, His Bundle, and Ventricular Myocardium, 633
 Arrhythmias and the Autonomic Nervous System, 635

BASIC ELECTROPHYSIOLOGIC PRINCIPLES, 637

Physiology of Ion Channels, 637
 Intercalated Discs, 638
 Phases of the Cardiac Action Potential, 639
 Normal Automaticity, 644

MECHANISMS OF ARRHYTHMOGENESIS, 646

Disorders of Impulse Formation, 646
 Disorders of Impulse Conduction, 651
 Tachycardias Caused by Reentry, 653

REFERENCES, 660

ANATOMY OF THE CARDIAC CONDUCTION SYSTEM

Sinoatrial Node

In humans, the sinoatrial node is a spindle-shaped structure composed of a fibrous tissue matrix with closely packed cells. It is 10 to 20 mm long and 2 to 3 mm wide and thick and tends to narrow caudally toward the inferior vena cava. It lies less than 1 mm from the epicardial surface, laterally in the right atrial sulcus terminalis at the junction of the superior vena cava and right atrium (**Figs. 33-1 and 33-2**). The artery supplying the sinoatrial node branches from the right (55% to 60% of the time) or the left (40% to 45%) circumflex coronary artery and approaches the node from a clockwise or counterclockwise direction around the junction of the superior vena cava and right atrium.

Cellular Structure. Cells from the sinoatrial node region exhibit a wide variety of morphologic features, including spindle- and spider-shaped cells, rod-shaped atrial cells with clear striations, and small round cells corresponding to endothelial cells.¹ Only the spindle- and spider-shaped cells exhibit the typical electrophysiologic characteristics of pacemaker cells, including the hyperpolarization-activated current I_P¹ and spontaneous beating under physiologic conditions.²

Function. The ionic mechanism underlying sinoatrial node cell automaticity has been controversial. Some groups promote a model in which hyperpolarization-activated cyclic nucleotide-gated (HCN) ion channels are the main regulator of the heart rate, whereas other groups promote a model in which intracellular Ca²⁺ oscillations affecting Ca²⁺-sensitive ion channels and ion transporters in the outer membrane give rise to diastolic membrane depolarizations, which then trigger a propagating sinoatrial node action potential^{3,4} (see later). Similarly, the mechanism of entrainment that enables synchronization of the electrical activity of multiple individual sinoatrial node cells to give rise to discharge of the sinoatrial node has been uncertain. Very probably, no single cell in the sinoatrial node serves as the pacemaker. Rather, sinoatrial nodal cells function as electrically coupled oscillators that discharge synchronously. The interaction depends on the degree of coupling and the electrophysiologic characteristics of the individual sinoatrial node cell. The resulting rate is not just a simple average of each of the cells. With an individual pacemaker cell coupled to an average of five other cells, each with potentially different electrophysiologic properties, the resulting discharge rate is not obvious. Functioning of the sinoatrial node as a pacemaker requires a delicate balance of intercellular electrical coupling. Excess electrical coupling depresses sinoatrial node automaticity because the sinoatrial node membrane potential is damped by the surrounding atrial myocardium to a more negative potential than the normal maximal diastolic potential, thereby inhibiting spontaneous diastolic depolarization (see **Fig. 33-18**). Too little coupling can prevent transmission of impulses to the adjacent atrial muscle. Restriction of the hyperpolarizing influence of the atrial muscle on the sinoatrial node while maintaining exit of impulses into the adjacent atrial myocardium is achieved by the composition and

spatial organization of connexins, proteins that form gap junction channels responsible for intercellular ion fluxes (see later, **Intercalated Discs**). Connexins 40 and 45, but not connexin 43, are expressed in the central sinoatrial node (**Fig. 33-3**). The major part of the crista terminalis-sinoatrial node border exhibits a sharp demarcation boundary of connexin 43-expressing atrial myocytes and connexin 40/45-expressing myocytes. On the endocardial side, a transitional zone (paranodal area; see **Fig. 33-2**) exists between the crista terminalis and the peripheral node in which connexins 45 and 43 are colocalized. This colocalization of different connexin isoforms raises the possibility that individual gap junctional channels in the transitional zone are formed by more than one connexin isoform.²

These disparate connexin phenotypes may create specific types of hybrid channels with rectifying electrical properties that ensure the maintenance of sinoatrial node pacemaker activity but diminish electrotropic interference from the atrial muscle.⁵ At the level of the intact sinoatrial node *in situ*, more recent studies combining immunohistochemistry and high-resolution optical mapping of action potentials have provided structural and functional evidence of the existence of discrete exit pathways that electrically connect the sinoatrial node and atria in canines, whose three-dimensional sinoatrial node structure closely resembles that of humans. In this model (**Fig. 33-4**), electrical excitation during sinoatrial rhythm originates in the central portion of the sinoatrial node and spreads bidirectionally at low speed (1 to 14 cm/sec) within the sinoatrial node, with failure to conduct laterally to the crista terminalis and interatrial septum. After a conduction delay of approximately 50 milliseconds within the sinoatrial node, the impulse reaches the atrial myocardium via two main superior or inferior exit pathways located a few millimeters from the leading pacemaker site. The ellipsoidal sinoatrial node is thus functionally insulated from the adjacent working myocardium. This insulation coincides with the lack of connexin 43 expression and the presence of connective tissue and coronary arteries at the sinoatrial border (see **Fig. 33-4C-F**).⁶ The intranodal location of the primary pacemaking site is not fixed but rather appears to shift under varying conditions (e.g., sympathetic stimulation; see later in this chapter).

A number of experimental studies have investigated the usefulness of gene delivery- or cell-based approaches to generate biologic pacemakers in the mammalian heart. Gene-based techniques included transduction of *in situ* left ventricular cardiomyocytes with genes encoding a dominant-negative inwardly rectifying potassium channel or isoforms of the HCN channel. Cell-based approaches have used human induced pluripotent stem cell (iPSC)-derived pacemaker-like cardiomyocytes and mesenchymal stem cells ectopically expressing HCN isoform 2. Clinical translatability of these approaches will require additional experimental testing.⁷

Innervation. The sinoatrial node is densely innervated by postganglionic adrenergic and cholinergic nerve terminals.⁸ Discrete vagal efferent pathways innervate both the sinoatrial and atrioventricular (AV) regions of the dog and nonhuman primate. Most efferent vagal fibers to the atria appear to converge first at a single fat pad between the medial portion of the superior vena cava and the aortic root, superior to the right pulmonary artery; the fibers then project onto two other fat pads found at the junction of the inferior vena cava and



Additional content is available online at ExpertConsult.

left atrium and the junction of the right pulmonary vein and atrium and subsequently project to both atria. Vagal fibers to the sinoatrial and AV nodes also converge at the superior vena cava–aortic root fat pad before projection to the right pulmonary vein and inferior vena cava fat pads.⁸ Although the sinoatrial nodal region contains amounts of norepinephrine equivalent to those in other parts of the right atrium, acetylcholine, acetylcholinesterase, and choline acetyltransferase (the enzyme necessary for the synthesis of acetylcholine) have been found in greatest concentration in the sinoatrial node, with the next highest concentration located in the right and then the left atrium. The concentration of acetylcholine in the ventricles is only 20% to 50% of that in the atria.

Neurotransmitters modulate the discharge rate of the sinoatrial node by stimulation of beta-adrenergic and muscarinic receptors. Both beta₁ and beta₂ adrenoceptor subtypes are present in the

sinoatrial node. Human sinoatrial nodes contain more than a threefold greater density of beta-adrenergic and muscarinic cholinergic receptors than adjacent atrial tissue does. The functional significance of beta adrenoceptor subtype diversity in the sinoatrial node is unclear. Binding of receptor agonists released from sympathetic nerve terminals causes a positive chronotropic response through a beta₁ receptor-activated pathway involving the stimulatory guanosine triphosphate (GTP) regulatory protein (G_s), activation of adenylyl cyclase, intracellular accumulation of cyclic adenosine monophosphate (cAMP), stimulation of cAMP-dependent protein kinase A, and phosphorylation of ion-handling proteins, which ultimately results in an increased sinoatrial node discharge rate (for a more detailed description of the ionic mechanisms underlying the acceleration of sinoatrial node action potential firing see later in this chapter).⁹ The negative chronotropic response of vagal stimulation is mediated by acetylcholine binding to and ensuing activation of M₂ muscarinic receptors.

In addition to its negative chronotropic effect, acetylcholine also prolongs intranodal conduction time, at times to the point of sinoatrial nodal exit block. Acetylcholine increases whereas norepinephrine decreases refractoriness in the center of the sinoatrial node. The phase (timing) in the cardiac cycle at which vagal discharge occurs and the background sympathetic tone importantly influence vagal effects on the sinus rate and conduction (see later). After cessation of vagal stimulation, sinoatrial nodal automaticity may accelerate transiently (postvagal tachycardia). The neurotransmitters neuropeptide Y (NPY) and vasoactive intestinal peptide (VIP) are localized in sympathetic and

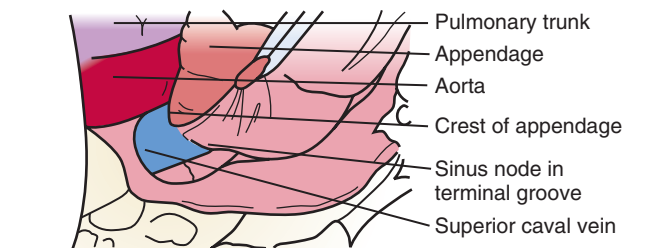


FIGURE 33-1 The human sinus node. This photograph, taken in the operating room, shows the location of the normal cigar-shaped sinus node along the lateral border of the terminal groove at the junction of the superior vena cava and atrium (arrowheads). (From Anderson RH, Wilcox BR, Becker AE: Anatomy of the normal heart. In Hurst JW, Anderson RH, Becker AE, Wilcox BR [eds]: *Atlas of the Heart*. New York, Gower, 1988, p 1.2.)

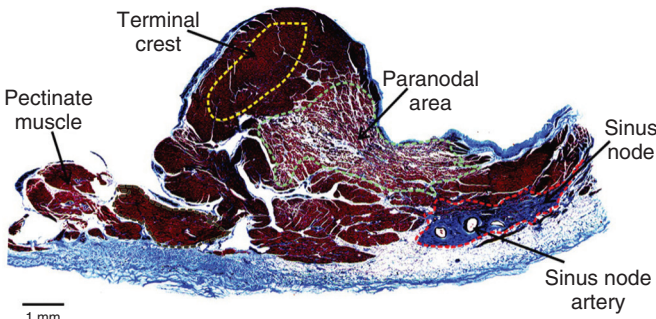


FIGURE 33-2 Masson trichrome-stained section through the human sinus node region. The node (red dashed line) is identified on the basis of the presence of the sinus node artery and the large amount of connective tissue (stained blue; myocytes stained purple-pink). The section also reveals the presence of a paranodal area (green dashed line) that is composed of loosely packed myocytes and sandwiched between the crista terminalis (yellow dashed line) and the sinus node. (From Chandler NJ, Greener ID, Tellez JO, et al: Molecular architecture of the human sinus node. *Circulation* 119:1562, 2009. By permission of the American Heart Association.)

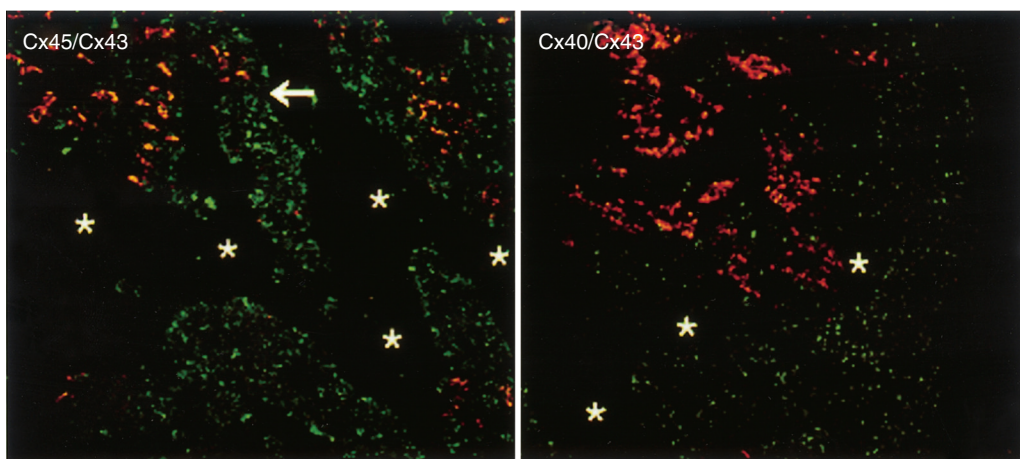


FIGURE 33-3 Sections through the sinoatrial node double-labeled with connexin 45 (Cx45/Cx43) (**left**) and CX40/Cx43 (**right**). Regions positive for Cx40/Cx43 (small punctate green signals) showing no detectable Cx43 signal (red) are sharply demarcated from adjacent Cx43-expressing regions of the crista terminalis. A zone of connective tissue (asterisks) contributes to separation between the zones, although elsewhere (arrow) the zones seem to be more closely approximated. (From Coppen SR, Kodama I, Boyett MR, et al: Connexin45, a major connexin of the rabbit sino-atrial node, is co-expressed with connexin43 in a restricted zone at the nodal–crista terminalis border. *J Histochem Cytochem* 47:907, 1999.)

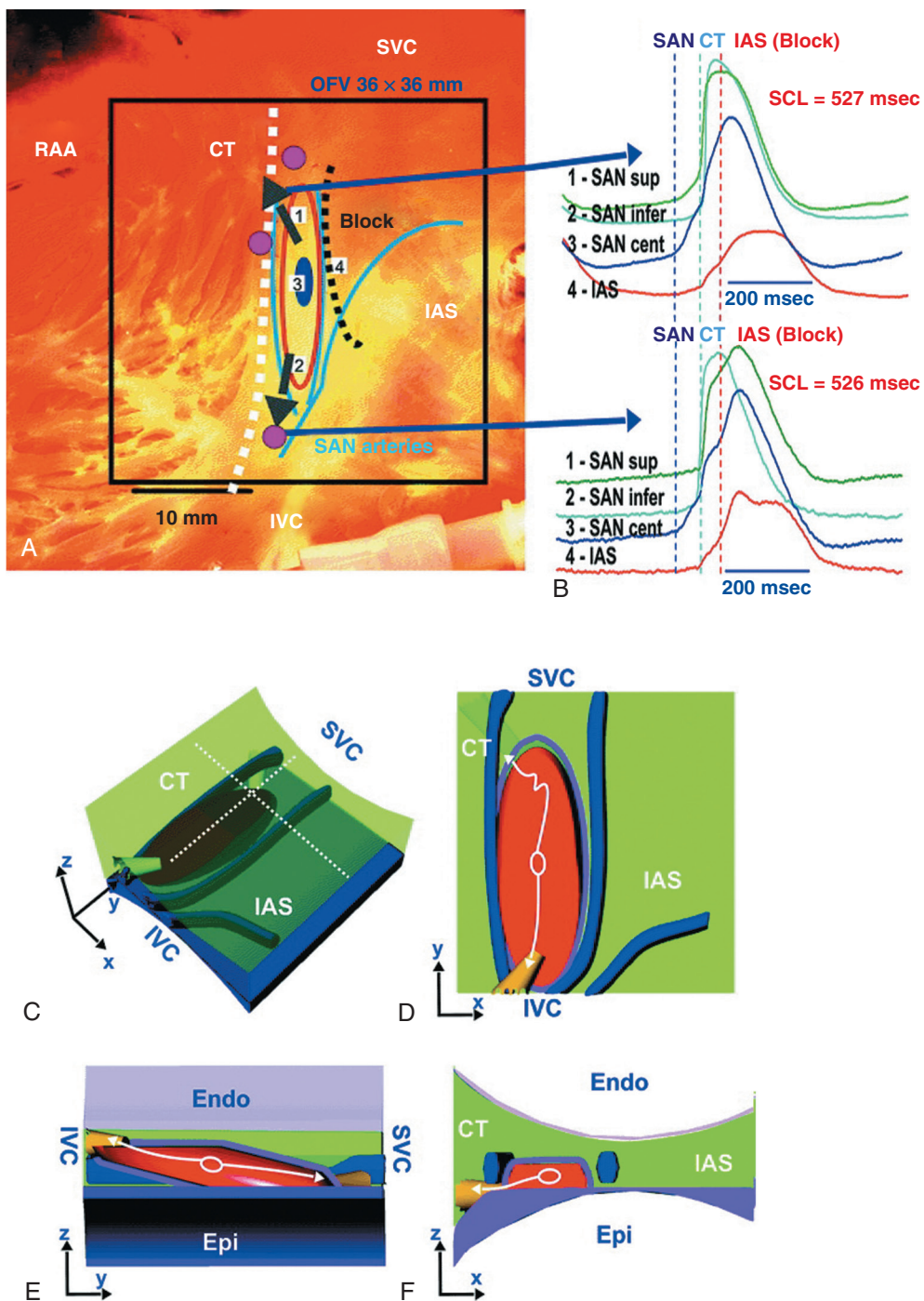


FIGURE 33-4 Endocardial optical voltage mapping in a canine right atrial preparation. **A**, Photograph of the endocardial aspect of the preparation. CT = crista terminalis; IAS = interatrial septum; OFV = optical field of view from which the optical recordings were taken; RAA = right atrial appendage; SVC and IVC = superior and inferior vena cava, respectively. The sinoatrial node (SAN; red oval) is flanked by branches of the SAN artery (drawn schematically in light blue). **B**, Optical action potentials recorded during sinus rhythm from sites 1 through 4 depicted in the photograph in **A**. Sites 1 and 2 are from the superior (SAN sup) and inferior (SAN infer) part of the SAN, near the SAN exit pathways. Site 3 is from the leading pacemaker site (SAN cent), and site 4 is from the IAS block zone. Electrical excitation originates in the central portion of the SAN (dark blue oval in **A**) and spreads bidirectionally within the SAN, with failure to conduct in a perpendicularly direction into the IAS and CT. After a conduction delay of approximately 50 milliseconds within the SAN, excitation reaches the atrial myocardium via superior (upper tracings in **B**) or inferior (lower tracings in **B**) sinoatrial exit pathways approximately 9 mm from the leading pacemaker site. The ellipsoidal SAN structure (red line in **A**) is functionally insulated from the atrial myocardium, as indicated by the dashed white and black lines in **A**, respectively, except for two (inferior and superior) exit pathways. Vertical dashed lines indicate the beginning of SAN, CT, and IAS activation. SCL denotes sinus cycle length. Numbers to the left of the optical action potential tracings correspond to the respective recording sites in the photograph in **A**. **C-F**, Three-dimensional model of the SAN. The green area represents the myocardium. The fibrotic tissue (purple) and coronary arteries (blue) enclose the SAN (red). The initial excitation during sinus rhythm is shown by a white oval. The arrows denote the two main directions of propagation of the impulse within the SAN. The yellow bundles show the sinus node exit pathways. **C** and **D** show side and top projections, respectively. **E** and **F** show cross sections in the z-y and z-x plane, respectively. (From Fedorov VV, Schuessler RB, Hemhill M, et al: Structural and functional evidence for discrete exit pathways that connect the canine sinoatrial node and atria. *Circ Res* 104:915, 2009. By permission of the American Heart Association.)

parasympathetic nerve terminals, respectively. VIP reversibly increases I_f , whereas NPY reversibly decreases I_f . The role of other peripheral neurotransmitters (such as calcitonin gene-related peptide, substance P) in controlling sinoatrial node electrophysiology is unclear.

Atrioventricular Junctional Area and Intraventricular Conduction System

Atrioventricular Node

Based on histology and immunolabeling, the normal AV junctional area (**Figs. 33-5 and 33-6**) is composed of multiple distinct structures, including transitional tissue, inferior nodal extension, compact portion, penetrating bundle, His bundle, atrial and ventricular muscle, central fibrous body, tendon of Todaro, and valves.^{10,11} **Figure 33-7A, B** shows a computer-generated three-dimensional reconstruction of the AV junctional area in a rabbit heart. At the level of the AV junction, the tract of nodal tissue is divided into two major components, the inferior nodal extension and the penetrating bundle (red and purple areas, respectively, in **Fig. 33-7A, B**). The inferior nodal extension is located between the coronary sinus and the tricuspid valve, and the end of the inferior nodal extension is covered by transitional tissue (light green area in **Fig. 33-7A, B**). The small myocytes in the inferior nodal extension are dispersed among connective tissue and do not express connexin 43, whereas myocytes in the transitional zone do express connexin 43; however, unlike the connexin 43-positive atrial myocytes in the working myocardium, they are loosely packed between collagen septa. The inferior nodal extension is continuous with the penetrating bundle, which penetrates the fibrous tissue separating the atria and ventricles and emerges in the ventricles as the bundle of His. Both structures are covered by connective tissue (sheaths in **Fig. 33-7A**) and are therefore enclosed. Myocytes in the penetrating bundle express connexin 43 and are dispersed among connective tissue. A tract of connexin 43-positive nodal tissue projects into the connexin 43-negative inferior nodal extension.

The compact portion of the AV node (yellow area in **Fig. 33-7A, B**) is a superficial structure lying just beneath the right atrial endocardium, anterior to the ostium of the coronary sinus, and directly above the insertion of the septal leaflet of the tricuspid valve. It is at the apex of a triangle formed by the tricuspid annulus and the tendon of Todaro (blue area in **Fig. 33-7A, B**), which originates in the central fibrous body and passes posteriorly through the atrial septum to continue with the eustachian valve (see **Figs. 33-5 and 33-6A**). The term *triangle of Koch*, however, has to be used with caution because histologic studies of anatomically normal adult hearts have demonstrated that the tendon of Todaro, which forms one side of the triangle of Koch, is absent in about two thirds of hearts. The compact node is located at the junction where the connexin 43-negative nodal tissue (red area in **Fig. 33-7A, B**) meets the connexin 43-positive nodal tissue (purple area in **Fig. 33-7A, B**). Myocytes in the nodal portion are small and weakly positive for connexin 43. In 85% to 90% of human hearts, the arterial supply to the AV node is derived from a branch of the right coronary artery that originates at the posterior intersection of the AV and interventricular grooves (crux). A branch of the circumflex coronary artery provides the arterial supply to the AV node in the remaining hearts. Fibers in the lower part of the AV node may exhibit automatic impulse formation.¹¹ The main function of the AV node is to delay transmission of atrial impulses to the ventricles, thereby coordinating atrial and ventricular contractions (**Fig. 33-7C, D**). During normal anterograde AV conduction, the action potential propagates from the sinoatrial node through atrial working myocardium (the existence of specialized internodal conduction pathways has been controversial) and enters the tract of nodal tissue at two points (see **Fig. 33-7C**; see also Video 33-1). The first point is at the end of the inferior nodal extension (next to the penetrating bundle) via the transitional tissue. This conduction pathway most likely corresponds to the fast-pathway route previously observed in electrical mapping experiments.¹¹ Second, the action potential enters toward the beginning of the inferior nodal extension. This conduction pathway probably constitutes the slow-pathway route. The action potential cannot enter the nodal tissue at other tissue points because the nodal and atrial tissues are isolated from each other by a vein along this length

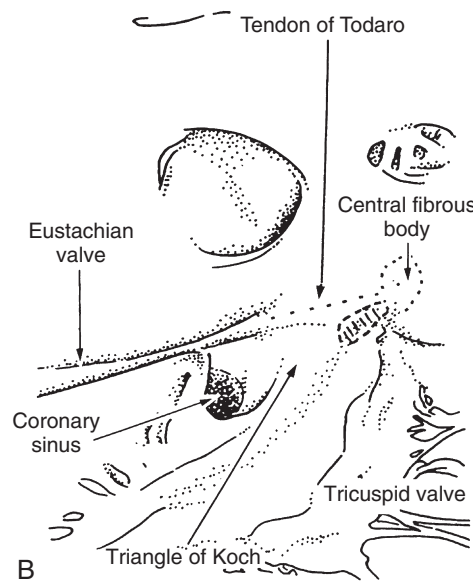


FIGURE 33-5 A, Photograph of a normal human heart showing the anatomic landmarks of the triangle of Koch. This triangle is delimited by the tendon of Todaro superiorly, by the fibrous commissure of the flap guarding the openings of the inferior vena cava and coronary sinus, by the attachment of the septal leaflet of the tricuspid valve inferiorly, and by the mouth of the coronary sinus at the base. **B,** The stippled area adjacent to the central fibrous body is the approximate site of the compact AV node. (From Janse MJ, Anderson RH, McGuire MA, et al: "AV nodal" reentry: I. "AV nodal" reentry revisited. *J Cardiovasc Electrophysiol* 4:561, 1993.)

of tissue (dark green area in **Fig. 33-7B, C**). From the two entry points, the action potentials propagate both anterogradely and retrogradely along the inferior nodal extension and eventually annihilate each other. The action potential entering the nodal tract via the transitional zone also propagates into the compact node and then reaches the His bundle and propagates down the left and right bundle branches. Transmembrane action potentials recorded from *in situ* cardiomyocytes at various locations within the nodal tract exhibit distinct shapes and time courses (see **Fig. 33-7D**). Action potentials from extranodal atrial tissue and the His bundle (locations 1 and 5, respectively, in **Fig. 33-7C**) have more hyperpolarized diastolic potentials and faster upstrokes than do myocytes in the transitional zone (location 3) and penetrating bundle (location 4). This smaller rate of depolarization results in slowing of conduction across the compact portion and penetrating bundle (conduction velocity, <10 cm/sec versus 35 cm/sec in atrial working myocardium), thereby giving rise to the AV conduction delay.

VIDEO 33-1

Simulation of anterograde conduction through the atrioventricular node (AVN) using an electroanatomical model. The preparation is stimulated at the interatrial septum as shown by the stimulating electrodes. There is a flash and click coincident with the stimulus. (From Li J, Greener ID, Inada S, et al: Computer three dimensional reconstruction of the atrioventricular node. Circ Res 102:975, 2008.)

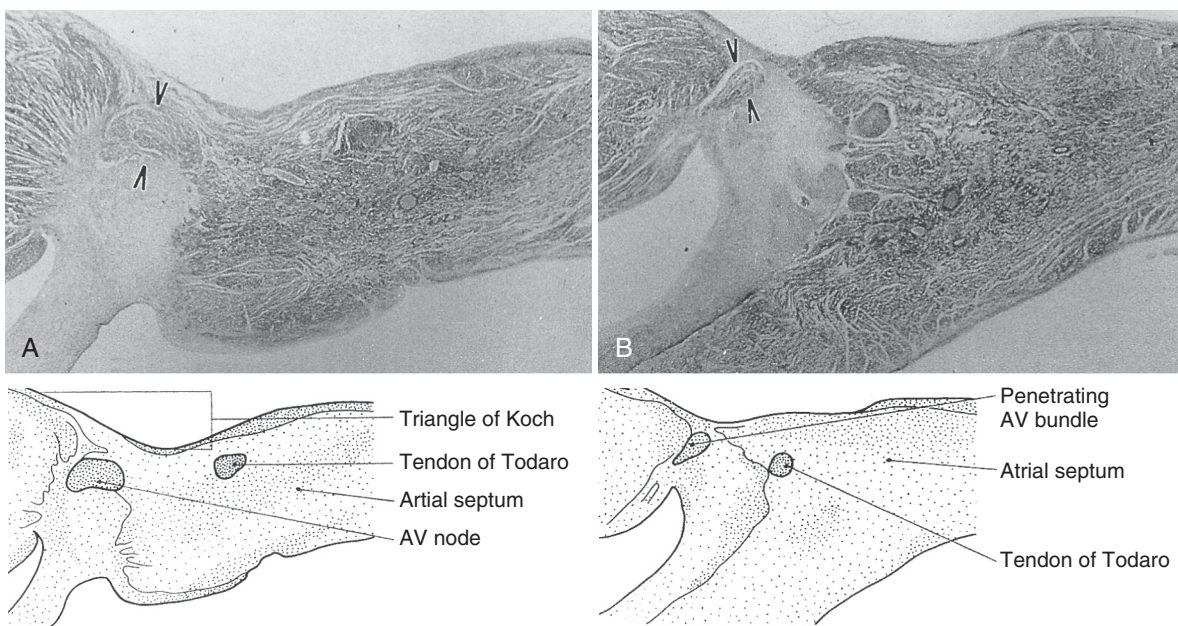


FIGURE 33-6 Sections through the AV junction show the position of the AV node (arrowheads) within the triangle of Koch (**A**) and the penetrating AV bundle of His (arrowheads) within the central fibrous body (**B**).

Bundle of His (Penetrating Portion of the Atrioventricular Bundle)

This structure is the continuation of the penetrating bundle on the ventricular side of the AV junction before it divides to form the left and right bundles (see Fig. 33-6A). Myocytes in the His bundle are small and connexin 43 positive (see Fig. 33-7C). However, large, well-formed fasciculoventricular connections between the penetrating portion of the AV bundle and the ventricular septal crest are rarely found in adult hearts. Branches from the anterior and posterior descending coronary arteries supply the upper muscular interventricular septum with blood, which makes the conduction system at this site more impervious to ischemic damage unless the ischemia is extensive.

Bundle Branches (Branching Portion of the Atrioventricular Bundle)

These structures begin at the superior margin of the muscular interventricular septum, immediately beneath the membranous septum, with cells of the left bundle branch cascading downward as a continuous sheet onto the septum beneath the noncoronary aortic cusp (Fig. 33-8A). The AV bundle may then give off other left bundle branches, sometimes constituting a true bifascicular system with an anterosuperior branch, in other hearts giving rise to a group of central fibers, and in still others appearing more as a network without clear division into a fascicular system (Fig. 33-8B). The right bundle branch continues intramyocardially as an unbranched extension of the AV bundle down the right side of the interventricular septum to the apex of the right ventricle and base of the anterior papillary muscle. In some human hearts, the His bundle traverses the right interventricular crest and gives rise to a right-sided narrow stem origin of the left bundle branch. The anatomy of the left bundle branch system can be variable and not conform to a constant bifascicular division. However, the concept of a trifascicular system remains useful to both electrocardiographers and clinicians (see Chapter 12).

Terminal Purkinje Fibers

These fibers connect with the ends of the bundle branches to form interweaving networks on the endocardial surface of both ventricles and transmit the cardiac impulse almost simultaneously to the entire right and left ventricular endocardium. Purkinje fibers tend to be less concentrated at the base of the ventricle and at the papillary

muscle tips. They penetrate the myocardium for varying distances, depending on the animal species. In humans, they apparently penetrate only the inner third of the endocardium, whereas in pigs, they almost reach the epicardium. Such variations could influence changes produced by myocardial ischemia, for example, because Purkinje fibers appear to be more resistant to ischemia than ordinary myocardial fibers are. Purkinje myocytes are found in the His bundle and bundle branches, cover much of the endocardium of both ventricles (see Fig. 33-8B), and align to form multicellular bundles in longitudinal strands separated by collagen. Although conduction of cardiac impulses appears to be their major function, free-running Purkinje fibers composed of many Purkinje cells in a series, sometimes called false tendons, are capable of contraction. Action potentials propagate within the thin Purkinje fiber bundles from the base to the apex before activation of the surrounding myocytes occurs. Purkinje myocytes largely lack transverse tubules (Fig. e33-1), which reduces membrane capacitance and thus accelerates action potential propagation.¹² Propagation of action potentials within the His-Purkinje system and working myocardium is mediated by connexins. Ventricular myocytes express mainly connexin 43, and Purkinje fibers express connexins 40 and 45. The molecular identity of the connexin type that enables transmission of impulses at the Purkinje fiber-myocyte junction (PMJ) is unclear. It is also still not clear how the small amount of depolarizing current provided by the thin bundle of Purkinje fibers can activate a much larger mass of ventricular muscle (current-to-load mismatch).¹³ It is possible that individual gap junctional channels at the PMJ are formed by more than one connexin isoform. These disparate connexin phenotypes may create specific types of hybrid channels with unique properties that ensure safe conduction at the PMJ. Because Purkinje cells have markedly longer repolarization times than surrounding myocytes do (see Fig. 33-17E), these connexin hybrids could also decrease entrainment of repolarization at the PMJ and thereby increase repolarization gradients.

Innervation of the Atrioventricular Node, His Bundle, and Ventricular Myocardium

Pathways of Innervation. The AV node and His bundle region are innervated by a rich supply of cholinergic and adrenergic fibers with densities exceeding those found in the ventricular myocardium.¹⁴

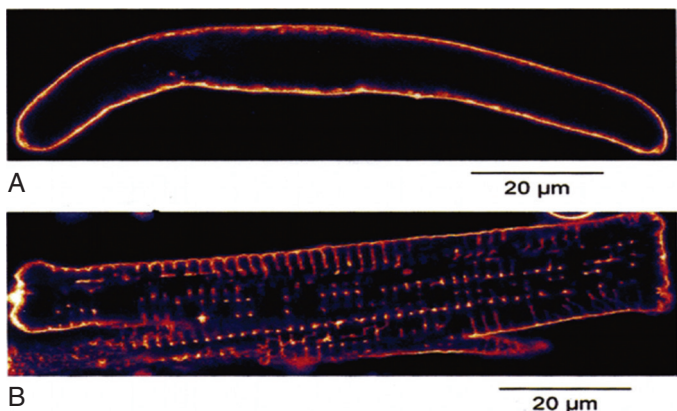


FIGURE e33-1 Confocal fluorescence images of a Purkinje cell (**A**) and left ventricular cardiomyocyte (**B**) isolated from a rabbit heart. The cells were stained with the membrane-selective fluorescent dye di-8-ANEPPS to visualize the sarcolemma. Ventricular myocytes typically exhibit regularly spaced lines of increased dye fluorescence intensity that run perpendicular to the outer membrane. These lines correspond to invaginations of the outer membrane, so-called *transverse tubuli*. Purkinje myocytes lack transverse tubuli. (From Cordeiro JM, Spitzer KW, Giles WR, et al: Location of the initiation site of calcium transients and sparks in rabbit heart Purkinje cells. *J Physiol* 531:301, 2001.)

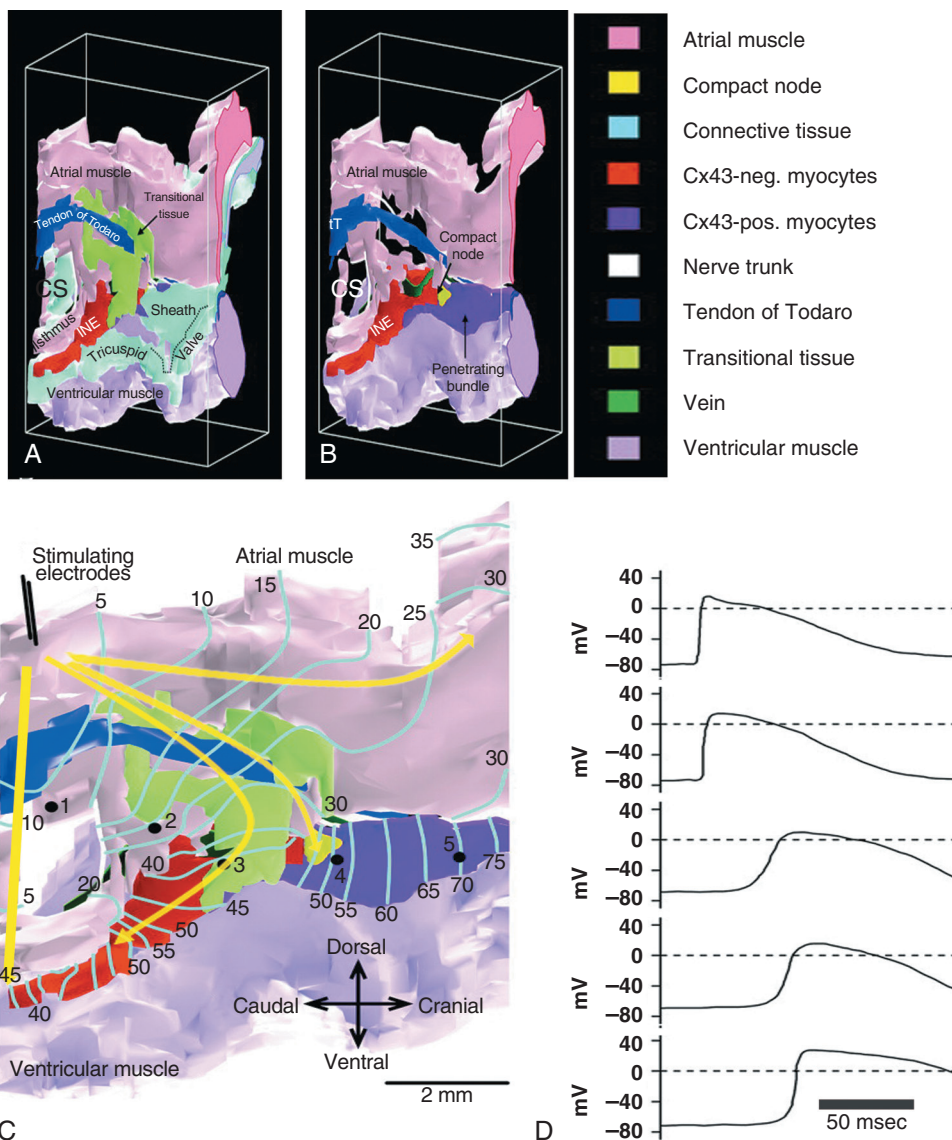


FIGURE 33-7 **A, B**, Computer-generated three-dimensional anatomic model of the AV node as viewed from the right atrium-ventricle. **A** shows all cell types. **B** shows the model after removal of transitional and connective tissue. The inferior nodal extension (INE) is located between the coronary sinus (CS) and the tricuspid valve, the end of the INE is covered by transitional tissue, the penetrating bundle begins at the apex of the triangle of Koch (formed by the CS, tendon of Todaro [tT], and tricuspid valve), and the penetrating bundle and His bundle are covered by connective tissue ("sheath"). After removal of the transitional and connective tissue, one sees protraction of a connexin 43 (Cx43)-positive portion of nodal tissue into the Cx43-negative INE. The compact node is located at the junction of Cx43-negative and Cx43-positive nodal tissue. **C, D**, Structure-function relationships of the AV node. **C**, Schematic representation of the sequence of anterograde AV conduction by using a combination of mathematical modeling and experimental mapping of action potential propagation. The preparation is electrically stimulated at the crista terminalis. The activation sequence is shown as isochrones at 5-millisecond intervals. Yellow arrows delineate the conduction pathways. (See also Video 33-1.) **D**, Transmembrane action potentials recorded at locations marked by black dots in C (numbered 1 through 5). (Modified from Li J, Greener ID, Inada S, et al: Computer three dimensional reconstruction of the atrioventricular node. *Circ Res* 102:975, 2008. By permission of the American Heart Association.)

Immunolabeling with markers for sympathetic and parasympathetic nerves revealed nonuniform innervation density in the AV junctional area. For example, the inferior nodal extension has been shown to exhibit a higher density of both nerve types than the working atrial myocardium does, whereas the opposite is true for the compact node.¹⁵ Ganglia, nerve fibers, and nerve nets lie close to the AV node. Parasympathetic nerves to the AV node region enter the canine heart at the junction of the inferior vena cava and the inferior aspect of the left atrium, adjacent to the entrance to the coronary sinus. Nerves in direct contact with AV nodal fibers have been noted, along with agranular and granular vesicular processes, which presumably represent cholinergic and adrenergic processes.

In general, autonomic neural input to the heart exhibits some degree of "sidedness," with the right sympathetic and vagal nerves

affecting the sinoatrial node more than the AV node and the left sympathetic and vagal nerves affecting the AV node more than the sinoatrial node. The distribution of neural input to the sinoatrial and AV nodes is complex because of substantial overlapping innervation. Despite the overlap, specific branches of the vagal and sympathetic nerves can be shown to innervate certain regions preferentially. Supersensitivity to acetylcholine follows vagal denervation. Stimulation of the right stellate ganglion produces sinus tachycardia with less effect on AV nodal conduction, whereas stimulation of the left stellate ganglion generally produces a shift in the sinus pacemaker to an ectopic site and consistently shortens AV nodal conduction time and refractoriness but inconsistently speeds the sinoatrial nodal discharge rate. Stimulation of the right cervical vagus nerve primarily slows the sinoatrial nodal discharge rate, and stimulation of the left vagus primarily prolongs AV nodal conduction time and refractoriness when sidedness is present. Neither sympathetic nor vagal stimulation affects normal conduction in the His bundle. The negative dromotropic response of the heart to vagal stimulation is mediated by the activation of $I_{K,ACh,Ade}$, which results in hyperpolarization of the AV nodal cells and thereby influences the conductive properties of the node. The positive dromotropic effect of sympathetic stimulation arises as a consequence of an increase in cytosolic cAMP levels and ensuing activation of the L-type Ca^{2+} current $I_{Ca,L}$ (see Table 33-3).

Most efferent sympathetic impulses reach the canine ventricles over the ansae subclaviae, branches from the stellate ganglia. Sympathetic nerves then synapse primarily in the caudal cervical ganglia and form individual cardiac nerves that innervate relatively localized parts of the ventricles. The major route to the heart is the recurrent cardiac nerve on the right side and the ventrolateral cardiac nerve on the left. In general, the right sympathetic chain shortens refractoriness primarily of the anterior portion of the ventricles, and the left affects primarily the posterior surface of the ventricles, although overlapping areas of distribution occur.

The intraventricular route of sympathetic nerves generally follows the coronary arteries. Functional data have suggested that afferent and efferent sympathetic nerves travel in the superficial layers of the epicardium and dive to innervate the endocardium, and anatomic observations have supported this conclusion. Vagal fibers travel intramurally or subendocardially and rise to the epicardium at the AV groove (Fig. 33-9A). Sympathetic nerve density in the left ventricle appears to be higher in the epicardial than in the endocardial portion of the ventricle, which at least in part results from transmural gradients in the expression of cytokines during cardiac development that attract and repel, respectively, sympathetic nerve growth (Fig. 33-9B).^{14,16}

Effects of Vagal Stimulation. The vagus modulates cardiac sympathetic activity at prejunctional and postjunctional sites by regulating the amount of norepinephrine released and by inhibiting cAMP-induced phosphorylation of cardiac proteins, including ion channels

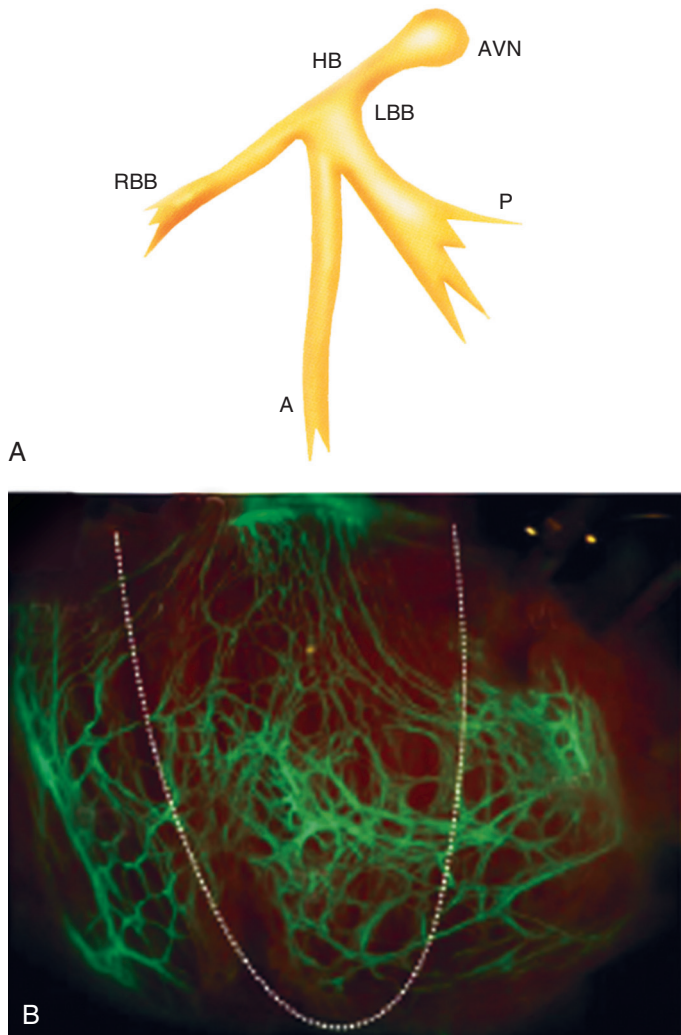


FIGURE 33-8 **A**, Schematic representation of the trifascicular bundle branch system. **B**, Structural organization of the His-Purkinje system in the mouse heart. Expression of a green fluorescent protein was specifically targeted to cells of the His-Purkinje system in mice. Green fluorescent cell networks in the left ventricular chamber are shown. The left ventricular free wall (LVFW) was incised from the base to the apex, and then the two parts of the LVFW were pulled back to expose the left flank of the interventricular septum (LF). The dotted line demarcates the border between the LF and the LVFW. A = anterosuperior fascicle of the left bundle branch; AVN = atrioventricular node; HB = His bundle; LBB = left bundle branch; P = posteroinferior fascicle of the left bundle branch; RBB = right bundle branch. (**A**, Modified from Rosenbaum MB, Elizari MV, Lazzari JO: *The Hemiblocks. Oldsmar, Fla, Tampa Tracings*, 1970, cover illustration; **B**, from Micquerol L, Meysen S, Mangoni M, et al: Architectural and functional asymmetry of the His-Purkinje system of the murine heart. *Cardiovasc Res* 63:77, 2004.)

and calcium pumps. The latter inhibition occurs at more than one level in the series of reactions constituting the adenylate cyclase–, cAMP-dependent protein kinase system. Neuropeptides released from the nerve fibers of both autonomic limbs also modulate autonomic responses. For example, NPY released from sympathetic nerve terminals inhibits cardiac vagal effects.

Tonic vagal stimulation produces a greater absolute reduction in the sinoatrial rate in the presence of tonic background sympathetic stimulation, a sympathetic-parasympathetic interaction termed *accentuated antagonism*. In contrast, changes in AV conduction during concomitant sympathetic and vagal stimulation are essentially the algebraic sum of the individual AV conduction responses to tonic vagal and sympathetic stimulation alone. Cardiac responses to brief vagal bursts begin after a short latency and dissipate quickly; in contrast, cardiac responses to sympathetic stimulation commence and dissipate slowly. The rapid onset and offset of responses to vagal stimulation allow dynamic beat-to-beat vagal modulation of the heart rate and AV conduction, whereas the slow temporal response to sympathetic

stimulation precludes any beat-to-beat regulation by sympathetic activity. Periodic vagal bursting, as may occur each time that a systolic pressure wave arrives at the baroreceptor regions in the aortic and carotid sinuses, induces phasic changes in sinus cycle length and can entrain the sinus node to discharge faster or slower at periods identical to those of the vagal burst. In a similar phasic manner, vagal bursts prolong AV nodal conduction time and are influenced by background levels of sympathetic tone. Because the peak vagal effects on sinus rate and AV nodal conduction occur at different times in the cardiac cycle, a brief vagal burst can slow the sinus rate without affecting AV nodal conduction or can prolong AV nodal conduction time and not slow the sinus rate. Bilateral but not unilateral vagal nerve stimulation increases and reverses the spatial dispersion of ventricular repolarization as the direction of repolarization from the apex to the base in sinus rhythm shifts from the base to the apex. This effect is attributable to more pronounced prolongation of the action potential at the apex than at the base of the heart (Fig. e33-2).¹⁷

Effects of Sympathetic Stimulation. Similar to bilateral vagal nerve stimulation, sympathetic nerve stimulation also increases and reverses the spatial gradients of ventricular repolarization as the direction of polarization from the apex to the base in sinus rhythm shifts from the base to the apex. This reversal results from a marked shortening of action potential duration at the base, with no or very little effect on the repolarization time course at the apex of the heart (see Fig. e33-2).¹⁷ Nonuniform distribution of sympathetic nerves—and thus norepinephrine levels—may in part contribute to some of the nonuniform electrophysiologic effects because the ventricular content of norepinephrine is greater at the base than at the apex of the heart.¹¹ In humans, both direct and reflex sympathetic stimulation increases regional differences in cardiac repolarization. The dispersion of repolarization is significantly enhanced in patients with ischemic cardiomyopathy.¹⁸ Afferent vagal activity appears to be higher in the posterior ventricular myocardium, which may account for the vagomimetic effects of inferior myocardial infarction.

The vagi exert minimal but measurable effects on ventricular tissue; they decrease the strength of myocardial contraction and prolong refractoriness. Under some circumstances, acetylcholine can cause a positive inotropic effect. It is now clear that the vagus (acetylcholine) can exert direct effects on some types of ventricular fibers, as well as indirect effects by modulating sympathetic influences.

Beyond the beat-to-beat regulation of rate and contractile force, sympathetic input to the heart, through both translational and post-translational modifications, also exerts long-term regulation of adrenergic receptor sensitivity and ionic channels. These long-term changes in autonomic responsiveness and cardiac electrical properties appear to be mediated, at least in part, by highly localized signaling cascades involving neurally released molecules such as NPY.¹⁹

Arrhythmias and the Autonomic Nervous System

Alterations in vagal and sympathetic innervation (autonomic remodeling) can influence the development of arrhythmias and result in sudden cardiac death from ventricular tachyarrhythmias.²⁰ Damage to nerves extrinsic to the heart, such as the stellate ganglia, and to intrinsic cardiac nerves from diseases that may affect primarily nerves, such as viral infections, or from diseases that secondarily cause cardiac damage may produce cardioneuropathy. Although the mechanisms by which altered sympathetic innervation modulates cardiac electrical properties are largely unknown, spatially heterogeneous sympathetic hyperinnervation could result in enhanced dispersion of myocardial excitability and refractoriness via patchy adrenergic stimulation of ionic currents, including $I_{Ca,L}$, I_Ks , and I_{Cl} (see Table 33-3). Sympathetic hypoinnervation has been shown to increase the sensitivity of adrenergic receptors to activation by circulating catecholamines (denervation supersensitivity).¹⁴

Numerous studies have suggested a primary role of altered cardiac sympathetic innervation in arrhythmogenesis. Chronic infusion of nerve growth factor into the left stellate ganglion in dogs with chronic myocardial infarction and complete AV block caused spatially heterogeneous sympathetic cardiac hyperinnervation (nerve sprouting) and dramatically increased the incidence of sudden death from ventricular tachyarrhythmias.²⁰ Ambulatory long-term recordings of left stellate ganglion nerve activity in these dogs revealed that most malignant ventricular arrhythmias were preceded by increased neuronal discharge,

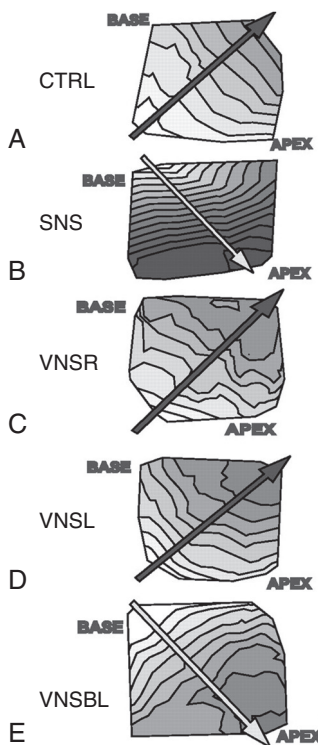


FIGURE e33-2 Reversal of the ventricular repolarization sequence during autonomic nerve stimulation in a rabbit heart. Each map represents the dispersion of repolarization for a single cardiac beat and is displayed as an isochronal map with lines 2 milliseconds apart. Light to dark shades represent early to late repolarization time points. Arrows point to the direction of the repolarization sequence. CTRL = control; SNS = sympathetic nerve stimulation; VNSBL = bilateral vagal nerve stimulation; VNSL = left vagal nerve stimulation; VNSR = right vagal nerve stimulation. (From Mantravadi R, Gabris B, Liu T, et al: Autonomic nerve stimulation reverses ventricular repolarization sequence in rabbit hearts. *Circ Res* 100:e72, 2007. With permission from the American Heart Association.)

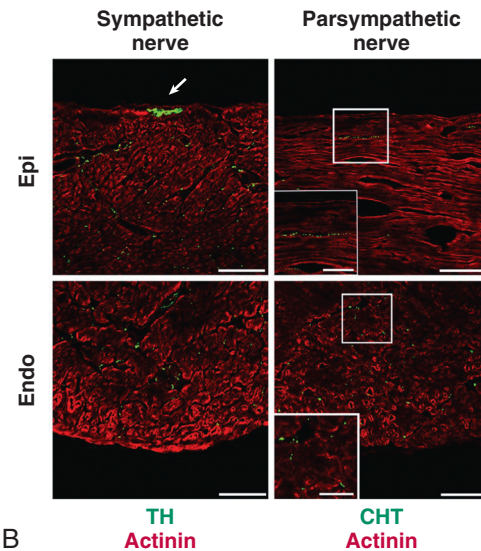
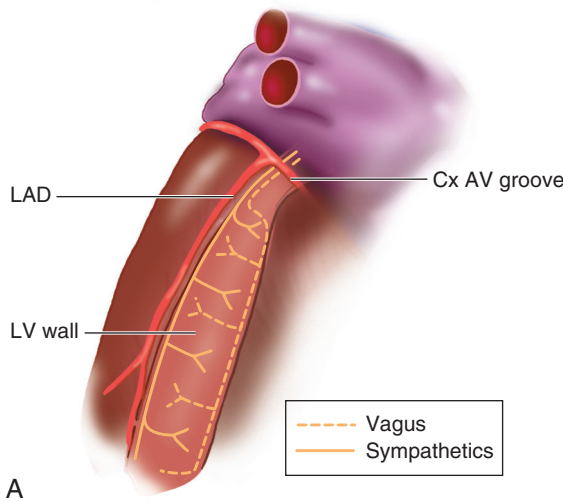


FIGURE 33-9 **A,** Intraventricular route of the sympathetic and vagal nerves to the left ventricle (LV). LAD = left anterior descending artery. **B,** Distribution of sympathetic and parasympathetic nerves in the mammalian heart. Immunofluorescence staining for the sympathetic and parasympathetic nerve markers tyrosine hydroxylase (TH) and choline transporter (CHT) is shown in the left ventricle of a rat heart (green: nerves; red: alpha-actinin, a cardiomyocyte marker). TH-positive nerves are more abundant in the subepicardial (epi) layer than in the subendocardial (endo) layer. The arrow indicates sympathetic nerves at the epicardial surface. No CHT-positive nerves are present at the epicardial surface, and CHT-positive nerves are more abundant in the subendocardial layer. Higher magnification views of the boxed regions are shown in the insets. Scale bars = 100 μ m. (**A**, From Ito M, Zipes DP: Efferent sympathetic and vagal innervation of the canine right ventricle. *Circulation* 90:1459, 1994. By permission of the American Heart Association; **B**, from Kanazawa H, Ieda M, Kimura K, et al: Heart failure causes cholinergic transdifferentiation of cardiac sympathetic nerves via gp130-signaling cytokines in rodents. *J Clin Invest* 120:408, 2010.)

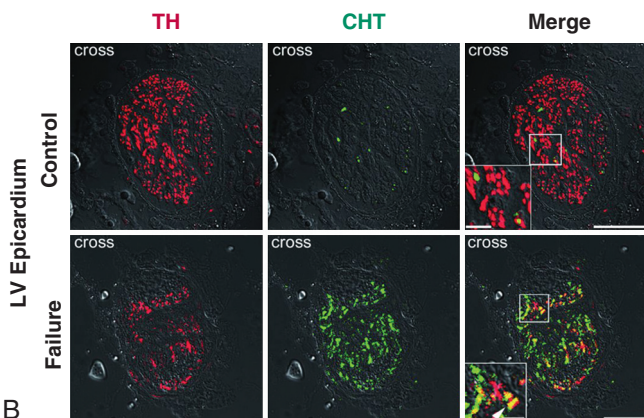
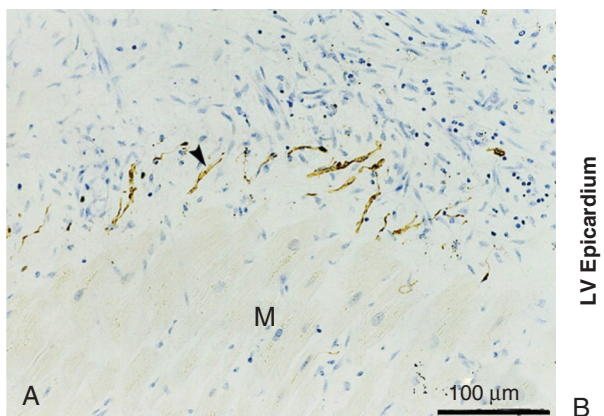


FIGURE 33-10 Sympathetic neural remodeling in diseased heart. **A,** Regional hyperinnervation (arrowhead) at the junction between necrotic and normal, surviving myocardium (M) in a patient with cardiomyopathy and ventricular tachyarrhythmias. **B,** Cholinergic transdifferentiation of cardiac sympathetic nerves in failing human hearts. Shown are representative cross sections of epicardial nerve bundles in the left ventricle of a nonfailing (**upper row**) and a failing human heart. Hearts were stained for tyrosine hydroxylase (TH; red) and choline transporter (CHT; green) as catecholaminergic and cholinergic nerve markers, respectively. The failing heart exhibits fewer TH-positive nerves and markedly more CHT-positive nerves than does the nonfailing heart, whereas overall nerve density appears to be similar. The **right** panels display merged images of the TH and CHT signal, which reveals that in the failing heart some nerves coexpress TH and CHT (yellow color because of the overlap of red TH and green CHT fluorescence). Higher magnification views of the boxed regions are shown in the insets. The arrowhead in the lower left corner of the far right image denotes a nerve coexpressing TH and CHT. Scale bar, 10 μ m; insets, 50 μ m. (**A**, From Cao J, Fishbein MC, Han JB, et al: Relationship between regional cardiac hyperinnervation and ventricular arrhythmia. *Circulation* 101:1960, 2000. By permission of the American Heart Association; **B**, from Kanazawa H, Ieda M, Kimura K, et al: Heart failure causes cholinergic transdifferentiation of cardiac sympathetic nerves via gp130-signaling cytokines in rodents. *J Clin Invest* 120:408, 2010.)

thus suggesting a causal role of sympathetic input in triggering arrhythmogenic sudden cardiac death.²¹ A high-cholesterol diet was reported to result in cardiac sympathetic hyperinnervation in rabbits and a marked increase in the incidence of ventricular fibrillation (VF).²² Explanted human hearts from transplant recipients with a history of arrhythmias exhibited a significantly higher and also more heterogeneous density of sympathetic nerve fibers than did those from patients without arrhythmias (Fig. 33-10A). Whether neural remodeling also involved parasympathetic nerve fibers in the heart was not examined in these studies. In patients with congestive heart failure, sympathetic neural tone is upregulated, and excess activation of the sympathetic nervous system leads to adverse myocardial effects, including lethal arrhythmias, and also causes depletion of cardiac norepinephrine content. This depletion of norepinephrine has recently been shown to result, at least partially, from neurotransmitter switching and

transdifferentiation from catecholaminergic into cholinergic neurons in the chronically failing heart (Fig. 33-10B).²³ This process is induced by release of cholinergic differentiation factors from failing cardiomyocytes. It remains to be determined, however, whether neurotransmitter switching is an adaptive response to protect the heart from excess sympathetic stimulation and thus lethal arrhythmias. Interestingly, beta adrenoceptor blockade in rats with coronary artery ligation reversed the myocardial sympathetic axon depletion in intact myocardium remote from the infarct but did not affect peri-infarct sympathetic hyperinnervation.²⁴ The junctions between pulmonary veins and the left atrium are highly innervated structures. Both sympathetic and parasympathetic nerves are colocated and concentrated in “ganglionated plexuses” around the pulmonary veins.²⁵ Selective ablation of ganglionated plexuses, as well as extensive regional ablation targeting anatomic areas containing ganglionated plexuses, has been shown to

reduce the incidence of paroxysmal atrial fibrillation (AF) in both clinical and experimental studies, thus further supporting a causal involvement of autonomic nerve activity in atrial arrhythmogenesis.^{26,27} On the other hand, spatially heterogeneous sympathetic denervation was similarly associated with an increased risk for atrial and ventricular arrhythmias. Mutations in genes encoding cardiac ion channel subunits also affect channel function in the central and peripheral autonomic nervous system and thereby result in abnormal firing properties of affected neurons.^{28,29} This observation may partially explain the clinical finding that sudden cardiac death in some variants of long-QT syndrome (LQTS; see Chapters 32, 34, and 37) is typically preceded by sympathetic arousal. Also, the antiarrhythmic efficacy of surgical left cardiac sympathetic denervation has previously been demonstrated in young patients with catecholaminergic polymorphic ventricular tachycardia (CPVT), an inherited arrhythmia caused by missense mutations in the gene encoding the cardiac ryanodine receptor Ca^{2+} release channel.³⁰ Thus the cardiac sympathetic nervous system provides a potentially useful target for treating patients at risk for clinical arrhythmias.³¹

BASIC ELECTROPHYSIOLOGIC PRINCIPLES

Physiology of Ion Channels

Electrical signaling in the heart involves the passage of ions through ionic channels. The Na^+ , K^+ , Ca^{2+} , and Cl^- ions are the major charge carriers, and their movement across the cell membrane creates a flow of current that generates excitation and signals in cardiac myocytes. Ion channels are macromolecular pores that span the lipid bilayer of the cell membrane (Fig. 33-11). Conformational transitions change (gate) a single ion channel from closed to open, which allows selected ions to flow passively down the electrochemical activity gradient at a very high rate (>106 ions per second). The high transfer rates and restriction to "downhill" fluxes not stoichiometrically coupled to the hydrolysis of energy-rich phosphates distinguish ionic channel mechanisms from those of other ion-transporting structures, such as sarcolemmal Na^+/K^+ -adenosine triphosphatase (ATPase) or sarcoplasmic reticular $\text{Mg}^{2+}/\text{Ca}^{2+}$ -ATPase (SERCA). Ion channels may be gated by extracellular and intracellular ligands, changes in transmembrane voltage, or mechanical stress (see Table 33-3). Gating of single ion channels can best be studied by means of the patch-clamp technique.

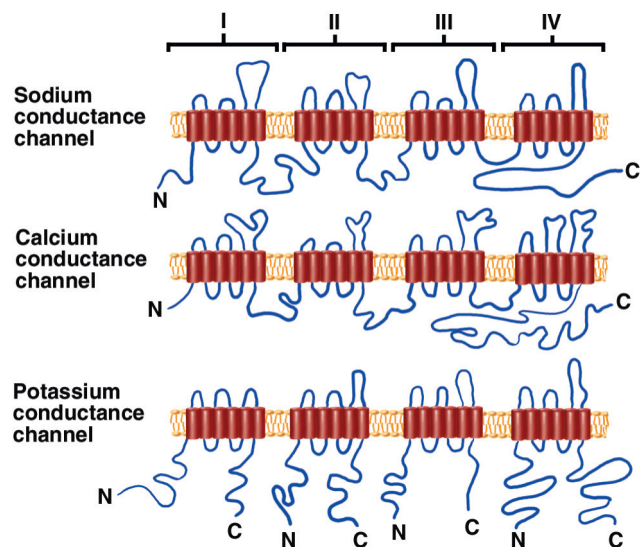


FIGURE 33-11 Structure of ion channels. Voltage-gated Na^+ and Ca^{2+} channels are composed of a single tetramer consisting of four covalently linked repeats of the six transmembrane-spanning motifs, whereas voltage-gated K^+ channels are composed of four separate subunits, each containing a single six transmembrane-spanning motif. Inwardly rectifying K^+ channels are formed by inward rectifier K^+ channel pore-forming (alpha) subunits. In contrast to voltage-gated K^+ channel alpha subunits, the Kir alpha subunits have only two (not six) transmembrane domains. (Modified from Katz AM: Molecular biology in cardiology, a paradigmatic shift. *J Mol Cell Cardiol* 20:355, 1988; and Shivkumar K, Weiss JN: Adenosine triphosphate-sensitive potassium channels. In Zipes DP, Jalife J [eds]: *Cardiac Electrophysiology: From Cell to Bedside*. Philadelphia, WB Saunders, 1999, pp 86-93.)

Ion channels are usually named after the strongest permeant ion— Na^+ , K^+ , Ca^{2+} , and Cl^- —but some channels are less selective or are not selective, as in gap junctional channels. Channels have also been named after neurotransmitters, as in acetylcholine-sensitive K^+ channels, I_{ACh} .

The ionic permeability ratio is a commonly used quantitative index of a channel's selectivity. It is defined as the ratio of the permeability of one ion type to that of the main permeant ion type. Permeability ratios of voltage-gated K^+ and Na^+ channels for monovalent and divalent (e.g., Ca^{2+}) cations are usually less than 1:10. Voltage-gated Ca^{2+} channels exhibit a more than 1000-fold discrimination against Na^+ and K^+ ions (e.g., $P_{\text{K}}/P_{\text{Ca}} = 1/3000$) and are impermeable to anions.

Because ions are charged, net ionic flux through an open channel is determined by both the concentration and electrical gradient across the membrane (electrodiffusion). The potential at which the passive flux of ions along the chemical driving force is exactly balanced by the electrical driving force is called the reversal or Nernst potential of the channel. In the case of a channel that is perfectly selective for one ion species, the reversal potential equals the thermodynamic equilibrium potential of that ion, E_s , which is given by the Nernst equation in the form

$$E_s = (RT/zF)\ln([S_o]/[S_i])$$

where $[S_i]$ and $[S_o]$ are the intracellular and extracellular concentrations of the permeant ion, respectively, z is the valence of the ion, R is the gas constant, F is the Faraday constant, T is the temperature (kelvin), and \ln is the logarithm to the base e. At membrane voltages more positive than the reversal potential of the channel, passive ion movement is outward, whereas it is inward at membrane potentials more negative than the Nernst potential of that channel. If the current through an open channel is carried by more than one permeant ion, the reversal potential becomes a weighted mean of all Nernst potentials.

Membrane voltages during a cardiac action potential are in the range of -94 to +30 mV (Table 33-1). With physiologic external K^+ (4 mM), E_K is approximately -91 mV, and passive movement of K^+ during an action potential is out of the cell. On the other hand, because the calculated reversal potential of a cardiac Ca^{2+} channel is +64 mV (assuming that $P_{\text{K}}/P_{\text{Ca}} = 1/3000$, $K_i = 150$ mM, $K_o = 4$ mM, $Ca_i = 100$ nM, and $Ca_o = 2$ mM), passive Ca^{2+} flux is into the cell. With physiologic internal and external chloride concentrations, E_{Cl} is -83 to -36 mV, and passive movement of Cl^- ions through open chloride channels can be both inward and outward at membrane potentials typically occurring during a cardiac action potential. In more general terms, the direction and magnitude of passive ion flux through a single open channel at any given transmembrane voltage are governed by the reversal potential of that ion and its concentration on the two sides of the membrane, with the net flux being larger when ions move from the more concentrated side.

Ion Flux Through Voltage-Gated Channels. Changes in transmembrane potential determine ion flux through voltage-gated channels, not only through the voltage dependence of the electrochemical driving force on the permeant ion but also through the voltage dependence of channel activation; that is, the fraction of time that a channel permits ions to permeate is determined by the membrane voltage. If the probability of a channel being activated (i.e., the open-state probability of that channel) exhibits voltage dependence, as is the case with the fast Na^+ channel or voltage-dependent K^+ channels in cardiac myocytes, activation increases with membrane depolarization. Note that channels do not have a sharp voltage threshold for opening. Rather, dependence of channel activation on membrane potential is a continuous function of voltage and follows a sigmoidal curve (Fig. 33-12, blue curve). The potential at which activation is half-maximal and the steepness of the activation curve determine the channel's activity during changes in membrane potential. Shifting the activation curve to potentials positive to the midpoint of activation and reducing the steepness of the channel's activation curve are two possible mechanisms by which ion channel blockers can inhibit ion channel activity.

As indicated in Figure 33-13, open channels enter a nonconducting conformation after a depolarizing change in membrane potential, a process termed *inactivation*. If membrane depolarization persists, the channel remains inactivated and cannot reopen. This steady-state inactivation increases with membrane depolarization in a sigmoidal fashion (see Fig. 33-12, gold curve). Inactivation curves of the various voltage-gated ion channel types in the heart differ in their slopes and

TABLE 33-1 Intracellular and Extracellular Ion Concentrations in Cardiac Muscle

ION	EXTRACELLULAR CONCENTRATION	INTRACELLULAR CONCENTRATION	RATIO OF EXTRACELLULAR TO INTRACELLULAR CONCENTRATION	E_1 (mV)
Na ⁺	145 mM	15 mM	9.7	+60
K ⁺	4 mM	150 mM	0.027	-94
Cl ⁻	120 mM	5-30 mM	4-24	-83 to -36
Ca ²⁺	2 mM	10^{-7} M	2×10^4	+129

Although intracellular Ca²⁺ content is about 2 mM, most of this Ca²⁺ is bound or sequestered in intracellular organelles (mitochondria and sarcoplasmic reticulum).

E_1 = equilibrium potential for a particular ion at 37°C.

Modified from Sperelakis N: Origin of the cardiac resting potential. In Berne RM, Sperelakis N, Geiger SR (eds): *Handbook of Physiology: The Cardiovascular System*. Bethesda, Md, American Physiological Society, 1979, p 193.

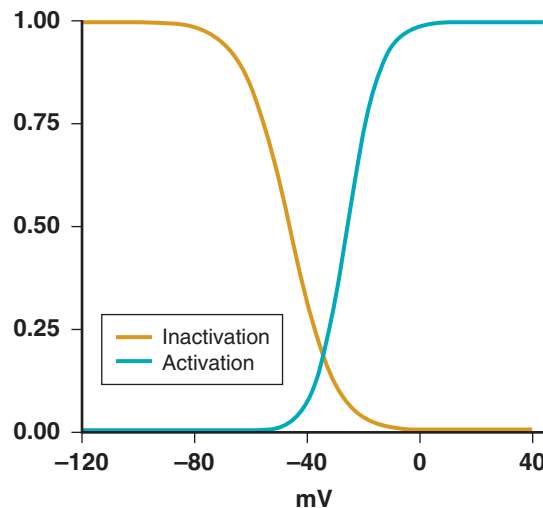


FIGURE 33-12 Voltage dependence of fast Na⁺ current steady-state activation (blue) and steady-state inactivation (gold). Fractional activation and inactivation (y axis) are plotted as a function of membrane potential. The inactivation and activation curves overlap within a voltage range from approximately -60 to approximately 0 mV, which demarcates the voltage range of the noninactivating Na⁺ window current.

midpoints of inactivation. For example, sustained cardiomyocyte membrane depolarization to -50 mV (as may occur in acutely ischemic myocardium) causes almost complete inactivation of the fast voltage-gated Na⁺ channel (see Fig. 33-12, gold curve), whereas the L-type Ca²⁺ channel exhibits only little inactivation at this membrane potential. Activation and inactivation curves can overlap, in which case a steady-state or noninactivating current flows. The existence of such a "window" current has been verified for both the voltage-gated Na⁺ current³² and the L-type Ca²⁺ current. The L-type Ca²⁺ current and the fast Na⁺ window current have been implicated in the genesis of triggered activity arising from early afterdepolarization (EAD) and delayed afterdepolarization (DAD).³³

Channels recover from inactivation and then enter the closed state, from which they can be reactivated (see Fig. 33-13). Rates of recovery from inactivation vary among the different types of voltage-dependent channels and usually follow monoexponential or multiexponential time courses, with the longest time constants ranging from a few milliseconds, for example, as for the fast sodium channel, to several seconds, as for some subtypes of K⁺ channels (see Table 33-3). Together, the activity of voltage-dependent ion channels in cardiomyocytes over the course of an action potential is tightly regulated by the orchestrated interplay of a number of time- and voltage-dependent gating mechanisms, including activation, inactivation, and recovery from inactivation. All these mechanisms represent potential targets for pharmacologic intervention.

Principles of Ionic Current Modulation. The whole-cell current amplitude I is the product of the number of functional channels in the membrane available for opening (N), the probability that a channel will open (P_o), and the single-channel current amplitude (i), or $I = N \cdot P_o \cdot i$. Modulation of current amplitudes in single cardiomyocytes therefore results from alterations in N, P_o , i, or any combination of these factors. Changes in the number of available channels in the cell

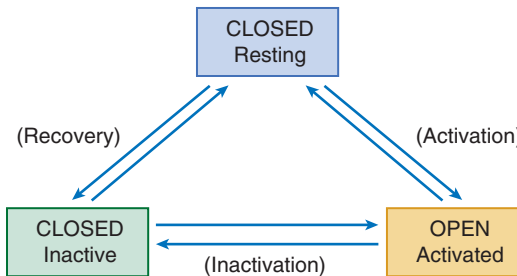


FIGURE 33-13 Simplest scheme for gating of voltage-gated ion channels.

membrane may result from alterations in the expression of ion channel-encoding genes. The magnitude of the single-channel current amplitude is dependent, among other factors, on the ionic concentration gradient across the membrane. For example, an increase in the extracellular Ca²⁺ concentration increases current through a single Ca²⁺ channel. Changes in channel activation can result from phosphorylation or dephosphorylation of the channel protein by second messenger-mediated activation of protein kinases and protein phosphatases, respectively. Channel phosphorylation or dephosphorylation causes a shift in the membrane potential dependence of a channel's activation or availability curve, or both, or modification of the sensitivity of channel activation or inactivation to changes in membrane potential. For example, Ca²⁺/calmodulin kinase II-mediated phosphorylation shifts the activation curve of the cardiac sodium current to more negative potentials.³⁴

Molecular Structure of Ion Channels. Electrophysiologic studies have detailed the functional properties of Na⁺, Ca²⁺, and K⁺ currents in cardiomyocytes, and molecular cloning has revealed a large number of pore-forming (alpha) and auxiliary (beta, delta, and gamma) subunits thought to contribute to formation of the cell surface ion channels. These studies have demonstrated that distinct molecular entities give rise to the various cardiac ion channels and shape the myocardial action potential. It has also been demonstrated that mutations in the genes encoding subunits underlying functional cardiac ion channels are responsible for several inherited cardiac arrhythmias (see Chapter 32).³⁵ The expression and functional properties of myocardial ion channels also change in a number of acquired disease states, and these alterations can predispose to cardiac arrhythmias.^{36,37}

A more detailed description of the molecular composition of sodium, calcium, potassium, and pacemaker channels is provided online at ExpertConsult.

Intercalated Discs

Another family of ion channel proteins is that containing the gap junctional channels. These dodecameric channels are found in the intercalated discs between adjacent cells. Three types of specialized junctions make up each intercalated disc. The macula adherens or desmosome and the fascia adherens form areas of strong adhesion between cells and may provide a linkage for the transfer of mechanical energy from one cell to the next. The nexus, also called the tight or gap junction, is a region in the intercalated disc where cells are in functional contact with each other. Membranes at these junctions are separated by only about 10 to 20 Å and are connected by a series of hexagonally packed subunit bridges. Gap junctions provide biochemical and low-resistance electrical coupling between adjacent cells by

establishing aqueous pores that directly link the cytoplasm of these adjacent cells. Gap junctions allow the movement of ions (e.g., Na^+ , Cl^- , K^+ , Ca^{2+}) and small molecules (e.g., cAMP, cyclic guanosine monophosphate [cGMP], inositol 1,4,5-triphosphate [IP_3]) between cells, thereby linking the interiors of adjacent cells.

Gap junctions permit a multicellular structure such as the heart to function electrically like an orderly, synchronized, interconnected unit and are probably responsible in part for the fact that conduction in the myocardium is anisotropic; that is, its anatomic and biophysical properties vary according to the direction in which they are measured. Usually, conduction velocity is two to three times faster longitudinally, in the direction of the long axis of the fiber, than it is transversely, in the direction perpendicular to this long axis.³⁸ Resistivity is lower longitudinally than transversely. Interestingly, the safety factor for propagation is greater transversely than horizontally. The safety factor for conduction determines the success of action potential propagation and has been defined as the ratio of electrical charge that is generated to charge that is consumed during the excitation cycle of a single myocyte in tissue.³⁸ Conduction delay or block occurs more commonly in the longitudinal direction than it does transversely. Cardiac conduction is discontinuous because of resistive discontinuities created by the gap junctions, which have an anisotropic distribution on the cell surface.³⁸ Because of anisotropy, propagation is discontinuous and can be a cause of reentry.

Gap junctions also provide "biochemical coupling," which permits cell-to-cell movement of ATP (or other high-energy phosphates), cyclic nucleotides, and IP_3 , the activator of the IP_3 -sensitive SR Ca^{2+} release channel,³⁹ thus demonstrating that diffusion of second-messenger substances through gap junctional channels constitutes a mechanism enabling coordinated responses of the myocardial syncytium to physiologic stimuli.

Gap junctions can also change their electrical resistance. When the intracellular calcium level rises, as in myocardial infarction, the gap junction may close to help seal off the effects of injured from noninjured cells. Acidosis increases and alkalosis decreases gap junctional resistance. Increased gap junctional resistance tends to slow the rate of action potential propagation, a condition that could lead to conduction delay or block. Cardiac-restricted inactivation of gap junctions decreases transverse conduction velocity to a greater degree than longitudinal conduction, thereby resulting in an increased anisotropic ratio, which may play a role in premature sudden death from ventricular arrhythmias.⁴⁰

Connexins are the proteins that form the intercellular channels of gap junctions. An individual channel is created by two hemichannels (connexons), each located in the plasma membrane of adjacent cells and composed of six integral membrane protein subunits (connexins). The hemichannels surround an aqueous pore and thereby create a transmembrane channel (Fig. 33-14). Connexin 43, a 43-kDa polypeptide, is the most abundant cardiac connexin, with connexins 40 and 45 being found in smaller amounts. Ventricular muscle expresses connexins 43 and 45, whereas atrial muscle and components of the specialized conduction system express connexins 43, 45, and 40. Expression of connexin 30.2 appears to be confined to the cardiac conduction system.⁴¹ Individual cardiac connexins form gap junctional channels with characteristic unitary conductances, voltage sensitivities, and permeabilities. Tissue-specific connexin expression and the spatial distribution of gap junctions determine the disparate conduction properties of cardiac tissue (see Fig. 33-7). The functional diversity of cardiac gap junctions is further enhanced by the ability of different connexin isoforms to form hybrid gap junctional channels with unique electrophysiologic properties. These channel chimeras appear to have a major function in controlling impulse transmission at the sinoatrial node–atrium border, the atrium–AV node transitional zone, and the Purkinje-myocyte border.⁵

Alterations in the distribution and function of cardiac gap junctions are associated with increased susceptibility to arrhythmias. Conduction slowing and arrhythmogenesis have been associated with redistribution of connexin 43 gap junctions from the end of cardiomyocytes to the lateral borders and with decreased phosphorylation of connexin 43 in a dog model of nonischemic dilated cardiomyopathy.^{42,43} Adult mice genetically engineered to express progressively decreasing levels of cardiac connexin 43 exhibited increased susceptibility to the induction of fatal tachyarrhythmias.^{44,45} Side-to-side electrical coupling between cardiomyocytes from the epicardial border zone of healing infarcts has been shown to be reduced, thereby exaggerating anisotropy and facilitating reentrant activity.⁴⁶ Finally, a rare single nucleotide polymorphism in the atrial-specific connexin 40 gene has been found to increase the risk for idiopathic AF.⁴⁷ Studies have suggested

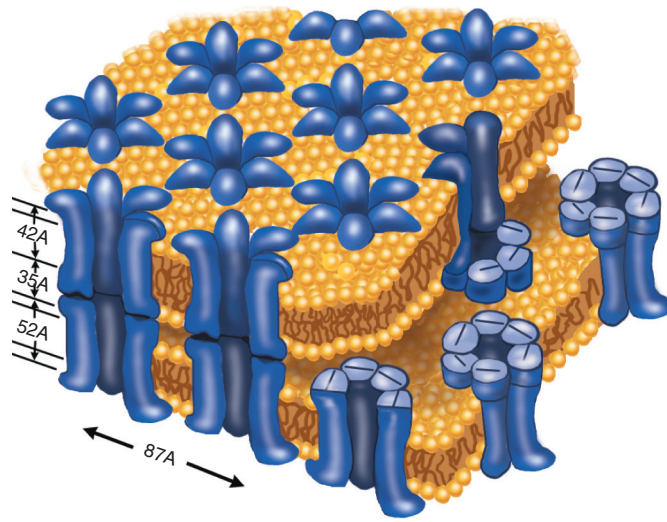


FIGURE 33-14 Model of the structure of a gap junction based on the results of x-ray diffraction studies. Individual channels are composed of paired hexamers that travel in the membranes of adjacent cells and adjoin in the extracellular gap to form an aqueous pore that provides continuity of the cytoplasm of the two cells. A = angstroms. (From Saffitz JE: Cell-to-cell communication in the heart. *Cardiol Rev* 3:86, 1995.)

that normal electrical coupling of cardiomyocytes via gap junctions depends on normal mechanical coupling via cell-cell adhesion junctions.⁴⁸ A defect in cell-cell adhesion or a discontinuity in the linkage between intercellular junctions and the cytoskeleton prevents normal localization of connexins in gap junctions, which in turn could contribute to sudden death from tachyarrhythmias. For example, Carvajal syndrome is caused by a recessive mutation in desmoplakin, a protein that links desmosomal adhesion molecules to desmin, a filament protein of the cardiomyocyte cytoskeleton.⁴⁹ Naxos disease is caused by a recessive mutation in plakoglobin, a protein that connects N-cadherins to actin and desmosomal cadherins to desmin.⁵⁰ Approximately 70% of the mutations linked to familial arrhythmogenic right ventricular cardiomyopathy are in the gene encoding the desmosomal protein plakophilin 2. Recent experiments have demonstrated that loss of plakophilin 2 expression leads to redistribution of connexin 43 to the intracellular space of cardiomyocytes, loss of gap junction plaques, and reduced functional coupling between cells.⁵¹ Further demonstration of the important role of other adhesion proteins in stabilizing gap junctions comes from a study wherein conditional loss of N-cadherin expression in mouse hearts resulted in a decrease in connexin 43 gap junctions and changes in conduction velocity with a concomitant increase in arrhythmogenicity (Fig. e33-3).⁴⁰

Phases of the Cardiac Action Potential

The cardiac transmembrane action potential consists of five phases: phase 0, upstroke or rapid depolarization; phase 1, early rapid repolarization; phase 2, plateau; phase 3, final rapid repolarization; and phase 4, resting membrane potential and diastolic depolarization (Figs. 33-15 and 33-16). These phases are the result of passive ion fluxes moving down the electrochemical gradients established by active ion pumps and exchange mechanisms. Each ion moves primarily through its own ion-specific channel. The following discussion explains the electrogenesis of each of these phases.

General Considerations. Ionic fluxes regulate membrane potential in cardiac myocytes in the following fashion. When only one type of ion channel opens, assuming that this channel is perfectly selective for that ion, the membrane potential of the entire cell would equal the Nernst potential of that ion. By solving the Nernst equation for the four major ions across the plasma membrane, the following equilibrium potentials are obtained: sodium, +60 mV; potassium, -94 mV; calcium, +129 mV; and chloride, -83 to -36 mV (see Table 33-1). Therefore, if a single K^+ -selective channel opens, such as the inwardly rectifying K^+ channel, the membrane potential approaches E_K (-94 mV). If a single Na^+ -selective channel opens, the transmembrane potential becomes E_{Na} (+60 mV). A quiescent cardiac myocyte (phase 4) has many more open potassium than sodium channels, and the

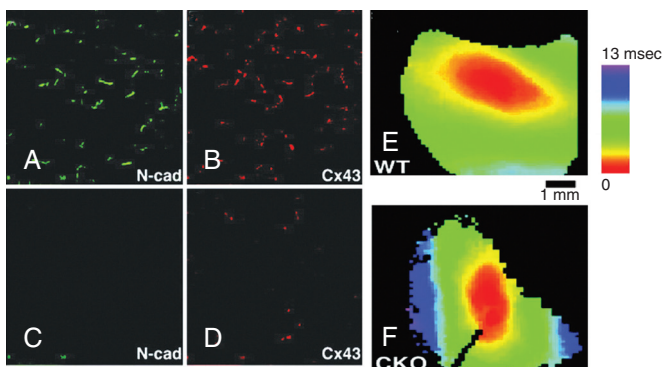


FIGURE e33-3 Cardiac restricted loss of N-cadherin leads to alteration in connexin 43 (Cx43) with conduction slowing. **A-D**, Anti-N-cadherin (**A**, **C**) and anti-Cx43 (**B**, **D**) immunoreactivity in a control mouse heart (**A**, **B**) and in a genetically manipulated mouse heart with knocked-out N-cadherin expression (**C**, **D**). N-cadherin was lost from intercalated disc in the knocked-out heart, whereas Cx43 was significantly decreased. **E, F**, Optical mapping of electrical activation in the left ventricular epicardium of a control (**E**) and N-cadherin knocked-out heart (**F**) with a voltage-sensitive fluorescent dye. The heart was paced at the lateral wall and activation maps were generated. Color-coded isochrone maps show that conduction was more impaired in the longitudinal than in the lateral direction, thereby increasing conduction anisotropy. (From Li J, Patel VV, Kostetskii I, et al: Cardiac-specific loss of N-cadherin leads to alteration in connexins with conduction slowing and arrhythmogenesis. *Circ Res* 97:474, 2005. With permission from the American Heart Association.)

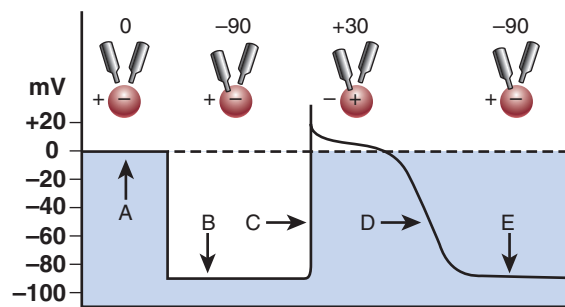


FIGURE 33-15 Demonstration of action potentials recorded during impalement of a cardiac cell. **Upper row:** Shown are a cell (circle), two microelectrodes, and stages during impalement of the cell and its activation and recovery. Both microelectrodes are extracellular (A), and no difference in potential exists between them (0 potential). The environment inside the cell is negative and the outside is positive because the cell is polarized. One microelectrode has pierced the cell membrane (B) to record the intracellular resting membrane potential, which is -90 mV with respect to the outside of the cell. The cell has depolarized (C), and the upstroke of the action potential is recorded. At its peak voltage, the inside of the cell is approximately $+30\text{ mV}$ with respect to the outside of the cell. The repolarization phase (D) is shown, with the membrane returning to its former resting potential (E). (From Cranefield PF: *The Conduction of the Cardiac Impulse*. Mount Kisco, NY, Futura, 1975.)

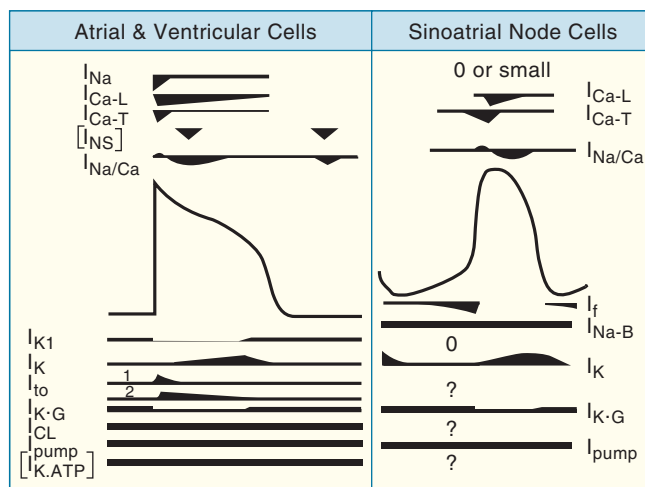


FIGURE 33-16 Currents and channels involved in generating resting and action potentials. The time course of a stylized action potential of atrial and ventricular cells is shown on the left, and that of sinoatrial node cells is on the right. Above and below are the various channels and pumps that contribute the currents underlying the electrical events. See Table 33-3 for identification of the symbols and description of the channels or currents. Where possible, the approximate time courses of the currents associated with the channels or pumps are shown symbolically without trying to represent their magnitudes relative to each other. I_K incorporates at least two currents, I_{K1} and I_{Ks} . There appears to be an ultrarapid component as well, designated I_{Kur} . The heavy bars for I_{CL} , I_{pump} , and $I_{K,ATP}$ indicate only the presence of these channels or pump without implying magnitude of currents because the magnitude would vary with physiologic and pathophysiologic conditions. The channels identified by brackets (I_{NS} and $I_{K,ATP}$) are active only under pathologic conditions. I_{NS} may represent a swelling-activated cation current. For the sinoatrial node cells, I_{NS} and I_{K1} are small or absent. Question marks indicate that experimental evidence is not yet available to determine the presence of these channels in sinoatrial cell membranes. Although it is likely that other ionic current mechanisms exist, they are not shown here because their roles in electogenesis are not sufficiently well defined. (From Members of the Sicilian Gambit: *Antiarrhythmic Therapy: A Pathophysiologic Approach*. Mount Kisco, NY, Futura, 1994, p 13.)

cell's transmembrane potential is close to E_K (Table 33-2). When two or more types of ion channels open simultaneously, each type tries to make the membrane potential go to the equilibrium potential of that channel. The contribution of each ion type to the overall membrane potential at any given moment is determined by the instantaneous permeability of the plasma membrane to that ion. For example, deviation of the measured resting membrane potential from E_K (see Table 33-1) would predict that other ion types with equilibrium potentials positive to E_K are contributing to the resting membrane potential in cardiac myocytes. If it is assumed that Na^+ , K^+ , and Cl^- are the

permeant ions at resting potential, their individual contributions to the resting membrane potential V can be quantified by the Goldman–Hodgkin–Katz voltage equation in the form

$$V = (RT/F)\ln[(P_K[\text{Na}]_o + P_C[\text{Cl}])/P_K[K] + P_{\text{Na}}[\text{Na}]P_C[\text{Cl}]]$$

where the symbols have the meanings outlined previously. With only one permeant ion, V becomes the Nernst potential for that ion. With several permeant ion types, V is a weighted mean of all the Nernst potentials.

Intracellular electrical activity can be recorded by inserting a glass microelectrode filled with an electrolyte solution and with a tip diameter smaller than $0.5\text{ }\mu\text{m}$ into a single cell. The electrode produces minimal damage, its entry point apparently being sealed by the cell. The transmembrane potential is recorded by using this electrode in reference to an extracellular ground electrode placed in the tissue bath near the cell membrane and represents the potential difference between intracellular and extracellular voltage (see Fig. 33-15). Alternatively, the patch-clamp technique in current clamp mode can be used to measure transmembrane potentials.

Phase 4: Resting Membrane Potential. The intracellular potential during electrical quiescence in diastole is -50 to -95 mV , depending on the type of cell (see Table 33-2). Therefore the inside of the cell is 50 to 95 mV negative relative to the outside of the cell because of the distribution of ions such as K^+ , Na^+ , and Cl^- .

Because cardiac myocytes have an abundance of open K^+ channels at rest, the cardiac transmembrane potential (in phase 4) is close to E_K . Potassium outward current through open, inwardly rectifying K^+ channels (I_{K}) under normal conditions contributes to the resting membrane potential mainly in atrial and ventricular myocytes, as well as in Purkinje cells. Deviation of the resting membrane potential from E_K is the result of movement of monovalent ions with an equilibrium potential greater than the E_K , for example, Cl^- efflux through activated chloride channels, such as $I_{\text{Cl},\text{cAMP}}$, $I_{\text{Cl},\text{Ca}}$, and $I_{\text{Cl},\text{swell}}$. Calcium does not contribute directly to the resting membrane potential, but changes in intracellular free calcium concentration can affect other membrane conductance values. For example, an increase in sarcoplasmic reticulum (SR) Ca^{2+} load can cause spontaneous intracellular Ca^{2+} waves, which in turn activate the Ca^{2+} -dependent chloride conductance $I_{\text{Cl},\text{Ca}}$ and thereby lead to spontaneous transient inward currents and concomitant membrane depolarization.⁵² Increases in $[\text{Ca}^{2+}]_i$ can also stimulate the $\text{Na}^+/\text{Ca}^{2+}$ exchanger $I_{\text{Na}/\text{Ca}}$. This protein exchanges three Na^+ ions for one Ca^{2+} ion; the direction is dependent on the sodium and calcium concentrations on the two sides of the membrane and the transmembrane potential difference. At resting membrane potential and during a spontaneous SR Ca^{2+} release event, this exchanger would generate a net Na^+ influx, possibly causing transient membrane depolarizations (see Fig. 33-20).⁵³ $[\text{Ca}^{2+}]_i$ has also been shown to activate I_{K} in cardiac myocytes, thereby indirectly contributing to cardiac resting membrane potential. Because of the Na-K pump, which pumps Na^+ out of the cell against its electrochemical gradient and simultaneously pumps K^+ into the cell against its chemical gradient, the intracellular K^+ concentration remains high and the intracellular Na^+ concentration remains low. This pump, fueled by an Na^+,K^+ -ATPase enzyme that hydrolyzes ATP for energy, is bound to the membrane. It requires both Na^+ and K^+ to function and can transport three Na^+ ions outward for two K^+ ions inward. Therefore the pump can be electrogenic and generate a net outward movement of positive charges. The rate of Na^+,K^+ pumping to maintain the same ionic gradients must increase as the heart rate increases because the cell gains a slight amount of Na^+ and loses a slight amount of K^+ with each depolarization. Cardiac glycoside-induced block of Na^+,K^+ -ATPase increases contractility through an increase in intracellular Na^+ concentration, which in turn reduces Ca^{2+} extrusion through the $\text{Na}^+/\text{Ca}^{2+}$ exchanger (see later) and ultimately increases myocyte contractility.⁵³

Phase 0: Upstroke or Rapid Depolarization. A stimulus delivered to excitable tissue evokes an action potential characterized by a sudden change in voltage caused by transient depolarization followed by repolarization. The action potential is conducted throughout the heart and is responsible for initiating each heartbeat. Electrical changes in action potential follow a relatively fixed time and voltage relationship that differs according to specific cell types (Fig. 33-17). In nerve, the entire process takes several milliseconds, whereas action potentials in human cardiac fibers last several hundred milliseconds. Normally, the action potential is independent of the size of the depolarizing stimulus if the latter exceeds a certain threshold potential. Small subthreshold depolarizing stimuli depolarize the membrane in

**TABLE 33-2** Properties of Transmembrane Potentials in Mammalian Hearts

PROPERTY	SINUS NODAL CELL	ATRIAL MUSCLE CELL	AV NODAL CELL	PURKINJE FIBER	VENTRICULAR MUSCLE CELL
Resting potential (mV)	-50 to -60	-80 to -90	-60 to -70	-90 to -95	-80 to -90
Action potential					
Amplitude (mV)	60-70	110-120	70-80	120	110-120
Overshoot (mV)	0-10	30	5-15	30	30
Duration (msec)	100-300	100-300	100-300	300-500	200-300
\dot{V}_{max} (V/sec)	1-10	100-200	5-15	500-700	100-200
Propagation velocity (m/sec)	<0.05	0.3-0.4	0.1	2-3	0.3-0.4
Fiber diameter (μm)	5-10	10-15	1-10	100	10-16

\dot{V}_{max} = maximal rise of membrane potential.

Modified from Sperelakis N: Origin of the cardiac resting potential. In Berne RM, Sperelakis N, Geiger SR (eds): *Handbook of Physiology: The Cardiovascular System*. Bethesda, Md, American Physiological Society, 1979, p 190.

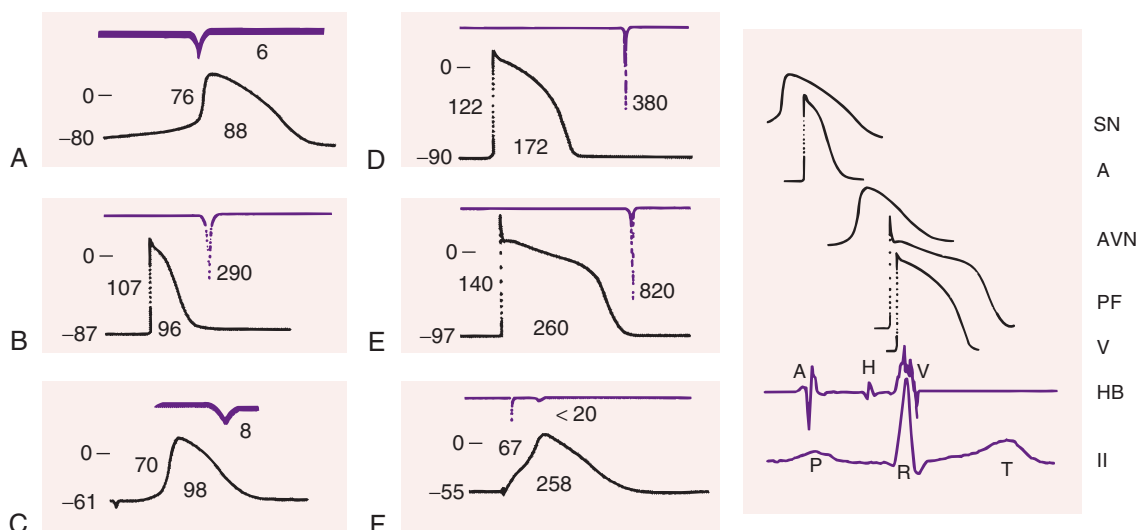


FIGURE 33-17 Action potentials recorded from different tissues in the heart (left) remounted along with a His bundle recording and scalar electrocardiogram from a patient (right) to illustrate the timing during a single cardiac cycle. In panels A to F, the top tracing is dV/dt of phase 0 and the second tracing is the action potential. For each panel, the numbers (from left to right) indicate maximum diastolic potential (mV), action potential amplitude (mV), action potential duration at 90% of repolarization (milliseconds), and \dot{V}_{max} of phase 0 (V/sec). Zero potential is indicated by the short horizontal line next to the zero on the upper left of each action potential. **A**, Rabbit sinoatrial node. **B**, Canine atrial muscle. **C**, Rabbit AV node. **D**, Canine ventricular muscle. **E**, Canine Purkinje fiber. **F**, Diseased human ventricle. Note that the action potentials recorded in **A**, **C**, and **F** have reduced resting membrane potentials, amplitudes, and \dot{V}_{max} relative to the other action potentials. A = atrial muscle potential; AVN = atrioventricular nodal potential; HB = His bundle recording; II = lead II; PF = Purkinje fiber potential; SN = sinus nodal potential; V = ventricular muscle potential. Horizontal calibration on the left: 50 milliseconds for **A** and **C**, 100 milliseconds for **B**, **D**, **E**, and **F**; 200 milliseconds on the right. Vertical calibration on the left: 50 mV; horizontal calibration on the right: 200 milliseconds. (Modified from Gilmour RF Jr, Zipes DP: Basic electrophysiology of the slow inward current. In Antman E, Stone PH [eds]: *Calcium Blocking Agents in the Treatment of Cardiovascular Disorders*. Mount Kisco, NY, Futura, 1983, pp 1-37.)

proportion to the strength of the stimulus. However, when the stimulus is sufficiently intense to reduce membrane potential to a threshold value in the range of -70 to -65 mV for normal Purkinje fibers, more intense stimuli do not produce larger action potential responses, and an "all-or-none" response results. In contrast, hyperpolarizing pulses, stimuli that render the membrane potential more negative, elicit a response proportional to the strength of the stimulus.

Mechanism of Phase 0. The upstroke of the cardiac action potential in atrial and ventricular muscle and His-Purkinje fibers is the result of a sudden increase in membrane conductance of Na^+ . An externally applied stimulus or a spontaneously generated local membrane circuit current in advance of a propagating action potential depolarizes a sufficiently large area of membrane at a sufficiently rapid rate to open the Na^+ channels and depolarize the membrane further. When the stimulus activates enough Na^+ channels, Na^+ ions enter the cell down their electrochemical gradient. The excited membrane no longer behaves like a K^+ electrode, that is, exclusively permeable to K^+ , but more closely approximates an Na^+ electrode, and the membrane moves toward the Na^+ equilibrium potential.

The rate at which depolarization occurs during phase 0, that is, the maximum rate of change in voltage over time, is indicated by the expression dV/dt_{max} or \dot{V}_{max} (see Table 33-2), which is a reasonable approximation of the rate and magnitude of Na^+ entry into the cell

and a determinant of conduction velocity for the propagated action potential. The transient increase in sodium conductance lasts 1 to 2 milliseconds. The action potential, or more properly the Na^+ current (I_{Na}), is said to be regenerative; that is, intracellular movement of a little Na^+ depolarizes the membrane more, which increases conductance of Na^+ more and allows more Na^+ to enter, and so on. As this process is occurring, however, $[\text{Na}^+]$, and positive intracellular charges increase and reduce the driving force for Na^+ . When the equilibrium potential for Na^+ (E_{Na}) is reached, Na^+ no longer enters the cell; that is, when the driving force acting on the ion to enter the cell balances the driving force acting on the ion to exit the cell, no current flows. In addition, Na^+ conductance is time dependent, so when the membrane spends some time at voltages less negative than the resting potential, Na^+ conductance decreases (inactivation; see earlier). Therefore an intervention that reduces membrane potential for a time (acute myocardial ischemia), but not to threshold, partially inactivates Na^+ channels, and if the threshold is now achieved, the magnitude and rate of Na^+ influx are reduced, which causes conduction velocity to slow.

In cardiac Purkinje fibers, sinoatrial cells, and to a lesser extent, ventricular muscle, two different populations of Na^+ channels exist: the tetrodotoxin (TTX)-sensitive, neuronal Na^+ channel isoform (Nav1.1) and the TTX-resistant Nav1.5 isoform, the latter being the



predominant isoform in cardiac muscle. Although the precise role of Nav1.1 channels in ventricular or atrial cardiomyocytes has not been defined, this channel is an important modulator of sinoatrial node pacemaking⁵⁴ and in determining Purkinje myocyte action potential duration.

Upstroke of the Action Potential. In normal atrial and ventricular muscle and in fibers in the His-Purkinje system, action potentials have very rapid upstrokes with a large V_{max} and are called fast responses. Action potentials in the normal sinoatrial and AV nodes and many types of diseased tissue have very slow upstrokes with a reduced V_{max} and are called slow responses (Table 33-3; see also Figs. 33-4, 33-7, and 33-17). Upstrokes of slow responses are mediated by a slow inward, predominantly L-type voltage-gated (Cav) Ca^{2+} current ($I_{\text{Ca,L}}$) rather than by the fast inward I_{Na} . These potentials have been termed *slow response potentials* because the time required for activation and inactivation of the slow inward current ($I_{\text{Ca,L}}$) is approximately an order of magnitude slower than that for the fast inward Na^+ current (I_{Na}). Recovery from inactivation also takes longer. Calcium entry and $[\text{Ca}^{2+}]_i$ help promote inactivation. The slow channel requires more time after a stimulus to be reactivated. In fact, recovery of excitability outlasts full restoration of maximum diastolic potential, which means that even though the membrane potential has returned to normal, the cell has not recovered excitability completely because the latter depends on the elapse of a certain amount of time (i.e., is time dependent) and not just on recovery of a particular membrane potential (i.e., voltage dependent), a phenomenon termed *postrepolarization refractoriness*.

The threshold for activation of $I_{\text{Ca,L}}$, that is, the voltage that the cell must reach to "turn on" the slow inward current, is about -30 to -40 mV. In fibers of the fast response type, $I_{\text{Ca,L}}$ is normally activated during phase 0 by the regenerative depolarization caused by the fast sodium current. Current flows through both fast and slow channels during the latter part of the action potential upstroke. However, $I_{\text{Ca,L}}$ is much smaller than the peak Na^+ current and therefore contributes little to the action potential until the fast Na^+ current is inactivated after completion of phase 0. Thus $I_{\text{Ca,L}}$ affects mainly the plateau of action potentials recorded in atrial and ventricular muscle and His-Purkinje fibers. In addition, $I_{\text{Ca,L}}$ may play a prominent role in partially depolarized cells in which the fast Na^+ channels have been inactivated if conditions are appropriate for slow-channel activation.

Ca^{2+} entry through activated L-type Cav channels triggers release of Ca^{2+} from SR stores and is an essential component of cardiac excitation-contraction coupling in atrial and ventricular myocardium (see Chapter 21). L-type Cav channels are also expressed in sinoatrial and AV nodal cells, where they play a role in controlling automaticity and action potential propagation, respectively. Cardiac L-type Cav channels undergo rapid voltage- and Ca^{2+} -dependent inactivation, the time course of which importantly affects the action potential waveform and the time course of repolarization. Although T-type Cav channels have not been detected in human myocardium, experimental evidence in animals has suggested that these channels play an important role in determining sinoatrial node automaticity and AV nodal conduction.³⁰ Whether Ca^{2+} influx through open T-type channels provides a sufficient trigger for release of Ca^{2+} from the SR is controversial. The density of T-type Ca^{2+} channels has been found to be increased in myocytes from hearts with experimentally induced hypertrophy, but the role of enhanced T-type channel density under these conditions remains to be determined.

Other significant differences exist between the fast and slow channels. Drugs that elevate cAMP levels, such as beta adrenoceptor agonists, phosphodiesterase inhibitors such as theophylline, and the lipid-soluble derivative of cAMP, dibutyryl cAMP, increase $I_{\text{Ca,L}}$. Binding of the beta adrenoceptor agonist to specific sarcolemmal receptors facilitates the dissociation of two subunits of a regulatory protein (G protein; see Chapter 21), one of which (G_s) activates adenylate cyclase and thus increases intracellular levels of cAMP. The latter binds to a regulatory subunit of a cAMP-dependent protein kinase that promotes phosphorylation of specific phosphorylation sites on the channel protein, which ultimately results in an enhanced open-state probability of the channel. Although Nav channels are sensitive to increases in cAMP, the net effect (decrease versus increase) appears to be species dependent.

Acetylcholine reduces $I_{\text{Ca,L}}$ by decreasing adenylate cyclase activity. However, acetylcholine stimulates the accumulation of cGMP. cGMP has negligible effects on basal $I_{\text{Ca,L}}$ but decreases the $I_{\text{Ca,L}}$ levels that have been elevated by beta adrenoceptor agonists. This effect is mediated by cAMP hydrolysis through a cGMP-stimulated cyclic nucleotide phosphodiesterase.

Differences Between Channels. Fast and slow channels can be differentiated on the basis of their pharmacologic sensitivity. Drugs that block the slow channel with a fair degree of specificity include verapamil, nifedipine, diltiazem, and D-600 (a methoxy derivative of verapamil). Antiarrhythmic agents such as lidocaine, quinidine, procainamide, and disopyramide (see Chapter 35) affect the fast channel and not the slow channel.

Normal action potentials recorded from the sinus node and the compact node of the AV junction have a reduced resting membrane potential, action potential amplitude, overshoot, upstroke, and conduction velocity when compared with action potentials in muscle or Purkinje fibers (see Figs. 33-7 and 33-17).

Slow-channel blockers suppress sinus and AV nodal action potentials. The prolonged time for reactivation of $I_{\text{Ca,L}}$ probably accounts for the fact that sinoatrial and AV nodal cells remain refractory longer than the time that it takes for full voltage repolarization to occur. Thus premature stimulation immediately after the membrane potential reaches full repolarization leads to action potentials with reduced amplitudes and upstroke velocities. Therefore slow conduction and prolonged refractoriness are characteristic features of nodal cells. These cells also have a reduced "safety factor for conduction" (see earlier), which means that the stimulating efficacy of the propagating impulse is low and conduction block occurs easily.

Inward Currents. Thus I_{Na} and $I_{\text{Ca,L}}$ represent two important inward currents. Another important inward current is I_f , also called the pacemaker or "funny" current.⁵⁵ This current is activated by hyperpolarization and is carried by Na^+ and K^+ . It generates phase 4 diastolic depolarization in the sinoatrial node. I_f modulation is one major mechanism whereby beta-adrenergic and cholinergic neurotransmitters regulate cardiac rhythm under physiologic conditions. Catecholamines increase the probability of channel opening by shifting the channel's activation curve to more positive potentials, which leads to increased current availability for the generation of diastolic depolarization and hence steepens its rate. Cholinergic action, in general, exerts the opposite effect.⁴⁶ Fish oil depresses I_f .⁵⁶ The electrophysiologic changes accompanying acute myocardial ischemia may represent a depressed form of a fast response in the center of the ischemic zone and a slow response in the border area. Probable slow-response activity has been shown in myocardium resected from patients undergoing surgery for recurrent ventricular tachyarrhythmias (see Fig. 33-17F). Whether and how slow responses play a role in the genesis of ventricular arrhythmias in these patients have not been established.

Phase 1: Early Rapid Repolarization. Following phase 0, the membrane repolarizes rapidly and transiently to almost 0 mV (early notch), partly because of inactivation of I_{Na} and concomitant activation of several outward currents.

I_{to} . The 4-aminopyridine-sensitive transient outward K^+ current, commonly termed I_{to} (or I_{to1}), is turned on rapidly by depolarization and then rapidly inactivates. Both the density and recovery of I_{to} from inactivation exhibit transmural gradients in the left ventricular free wall, with the density decreasing and reactivation becoming progressively prolonged from epicardium to endocardium.²⁹ Transmural differences in the expression of KCNIP2, the auxiliary subunit to Kv4.3 pore-forming alpha subunits, appears to be the primary determinant of the transmural gradient in I_{to} properties and densities in the human heart.⁵⁷ This gradient gives rise to regional differences in action potential shape, with increasingly slower phase 1 restitution kinetics and diminution of the notch along the transmural axis (Fig. e33-4).

These regional differences might create transmural voltage gradients, specifically at higher rates, thereby increasing dispersion of repolarization, a putative arrhythmogenic factor (Brugada syndrome; see Chapters 32 and 37). However, elimination of the physiologic repolarization gradient appears to be similarly arrhythmogenic.⁵⁷ Downregulation of I_{to} is at least partially responsible for slowing of phase 1 repolarization in failing human myocytes. Studies have demonstrated that these changes in the phase 1 notch of the cardiac action potential cause a reduction in the kinetics and peak amplitude of the action potential-evoked intracellular Ca^{2+} transient because of failed recruitment and synchronization of SR Ca^{2+} release through $I_{\text{Ca,L}}$ (Fig. e33-5). Thus modulation of I_{to} appears to play a significant physiologic role in controlling cardiac excitation-contraction coupling,⁵⁸ and it remains to be determined whether transmural differences in phase 1 repolarization translate into similar differences in regional contractility.

$I_{\text{Cl,Ca}}$. The 4-aminopyridine-resistant, Ca^{2+} -activated chloride current $I_{\text{Cl,Ca}}$ (or I_{to2}) also contributes a significant outward current during phase 1 repolarization.⁵⁹ This current is activated by the action potential-evoked intracellular Ca^{2+} transient. Therefore interventions that augment the amplitude of the Ca^{2+} transient associated with the twitch (such as beta-adrenergic receptor stimulation) also enhance



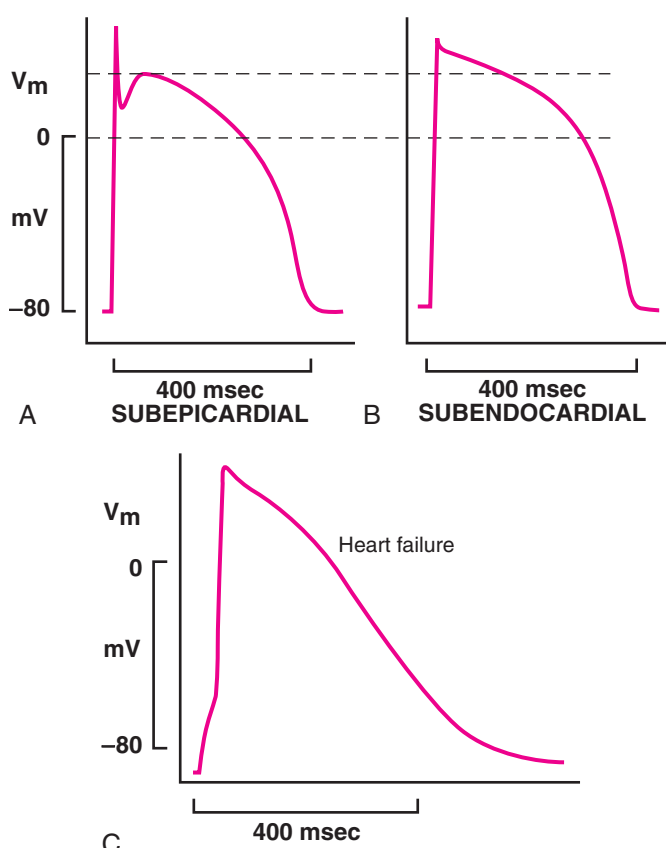


FIGURE e33-4 Action potential plots demonstrating differences in the action potential shape of human ventricular myocytes of subepicardial (**A**) and subendocardial (**B**) origin. Subepicardial myocytes present a prominent notch during phase 1 repolarization of the action potential, most likely caused by a larger I_{to} in these cells. The notch is absent in subendocardial cells. The peak plateau potential is higher in subendocardial than in subepicardial myocytes, and the action potential duration tends to be shorter in subepicardial cells. **C**, Transmembrane action potential in a human ventricular cardiomyocyte of a failing heart. Note loss of the prominent phase 1 notch and delayed repolarization. Recording temperature = 35°C; V_m = membrane potential. (**A, B**, From Nähauer M, Beuckelmann DJ, Überfuhr P, Steinbeck G: Regional differences in current density and rate-dependent properties of the transient outward current in subepicardial and subendocardial myocytes of human left ventricle. *Circulation* 93:168, 1996. By permission of the American Heart Association; **C**, from Priebe L, Beuckelmann DJ: Simulation studies of cellular electrical properties in heart failure. *Circ Res* 82:1206, 1998.)

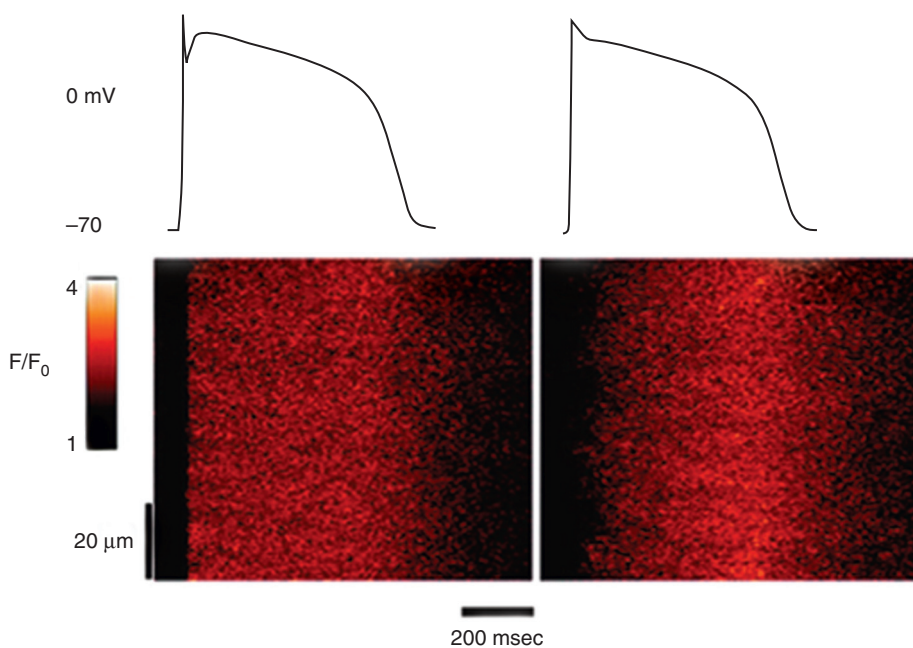


FIGURE e33-5 Diminution of phase 1 amplitude (“notch”) causes asynchronous SR Ca^{2+} release. Normal cardiomyocytes were voltage-clamped with action potential profiles having a normal or congestive heart failure wave shape, and local changes in intracellular calcium were recorded simultaneously. When the myocyte was clamped with a normal action potential profile having the early phase 1 repolarization notch (**left**), there was uniform Ca^{2+} release. However, when a congestive heart failure action potential profile without early rapid phase 1 repolarization was used, Ca^{2+} release was dysynchronous. This dysynchrony causes slowing in the rate of rise of the Ca^{2+} transient and loss of spatial and temporal release uniformity. F/F_0 = fluorescence of the Ca^{2+} indicator normalized to its baseline fluorescence. (From Harris DM, Mills GD, Chen X, et al: Alterations in early action potential repolarization causes localized failure of sarcoplasmic reticulum Ca^{2+} release. *Circ Res* 96:543, 2005. By permission of the American Heart Association.)

**TABLE 33-3** Synopsis of Transsarcolemmal Ionic Currents in Mammalian Cardiac Myocytes

CURRENT	SUBUNIT	FUNCTIONAL PROPERTIES
I_{Na}	Nav1.5, Nav1.1, Nav1.3, Nav1.6, Nav1.8 (alpha subunits)	TTX-resistant (Nav1.5, Nav1.8) and TTX-sensitive (Nav1.1, Nav1.3, Nav1.6) voltage-gated currents; Nav1.5 is the major cardiac isoform; neuronal Na^+ channel isoforms contribute to sinoatrial node pacemaking and ventricular repolarization
$I_{Ca,L}$	Cav1.2 (alpha subunit)	L-type (long lasting, large conductance) Ca^{2+} currents through voltage-gated Ca^{2+} (Cav) channels blocked by dihydropyridine-type antagonists (e.g., nifedipine), phenylalkylamines (e.g., verapamil), benzothiazepines (e.g., diltiazem), and various divalent ions (e.g., Cd^{2+}); activated by dihydropyridine-type agonists (e.g., Bay K 8644); responsible for phase 0 depolarization and propagation in sinoatrial and AV nodal tissue and contributing to the plateau of atrial, His-Purkinje, and ventricular cells; main trigger of Ca^{2+} release from the SR (Ca^{2+} -induced Ca^{2+} release); the noninactivating or "window" component underlies EADs
$I_{Ca,T}$	Cav3.1/alpha _G (alpha subunit)	T-type (transient current, tiny conductance) Ca^{2+} currents through Cav channels blocked by mibepradil and efonidipine but insensitive to dihydropyridines; may contribute an inward current to the later phase of phase 4 depolarization in pacemaker cells and action potential propagation in AV nodal cells; role in triggering Ca^{2+} -induced Ca^{2+} release uncertain
I_f	HCN4 (alpha subunit)	Hyperpolarization-activated "funny" current carried by Na^+ and K^+ in sinoatrial and AV nodal cells and His-Purkinje cells; involved in generating phase 4 depolarization; increases the rate of impulse initiation in pacemaker cells
I_K	Kir2.1 (alpha subunit)	K^+ current through inwardly rectifying K^+ (Kir) channels, voltage-dependent block by Ba^{2+} at micromolar concentrations; responsible for maintaining resting membrane potential in atrial, His-Purkinje, and ventricular cells; channel activity is a function of both membrane potential and $[K^+]$; inward rectification appears to result from depolarization-induced internal block by Mg^{2+} and neutral or positively charged amino acid residues in the cytoplasmic channel pore
$I_{K,G}$ ($I_{K,ACh}$, $I_{K,Ade}$)	Kir3.1/Kir3.4 (alpha subunit)	Inwardly rectifying K^+ current activated by muscarinic (M_2) and purinergic (type 1) receptor stimulation via GTP regulatory (G) protein signal transduction; expressed in sinoatrial and AV nodal cells and atrial cells, where it causes hyperpolarization and action potential shortening; activation causes negative chronotropic and dromotropic effects
I_Ks	KvLQT1 (alpha subunit)/minK (beta subunit)	K^+ current carried by a voltage-gated K^+ (Kv) channel (delayed rectifier K^+ channel); plays a major role in determining phase 3 of the action potential
I_{Kr}	hERG (alpha subunit)/MiRP1 (beta subunit)	Rapidly activating component of delayed rectifier K^+ current; I_{Kr} specifically blocked by dofetilide and sotalol in a reverse use-dependent manner; inward rectification of I_{Kr} results from depolarization-induced fast inactivation; plays a major role in determining the action potential duration
I_{Kur}	Kv1.5 (alpha subunit)	K^+ current through a Kv channel with ultrarapid activation but ultraslow inactivation kinetics; expressed in atrial myocytes; determines the action potential duration
$I_{K,Ca}$	SK2 (alpha subunit)	K^+ current through small-conductance Ca^{2+} -activated channels; blocked by apamine and dequalinium chloride; expressed in human atrial and ventricular myocytes; determines the action potential duration; upregulated in failing cardiomyocytes
I_{to} (I_{to1} , I_A)	Kv4.3 (alpha subunit)/KChIP2 (beta subunit)	Transient outward K^+ current through voltage-gated (Kv) channels; exhibits fast activation and inactivation and recovery kinetics; blocked by 4-aminopyridine in a reverse use-dependent manner; contributes to the time course of phase 1 repolarization; transmural differences in I_{to} properties contribute to regional differences in early repolarization
$I_{Cl,Ca}$ (I_{to2})	?	4-Aminopyridine-resistant transient outward current carried by Cl^- ions; activated by an increase in intracellular calcium level; blocked by stilbene derivatives (SITS, DIDS); contributes to the time course of phase 1 repolarization; may underlie spontaneous transient inward currents under conditions of Ca^{2+} overload; molecular correlate uncertain
$I_{Cl,cAMP}$?	Time-independent chloride current regulated by the cAMP/adenylate cyclase pathway; slightly depolarizes resting membrane potential and significantly shortens the action potential duration; antagonizes action potential prolongation associated with beta-adrenergic stimulation of $I_{Ca,L}$
$I_{Cl,swell}$ or $I_{Cl,vol}$?	Outwardly rectifying, swelling-activated Cl^- current; inhibited by 9-anthracene carboxylic acid; activation causes resting membrane depolarization and action potential shortening
$I_{K,ATP}$	Kir6.2 (alpha subunit)/SUR	Time-independent K^+ current through Kir channels activated by a fall in intracellular ATP concentration; inhibited by sulfonylurea drugs, such as glibenclamide; activated by pinacidil, nicorandil, cromakalim; causes shortening of the action potential duration during myocardial ischemia or hypoxia
$I_{Cir,swell}$?	Inwardly rectifying, swelling-activated cation current; permeable to Na^+ and K^+ ($P_{Na}/P_K = 8$); inhibited by Gd^{3+} ; depolarizes resting membrane potential and prolongs terminal (phase 3) repolarization
$I_{Na/Ca}$	NCX1.1	Current carried by Na^+/Ca^{2+} exchanger; causes net Na^+ outward current and Ca^{2+} inward current (reverse mode) or net Na^+ inward and Ca^{2+} outward current (3 Na^+ for 1 Ca^{2+}); direction of Na^+ flux depends on membrane potential and intracellular and extracellular concentrations of Na^+ and Ca^{2+} ; Ca^{2+} influx mediated by $I_{Na/Ca}$ can trigger SR Ca^{2+} release; underlies I_t (transient inward current) under conditions of intracellular Ca^{2+} overload
$I_{Na/K}$	Alpha subunit/ beta subunit	Na^+ outward current generated by Na^+/K^+ -ATPase (stoichiometry: 3 Na^+ leave and 2 K^+ enter); inhibited by digitalis
I_{ti}	?	Transient inward current activated by Ca^{2+} waves; I_{ti} possibly reflects 3 Ca^{2+} -dependent components: I_{NCX} , $I_{Cl,Ca}$, and a TRPM4 (transient receptor potential cation channel, member 4 gene)-mediated current
Electroneutral Ion-Exchanging Proteins		
Ca^{2+} -ATPase		Extrudes cytosolic calcium
Na/H	Cardiac myocytes express isoform NHE1	Exchanges intracellular H^+ for extracellular Na^+ ; specifically inhibited by the benzoylguanidine derivatives HOE 694 and HOE 642; inhibition causes intracellular acidification
Cl^- - HCO_3^-		Exchanges intracellular HCO_3^- for external Cl^- ; inhibited by SITS
Na^+ - K^+ - $2Cl^-$		Cotransporter blocked by amiloride

DIDS = 4,4'-diisothiocyanostilbene-2,2'-disulfonic acid; SITS = 4-acetamido-4'-isothiocyanostilbene-2,2'-disulfonic acid.



outward $I_{Cl,Ca}$. It is not currently known whether human cardiac myocytes express Ca^{2+} -activated chloride channels. Other, time-independent chloride currents may also play a role in determining the time course of early repolarization, such as the cAMP- or swelling-activated chloride conductances $I_{Cl,cAMP}$ and $I_{Cl,swell}$.

Na/Ca Exchanger. A third current contributing to early repolarization is Na^+ outward movement through the Na^+/Ca^{2+} exchanger operating in reverse mode (see Fig. 33-16).⁶⁰ Overexpression of the exchanger in transgenic mice caused accentuation of the early notch in left ventricular myocytes.

Sometimes, a transient depolarization follows phase 1 repolarization. This notch is well defined and separated from phase 2 in Purkinje fibers and left ventricular epicardial and midmyocardial myocytes (see Fig. e33-4).

Phase 2: Plateau. During the plateau phase, which may last several hundred milliseconds, membrane conductance of all ions falls to rather low values. Thus less change in current is required near plateau levels than near resting potential levels to produce the same changes in transmembrane potential. The plateau is maintained by competition between the outward current carried by K^+ and Cl^- ions and the inward current carried by Ca^{2+} moving through open L-type Ca^{2+} channels and Na^+ being exchanged for internal Ca^{2+} by the Na^+/Ca^{2+} exchanger operating in forward mode. After depolarization, potassium conductance falls to plateau levels as a result of inward rectification despite the large electrochemical driving force on K^+ ions.

Rectification simply means that membrane conductance changes with voltage. Specifically, inward rectification means that K^+ channels are open at negative potentials but closed at less negative or positive voltages. Membrane depolarization-induced internal block by intracellular ionized magnesium is thought to underlie inward rectification of cardiac I_{K1} channels. Inward rectification can also be induced by neutral and positively charged amino acid residues in the cytoplasmic channel pore that is formed by four Kir2.1 subunits.⁶¹ The mechanism underlying rectification of the rapid component of the delayed rectifier K^+ current (I_{Kr}) in cardiac cells is the inactivation that channels rapidly undergo during depolarizing pulses. More I_{Kr} channels enter the inactivated state with stronger depolarizations, thereby causing inward rectification. This fast inactivation mechanism is sensitive to changes in extracellular K^+ in the physiologic range, with inactivation being more accentuated at low extracellular K^+ concentrations. Thus hypokalemia would decrease outward I_{Kr} , thereby prolonging the action potential duration.

Outward K^+ movement carried by the slow component of the delayed rectifier K^+ current (I_{Ks}) also contributes to plateau duration: (1) I_{Ks} density has been shown to be correlated with the action potential duration, and (2) isolated defects in the KvLQT1 subunit, which in combination with the I_{Ks} subunit (minK) reconstitutes the cardiac I_{Ks} current, are associated with abnormally prolonged ventricular repolarization (LQTS type 1; see Chapters 32 and 37). Although I_{Ks} activates slowly in comparison to the action potential duration, it is only slowly inactivated. Therefore increases in heart rate can cause this activation to accumulate during successive depolarizations, and cumulative activation can determine the contribution to repolarization of K^+ currents that are active during the plateau of the action potential. In conditions of reduced intracellular ATP concentration (e.g., hypoxia, ischemia), K^+ efflux through activated K_{ATP} channels is enhanced, thereby shortening the plateau phase of the action potential. Other ionic mechanisms that control plateau potential and duration include the kinetics of inactivation of the L-type Ca^{2+} current. Reduced efficiency of intracellular free Ca^{2+} in inducing Ca^{2+} -dependent inactivation, such as in myocytes from hypertrophic hearts, can result in delayed repolarization. Steady-state components of both I_{Na} and $I_{Ca,L}$ (window currents) also shape the plateau phase.³³ Na^+/K^+ -ATPase generates a net outward current by pumping out three Na^+ ions in exchange for two K^+ ions. Noninactivating chloride currents, such as $I_{Cl,swell}$ and $I_{Cl,cAMP}$, may produce significant outward currents during the plateau phase under certain conditions, thereby significantly shortening the action potential duration. A nonselective, swelling-induced cation current has been shown to cause prolongation of action potentials in myocytes from failing ventricles.

Phase 3: Final Rapid Repolarization. In this portion of the action potential, repolarization proceeds rapidly at least in part because of two currents: time-dependent inactivation of $I_{Ca,L}$, with a decrease in the intracellular movement of positive charges, and activation of repolarizing K^+ currents, including the slow and rapid components of the delayed rectifier K^+ currents I_{Ks} and I_{Kr} , and the inwardly rectifying K^+ currents I_{K1} and $I_{K,Ach}$, which all cause an increase in the movement of positive charges out of the cell. The net membrane current becomes

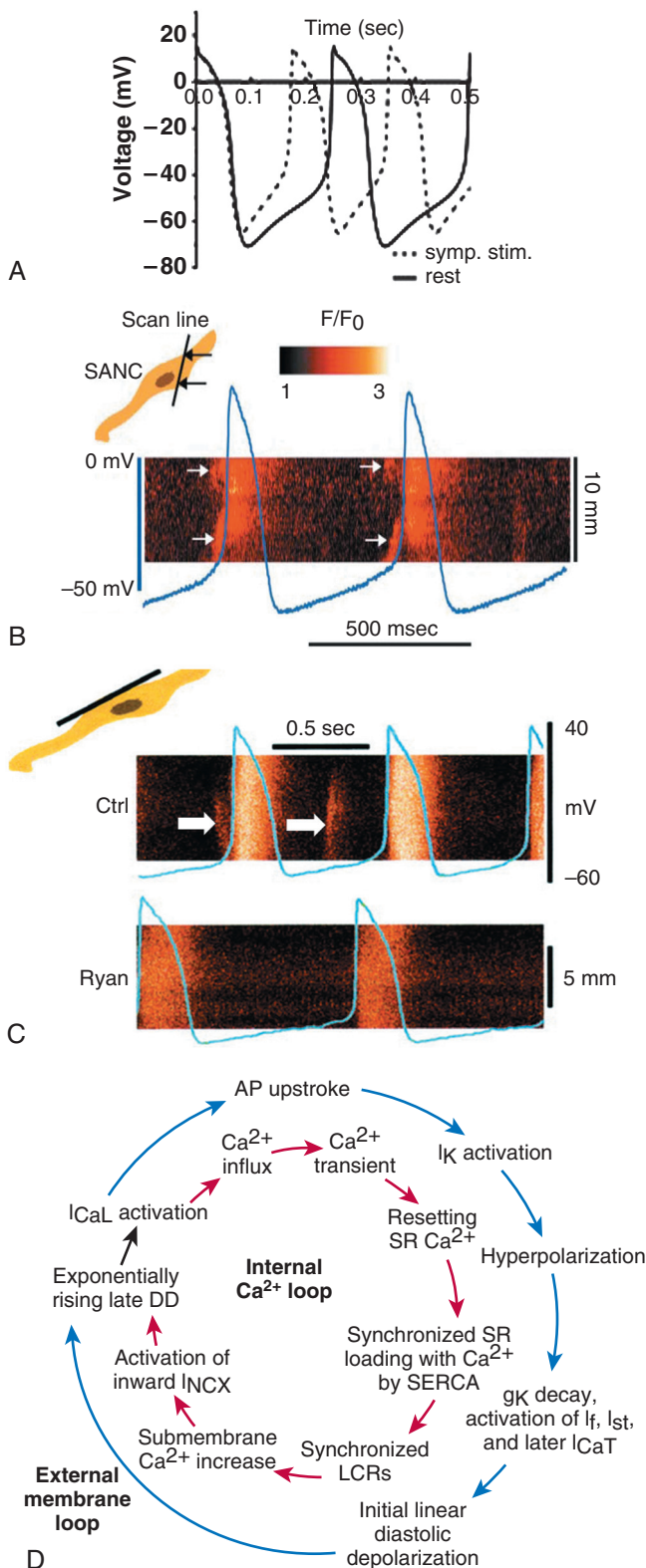
more outward, and the membrane potential shifts to the resting potential. A small-conductance Ca^{2+} -activated K^+ current, $I_{K,Ca}$, is expressed in human atrial myocytes, where it controls the time course of phase 3 repolarization.⁶² Loss-of-function mutations in the human ether-a-go-go-related gene (*HERG*), which is responsible for I_{Kr} , prolong phase 3 repolarization, thereby predisposing to the development of torsades de pointes. Macrolide antibiotics such as erythromycin, antihistamines such as terfenadine, and antifungal drugs such as ketoconazole inhibit I_{Kr} and have been implicated in the acquired form of LQTS (see Chapters 32 and 39). A decrease in I_{K1} activity, as is the case in left ventricular myocytes from failing hearts, causes prolongation of the action potential by slowing of phase 3 repolarization and resting membrane depolarization. A reduction in the outward potassium current through open inwardly rectifying K^+ channels renders the failing cardiomyocyte more susceptible to the induction of DADs triggered by spontaneous intracellular Ca^{2+} release events and therefore plays a major role in arrhythmogenesis in the failing heart (see Fig. 33-20).

Phase 4: Diastolic Depolarization. Under normal conditions the membrane potential of atrial and ventricular muscle cells remains steady throughout diastole. I_{K1} is the current responsible for maintaining the resting potential near the K^+ equilibrium potential in atrial, His-Purkinje, and ventricular cells. I_{K1} is the inward rectifier and shuts off during depolarization. In other fibers found in certain parts of the atria, in the muscle of the mitral and tricuspid valves, in His-Purkinje fibers, and in the sinoatrial node and portions of the AV nodal tract, the resting membrane potential does not remain constant in diastole but gradually depolarizes (see Figs. 33-4, 33-7, and 33-17A). The property possessed by spontaneously discharging cells is called phase 4 diastolic depolarization; when it leads to initiation of action potentials, automaticity results. The discharge rate of the sinoatrial node normally exceeds the discharge rate of other potentially automatic pacemaker sites and thus maintains dominance of the cardiac rhythm. The discharge rate of the sinoatrial node is usually more sensitive than the discharge rate of ventricular muscle cells to the effects of norepinephrine and acetylcholine. Normal or abnormal automaticity at other sites can cause discharge at rates faster than the sinoatrial nodal discharge rate and can thus usurp control of the cardiac rhythm for one cycle or many (see Chapter 34).

Normal Automaticity

Two models of sinoatrial node pacemaking have been proposed. In the first model, HCN channels are activated by hyperpolarizations in the normal range of diastolic membrane potentials. During the hyperpolarized diastolic membrane potential between consecutive action potentials, HCN channels will increase their probability of being open (see earlier). Open HCN channels conduct both Na^+ and K^+ , but at these negative membrane potentials they let mainly Na^+ into the cells. It is this inward Na^+ current through HCN channels (together with inflow of Ca^{2+} through voltage-activated Ca^{2+} channels, inward currents through Na^+/Ca^{2+} exchangers, and decaying outward K^+ currents; see Fig. 33-16) at diastolic membrane potentials that is thought to depolarize the pacemaker cells to threshold and thus trigger the next action potential and generate a periodically firing pacemaker (see Fig. 33-17A).⁶³

In the model proposed by proponents of Ca^{2+} oscillations operating as the primary pacemaking mechanism ("Ca²⁺ clock"), periodic increases in $[Ca^{2+}]_i$ serve as an internal generator ("calcium clock") of rhythmic signals that are transformed into changes in membrane voltage via modulation of calcium-sensitive ion channels and transporters in the outer membrane ("membrane clock").⁶⁴ This novel concept is illustrated in Figure 33-18, in which simultaneous $[Ca^{2+}]_i$ and action potential measurements in isolated sinoatrial myocytes are used as an example. Local submembrane increases in $[Ca^{2+}]_i$ (denoted by the white arrows in Fig. 33-18B, C) occurring during the later part of the spontaneous diastolic depolarization (transmembrane action potentials are shown in blue) precede the rapid upstroke of the action potential. These local submembrane increases in $[Ca^{2+}]_i$ are abolished by a specific blocker of the SR Ca^{2+} release channel, ryanodine (Ryan), concurrent with slowing of the beating frequency by this drug. The periodic SR Ca^{2+} release events rhythmically activate the Na^+/Ca^{2+} exchange inward (i.e., depolarizing) current (I_{NCX} ; Fig. 33-18D), which then results in an exponential increase in membrane potential that prompts activation of surface membrane L-type Ca^{2+} channels to initiate an action potential (see Fig. 33-18D). Thus the Na^+/Ca^{2+} exchanger operating in forward mode plays an essential role in converting the primary intracellular Ca^{2+} signals into membrane (i.e., voltage) signals. In this novel model of sinoatrial node pacemaking, spontaneous SR



Ca²⁺ release-induced membrane excitation initiates the sinoatrial node cell duty cycle, as schematically illustrated in Figure 33-18D. Once an action potential has been initiated, two highly interacting, concurrent series of events proceed during a normal sinoatrial node cell cycle (see Fig. 33-18D). In one event series (delimited to the outer membrane), depolarization-induced activation of the delayed rectifier K⁺ current I_K (see Table 33-3) leads to membrane hyperpolarization, which is followed by slow diastolic depolarization via activation of a number of inward currents, including I_f and I_{Ca,T} (see Table 33-3). In a

FIGURE 33-18 Sympathetic stimulation of heart rate in the sinoatrial node. **A**, Simulated sinoatrial node action potentials during baseline (solid line) and sympathetic stimulation (dashed line). Sympathetic stimulation increases the rate of diastolic depolarization and shifts the maximum diastolic potential to a less negative value, thereby accelerating action potential firing. **B-D**, Spontaneous SR Ca²⁺ release events trigger membrane excitation in sinoatrial node myocytes. **B**, **C**, Confocal line scan images of Ca²⁺ signals measured in spontaneously beating rabbit sinoatrial node cells with different orientation of the scanning line simultaneously with recording (blue lines) of transmembrane action potentials. **B**, Transversal orientation of the scan line (inset). Arrows in the confocal image show the local Ca²⁺ release in the submembrane space during late diastolic depolarization that precedes the rapid upstroke of the action potential. **C**, The scanned line was oriented parallel to the longitudinal axis of the cell near the cell's edge (inset). The specific blocker of the SR Ca²⁺ release channel, ryanodine (Ryan), slows the beating rate and is accompanied by abolition of local subsarcolemmal Ca²⁺ release during diastolic depolarization (arrows). **D**, Model of sinoatrial node cell pacemaking as suggested by Maltsev and coworkers. I_{NCX} = Na⁺/Ca²⁺ exchange current; DD = diastolic depolarization; LCR = local Ca²⁺ release. (**A**, From Larsson HP. How is the heart rate regulated in the sinoatrial node? Another piece to the puzzle. *J Gen Physiol* 136:237, 2010; **B-D**, from Maltsev VA, Vinogradova TM, Lakatta EG: The emergence of a general theory of the initiation and strength of the heartbeat. *J Pharmacol Sci* 100:338, 2006.)

second, parallel cycle of events, action potential-induced SR Ca²⁺ release is followed by Ca²⁺ reuptake into the SR, which subsequently gives rise to multifocal, synchronized spontaneous Ca²⁺ release events culminating in an increase in inward I_{NCX}. The role of late diastolic spontaneous SR Ca²⁺ release events in triggering the sinoatrial node action potential has recently been confirmed in canine hearts *in situ* (Fig. e33-6).⁶⁵

The rate of sinoatrial nodal discharge can be varied by several mechanisms in response to autonomic or other influences. The pacemaker locus can shift within or outside the sinoatrial node to cells discharging faster or more slowly.⁶³ If the pacemaker site remains the same, alterations in the slope of the diastolic depolarization, maximum diastolic potential, or threshold potential can speed or slow the discharge rate (Fig. 33-18A). For example, if the slope of diastolic depolarization steepens and if the resting membrane potential becomes less negative or the threshold potential more negative (within limits), the discharge rate increases. Opposite changes slow the discharge rate. The molecular mechanism that is primarily responsible for acceleration of the sinoatrial node discharge rate has been highly controversial. Proponents of the HCN pacemaker role consider an increase in inward HCN current via a shift of the HCN channel activation curve to more depolarized potentials the primary regulatory mechanism.^{3,65} In contrast, proponents of the Ca²⁺ clock model have suggested protein kinase A-mediated phosphorylation of Ca²⁺-handling proteins (ryanodine receptor, phospholamban [see Chapter 21], SERCA, voltage-gated Ca²⁺ channels) as the mechanism responsible for increased action potential firing: an increase in the level of cAMP (after beta-adrenergic receptor stimulation) augments the activity of protein kinase A, which then increases the rate of spontaneous SR Ca²⁺ release and SR Ca²⁺ reuptake via synergistic activation of these proteins, whereas a reduction in cAMP levels (after muscarinic receptor stimulation) has the opposite effect.¹ Acetylcholine activates K⁺ efflux through acetylcholine-sensitive inward rectifier K⁺ channels, which are expressed in both sinoatrial nodal and AV nodal cells, thereby shifting the maximum diastolic potential to more negative values. The same mechanism reduces input resistance at diastolic potentials, which means that a greater depolarizing current would be required to achieve the "threshold" for firing an action potential.

Passive Membrane Electrical Properties. Passive membrane properties, including membrane resistance, capacitance, and cable properties, play an important role in cardiac electrophysiology. Although the cardiac cell membrane is resistant to current flow, it also has capacitive properties, which means that it behaves like a battery and can store charges of opposite signs on its two sides—an excess of negative charges inside the membrane balanced by equivalent positive charges outside the membrane. These resistive and capacitive properties cause the membrane to take a certain amount of time to respond to an applied stimulus, rather than responding instantly, because the charges across the capacitive membrane must be altered first. A subthreshold rectangular current pulse applied to the membrane produces a slowly rising and decaying change in membrane voltage rather than a rectangular voltage change. A value called the time constant of the membrane reflects this property. The time

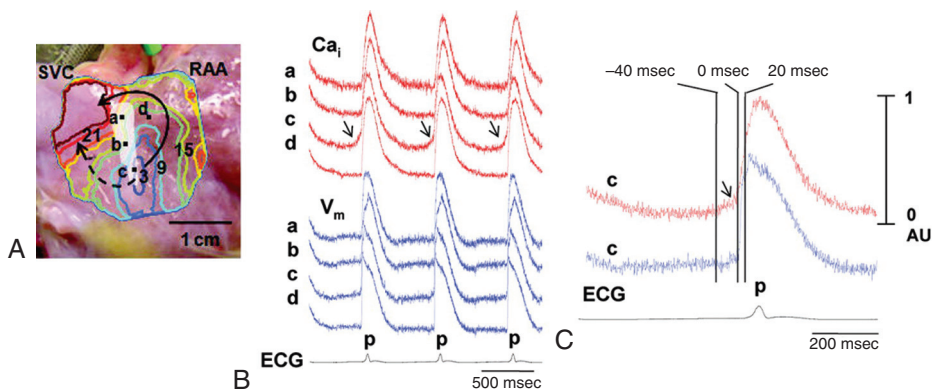


FIGURE e33-6 Demonstration of late diastolic intracellular calcium elevations in the sinoatrial node *in situ* by simultaneous optical mapping of changes in intracellular calcium (Ca_i) and transmembrane voltage (V_m) in an isolated canine right atrial preparation. **A**, Isochronal map of atrial activation during sinus rhythm superimposed on a photograph of the endocardial surface of the sinoatrial node region. The number on each isochronal line indicates the time of activation in milliseconds. The white shaded area is the sinoatrial node. SVC = superior vena cava; RAA = right atrial appendage. **B**, V_m (blue) and Ca_i (red) recordings from the superior (a), middle (b), and inferior (c) sinoatrial node and right atrium (d). Arrows indicate late diastolic elevations in Ca_i . Note the presence of slow diastolic depolarization in the V_m tracings through c, but not in d. **C**, Magnified views of Ca_i and V_m tracings of the inferior sinoatrial node. The late diastolic elevation in Ca_i (arrow) precedes rapid upstroke of the sinoatrial and atrial action potential and occurs much earlier than the P wave on the electrocardiogram (ECG). (From Joung B, Tang L, Maryama M, et al: Intracellular calcium dynamics and acceleration of sinus rhythm by β -adrenergic stimulation. *Circulation* 119:788, 2009. With permission from the American Heart Association.)

constant tau is equal to the product of membrane resistance R_m and cell capacitance C_m :

$$\tau = R_m \cdot C_m$$

This is the time taken by the membrane voltage to reach 63% of its final value after application of a steady current. The time course of changes in membrane potential after the application of a hyperpolarizing or depolarizing subthreshold current step is typically mono-exponential in all myocyte types, thus indicating that the entire sarcolemma (including the T-tubular membrane; see Fig. e33-1) is charging uniformly.

When aligned end to end, cardiac cells, particularly the His-Purkinje system, behave like a long cable in which current flows more easily inside the cell and to the adjacent cell across the gap junction than it does across the cell membrane to the outside. When current is injected at a point, most of it flows along inside the cell, but some leaks out. Because of this loss of current, the change in voltage of a cell at a site distant from the point of applied current is less than the change in membrane voltage at the point where the stimulus was applied. A measure of this property of a cable is called the space or length constant lambda (λ), which is the distance along the cable from the point of stimulation at which the voltage at steady state is $1/e$ (37%) of its value at the point of introduction.

Restated, λ describes how far current flows before leaking passively across the surface membrane to a value about a third of its initial value. This distance is normally approximately 2 mm for Purkinje fibers, 0.5 mm for the sinoatrial node, and 0.8 mm for ventricular muscle fibers. λ is about 10 times the length of an individual cell. As an example, if ϵ is approximately 2.7 and a hyperpolarizing current pulse in a Purkinje fiber produces a change in membrane voltage of 15 mV at the site of current injection, the change in membrane potential one space constant (2 mm) away would be $15/2.7 = 5.5$ mV.

Because the current loop in any circuit must be closed, current must flow back to its point of origin. Local circuit currents pass across gap junctions between cells and exit across the sarcolemmal membrane to close the loop and complete the circuit. Inward excitation currents in one area (carried by Na^+ in most regions) flow intracellularly along the length of the tissue (carried mostly by K^+), escape across the membrane, and flow extracellularly in a longitudinal direction. The outside local circuit current is the current recorded on an electrocardiogram. Through these local circuit currents the transmembrane potential of each cell influences the transmembrane potential of its neighbor because of the passive flow of current from one segment of the fiber to another across the low-resistance gap junctions.

As discussed earlier, the speed of conduction depends on active membrane properties such as the magnitude of the Na^+ current, a measure of which is V_{\max} . Passive membrane properties also contribute to conduction velocity and include the excitability threshold, which influences the capability of cells adjacent to the one that has been discharged to reach threshold; the intracellular resistance of the cell, determined by free ions in the cytoplasm; the resistance of the gap junction; and the cross-sectional area of the cell. The direction of propagation is crucial because of the influence of anisotropy, as mentioned earlier.

Loss of Membrane Potential and Development of Arrhythmia. Many acquired abnormalities of cardiac muscle or specialized fibers that result in arrhythmias produce a loss of membrane potential; that is, maximum diastolic potential becomes less negative. This change should be viewed as a symptom of an underlying abnormality, analogous to fever or jaundice, rather than as a diagnostic category in and of itself because both the ionic changes resulting in cellular depolarization and the more fundamental biochemical or metabolic abnormalities responsible for the ionic alterations probably have a number of causative factors.

Cellular depolarization can result from elevated $[K^+]_o$ or decreased $[K^+]_i$, an increase in membrane permeability to Na^+ (P_{Na} increases), or a decrease in membrane permeability to K^+ (P_K decreases). Reference to the GHK equation for V (see [Phases of the Cardiac Action Potential: General Considerations](#)) illustrates that these changes alone or in combination make membrane diastolic voltage less negative.

Normal cells perfused by an abnormal milieu (e.g., hyperkalemia), abnormal cells perfused by a normal milieu (e.g., healed myocardial infarction), or abnormal cells perfused by an abnormal milieu (e.g., acute myocardial ischemia and infarction) can exist alone or in combination and reduce resting membrane voltage. Each of these changes can have one or more biochemical or metabolic causes. For

example, acute myocardial ischemia results in decreased $[K^+]_i$ and increased $[K^+]_o$, release of norepinephrine, and acidosis, which may be related to an increase in intracellular Ca^{2+} and Ca^{2+} -induced transient inward currents and accumulation of amphipathic lipid metabolites and oxygen free radicals. All these changes can contribute to the development of an abnormal electrophysiologic environment and arrhythmias during ischemia and reperfusion. Knowledge of these changes may provide insight into therapy that actually reverses basic defects and restores membrane potential or other abnormalities to normal.

Effects of Reduced Resting Potential. The reduced resting membrane potential alters the depolarization and repolarization phases of the cardiac action potential. For example, partial membrane depolarization causes a decrease in the steady-state availability of fast sodium channels, thereby reducing the magnitude of peak I_{Na} during phase 0 of the action potential. The subsequent reduction in V_{\max} and action potential amplitude prolongs the conduction time of the propagated impulse, at times to the point of block.²⁸

Action potentials with reduced upstroke velocity resulting from partial inactivation of I_{Na} are called depressed fast responses (see Fig. 33-17F). Their contours often resemble and can be difficult to distinguish from slow responses, in which upstrokes are caused by $I_{\text{Ca,L}}$ (see Fig. 33-17F). Membrane depolarization to levels of -60 to -70 mV can inactivate a substantial portion of the available voltage-gated Na^+ channels, and depolarization to -50 mV or less can almost completely inactivate all the Na^+ channels (see Fig. 33-12). At membrane potentials positive to -50 mV, $I_{\text{Ca,L}}$ can be activated to generate phase 0 if conditions are appropriate. These changes in action potential are likely to be heterogeneous, with unequal degrees of Na^+ inactivation that create areas with minimally reduced velocity, more severely depressed zones, and areas of complete block. These uneven changes are conducive to the development of arrhythmias.

In these cells with reduced membrane potential, refractoriness can outlast voltage recovery of the action potential; that is, the cell can still be refractory or partially refractory after the resting membrane potential returns to its most negative value. Furthermore, if cardiac-impulse block occurs in a fairly localized area without significant slowing of conduction proximal to the site of block, cells in this proximal zone exhibit short action potentials and refractory periods because unexcited cells distal to the block (still in a polarized state) electrotonically speed recovery in cells proximal to the site of block.

If conduction slows gradually proximal to the site of block, the duration of these action potentials and their refractory periods can be prolonged. Some cells can exhibit abnormal electrophysiologic properties, even though they have a relatively normal resting membrane potential.

MECHANISMS OF ARRHYTHMOGENESIS

The mechanisms responsible for cardiac arrhythmias (Table 33-4) are generally divided into categories of disorders of impulse formation, disorders of impulse conduction, or combinations of both. However, our currently available diagnostic tools do not permit unequivocal determination of the electrophysiologic mechanisms responsible for many clinically occurring arrhythmias or their ionic bases. This is especially true for ventricular arrhythmias. It may be clinically difficult to separate microanatomic reentry from automaticity, and often one is left with the consideration that a particular arrhythmia is "most consistent with" or "best explained by" one or the other electrophysiologic mechanism. Some tachyarrhythmias can be started by one mechanism and be perpetuated by another. An episode of tachycardia caused by one mechanism can precipitate another episode caused by a different mechanism. For example, an initiating tachycardia or premature complex caused by abnormal automaticity can precipitate an episode of tachycardia sustained by reentry. However, by use of the features of entrainment (see later), arrhythmias caused by macroreentry circuits can be identified.

Disorders of Impulse Formation

Disorders in this category are characterized by an inappropriate discharge rate of the normal pacemaker, the sinoatrial node (e.g., sinus

**TABLE 33-4** Mechanisms of Arrhythmogenesis

DISORDER	EXPERIMENTAL EXAMPLES	CLINICAL EXAMPLES
Disorders of Impulse Formation		
Automaticity		
Normal automaticity	Normal <i>in vivo</i> or <i>in vitro</i> in sinoatrial nodal, AV nodal, and Purkinje cells	Sinus tachycardia or bradycardia inappropriate for the clinical situation; possibly ventricular parasystole
Abnormal automaticity	Depolarization-induced automaticity in Purkinje myocytes	Possibly accelerated ventricular rhythms after myocardial infarction
Triggered activity		
EADs	Drugs (sotalol, <i>N</i> -acetylprocainamide, terfenadine, erythromycin), cesium, barium, low [K ⁺],	Acquired LQTS and associated ventricular arrhythmias
DADs	Gain-of-function mutations in the gene encoding RyR2	Catecholaminergic polymorphic ventricular tachycardia
Disorders of Impulse Conduction		
Block		
Bidirectional or unidirectional without reentry	Sinoatrial, AV, bundle branch, Purkinje-muscle	Sinoatrial, AV, bundle branch block
Unidirectional block with reentry	AV node, Purkinje-muscle junction, infarcted myocardium	Reciprocating tachycardia in Wolff-Parkinson-White syndrome, AV nodal reentry tachycardia, ventricular tachycardia caused by bundle branch reentry
Reflection	Purkinje fiber with area of inexcitability	Unknown
Combined Disorders		
Interactions between automatic foci	Depolarizing or hyperpolarizing subthreshold stimuli speed or slow the automatic discharge rate	Modulated parasystole
Interactions between automaticity and conduction	Deceleration-dependent block, overdrive suppression of conduction, entrance and exit block	Similar to experimental

rates too fast or too slow for the physiologic needs of the patient), or discharge of an ectopic pacemaker that controls atrial or ventricular rhythm. Pacemaker discharge from ectopic sites, often called latent or subsidiary pacemakers, can occur in fibers located in several parts of the atria, coronary sinus and pulmonary veins, AV valves, portions of the AV junction, and His-Purkinje system. Ordinarily kept from reaching the level of threshold potential because of overdrive suppression by the more rapidly firing sinus node or electrotonic depression from contiguous fibers, ectopic pacemaker activity at one of these latent sites can become manifested when the sinus nodal discharge rate slows or block occurs at some level between the sinoatrial node and the ectopic pacemaker site, which permits *escape* of the latent pacemaker at the latter's normal discharge rate. A clinical example would be sinus bradycardia to a rate of 45 beats/min that permits an AV junctional escape complex to occur at a rate of 50 beats/min.

Alternatively, the discharge rate of the latent pacemaker can speed inappropriately and usurp control of cardiac rhythm from the sinoatrial node, which has been discharging at a normal rate, such as occurs with a premature ventricular complex (PVC) or a burst of ventricular tachycardia. Such disorders of impulse formation can be caused by speeding or slowing of a *normal* pacemaker mechanism (e.g., phase 4 diastolic depolarization that is ionically normal for the sinoatrial node or for an ectopic site such as a Purkinje fiber but occurs inappropriately fast or slow) or by an ionically *abnormal* pacemaker mechanism.

A patient with persistent sinus tachycardia at rest or sinus bradycardia during exertion exhibits inappropriate sinus nodal discharge rates, but the ionic mechanisms responsible for sinus nodal discharge can still be normal, although the kinetics or magnitude of the currents can be altered. Conversely, when a patient experiences ventricular tachycardia during acute myocardial infarction, ionic mechanisms ordinarily not involved in the formation of spontaneous impulses for this fiber type can be operative and generate the tachycardia. For example, although pacemaker activity is not generally found in ordinary working myocardium, the effects of myocardial infarction can perhaps depolarize these cells to membrane potentials

at which inactivation of I_K and activation of I_{Ca,L} cause automatic discharge. *In vitro* studies have demonstrated that myofibroblasts in infarct scars depolarize cardiomyocytes by heterocellular electrotonic interactions via gap junctions and also induce synchronized spontaneous activity in neighboring cardiomyocytes.⁶⁶

Abnormal Automaticity. The mechanisms responsible for normal automaticity were described earlier. Abnormal automaticity can arise from cells that have reduced maximum diastolic potentials, often at membrane potentials positive to -50 mV, when I_K and I_{Ca,L} may be operative.

Automaticity at membrane potentials more negative than -70 mV may be caused by I_f. When the membrane potential is between -50 and -70 mV, the cell may be quiescent. Electrotonic effects from surrounding normally polarized or more depolarized myocardium influence the development of automaticity.⁶⁴ Abnormal automaticity has been found in Purkinje fibers removed from dogs subjected to myocardial infarction, in rat myocardium damaged by epinephrine, in human atrial samples, and in ventricular myocardial specimens from patients undergoing aneurysmectomy and endocardial resection for recurrent ventricular tachyarrhythmias.

Abnormal automaticity can be produced in normal muscle or Purkinje fibers by appropriate interventions, such as passage of current that reduces diastolic potential. An automatic discharge rate speeds up with progressive depolarization, and hyperpolarizing pulses slow the spontaneous firing. It is possible that partial depolarization and failure to reach normal maximal diastolic potential can induce automatic discharge in most if not all cardiac fibers. Although this type of spontaneous automatic activity has been found in human atrial and ventricular fibers, its relationship to the genesis of clinical arrhythmias has not been established. Abnormal automaticity in Purkinje cells can also originate secondary to spontaneous, submembrane Ca²⁺ elevations via activation of calcium-sensitive membrane conductances, a process identical to that previously identified in sinoatrial nodal myocytes. Indeed, Purkinje myocytes isolated from mice heterozygous for an arrhythmia-causing mutation in the gene encoding the cardiac ryanodine receptor Ca²⁺ release channel (RyR2) display a greater propensity for the development of arrhythmogenic Ca²⁺-handling abnormalities than do mutant ventricular cardiomyocytes.⁶⁷ This proarrhythmic behavior is further exacerbated by catecholaminergic

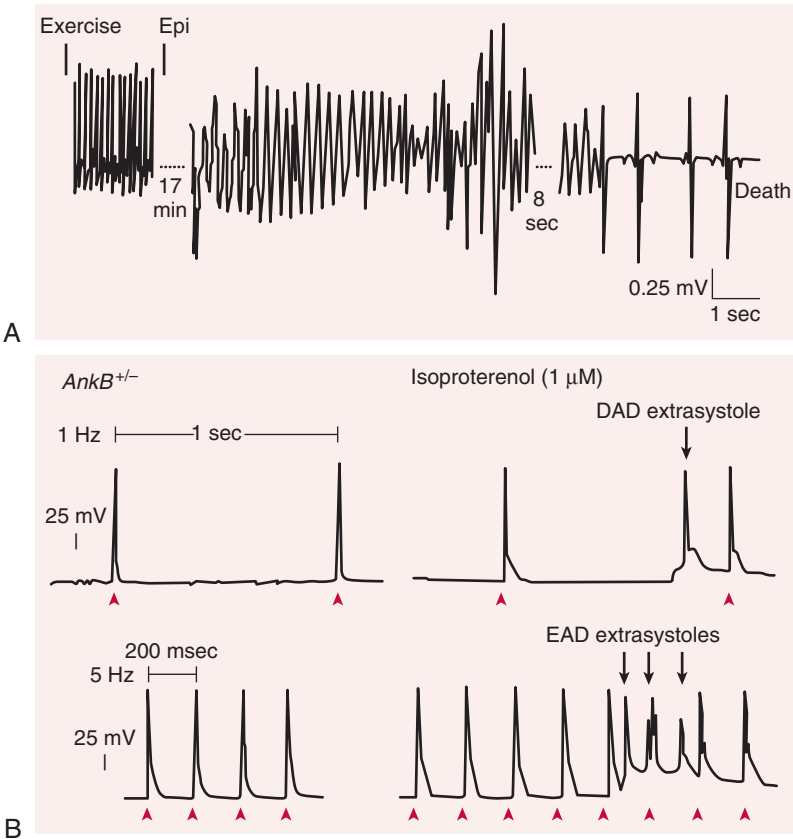


FIGURE 33-19 Polymorphic ventricular tachycardia and sudden death in an animal model of type 4 LQTS. **A**, Electrocardiogram after exercise and administration of epinephrine in a mouse heterozygous for a loss-of-function mutation in the gene encoding ankyrin-B (AnkB). Polymorphic ventricular tachycardia (*torsades de pointes*) occurred within about 17 minutes of epinephrine administration, followed by marked bradycardia and death 2 minutes after the arrhythmia. **B**, Transmembrane action potentials in single cardiomyocytes from Ank $B^{+/-}$ mice at the frequencies indicated. Acute exposure to isoproterenol induced both DADs and EADs, which led to extra beats. (From Mohler PJ, Schott J, Gramolini AO, et al: Ankyrin-B mutation causes type 4 long-QT cardiac arrhythmia and sudden cardiac death. *Nature* 421:634, 2003.)



stimulation with the development of triggered beats (Fig. e33-7), thus supporting the concept that Purkinje cells are critical contributors to arrhythmic triggers in animal models and humans with RyR2 mutations that are linked to CPVT. The occurrence of such spontaneous localized $[Ca^{2+}]_i$ transients has been confirmed in canine Purkinje cells (see Video 33-2).⁶⁸



Rhythms resulting from automaticity may be slow atrial, junctional, and ventricular escape rhythms; certain types of atrial tachycardias (e.g., those produced by digitalis or perhaps those coming from pulmonary veins); accelerated junctional (nonparoxysmal junctional tachycardia) and idioventricular rhythms; and parasytole (see Chapter 37).

Triggered Activity

Automaticity is the property of a fiber to initiate an impulse spontaneously, without need for prior stimulation, so that electrical quiescence does not occur. Triggered activity is initiated by afterdepolarizations, which are depolarizing oscillations in membrane voltage induced by one or more preceding action potentials. Thus triggered activity is pacemaker activity that results as a consequence of a preceding impulse or series of impulses, without which electrical quiescence occurs (Fig. 33-19). This triggering activity is not caused by an automatic self-generating mechanism, and the term *triggered automaticity* is therefore contradictory. These depolarizations can occur before or after full repolarization of the fiber and are best termed EADs when they arise from a reduced level of membrane potential during phases 2 (type 1) and 3 (type 2) of the cardiac action potential (see

Fig. e33-12) or late afterdepolarizations or DADs (see Fig. 33-19) when they occur after completion of repolarization (phase 4), generally at a more negative membrane potential than that from which EADs arise. Not all afterdepolarizations may reach threshold potential, but if they do, they can trigger another afterdepolarization and thus self-perpetuate.

Delayed Afterdepolarizations. DADs and triggered activity have been demonstrated in Purkinje fibers, specialized atrial fibers and ventricular muscle fibers exposed to digitalis preparations, pulmonary veins, normal Purkinje fibers exposed to Na-free superfusates from the endocardium of the intact heart, ventricular myocardial cells from failing hearts (Fig. 33-20) and from mouse hearts with ankyrin-B mutations (see Fig. 33-19) during beta-adrenergic stimulation, and endocardial preparations 1 day after a myocardial infarction.^{69,70} When fibers in the rabbit, canine, simian, and human mitral valves and in the canine tricuspid valve and coronary sinus are superfused with norepinephrine, they exhibit the capability for sustained triggered rhythmic activity.

Triggered activity caused by DADs has also been noted in diseased human atrial and ventricular fibers studied *in vitro*. Left stellate ganglion stimulation can elicit DADs in canine ventricles. In vivo, atrial and ventricular arrhythmias apparently caused by triggered activity have been reported in the dog and possibly in humans. It is tempting to ascribe certain clinical arrhythmias to DADs, such as some arrhythmias precipitated by digitalis or some cases of AF arising from DADs in pulmonary veins. The accelerated idioventricular rhythm 1 day after experimental canine myocardial infarction may be caused by DADs, and some evidence has suggested that certain ventricular tachycardias, such as those arising in the right ventricular outflow tract, may be caused by DADs, whereas other data suggest that EADs are responsible.⁷¹

Major Role of Intracellular Ca^{2+} -Handling Abnormalities in the Generation of Delayed Afterdepolarizations. It is well recognized that DADs result from the activation of a calcium-sensitive inward current elicited by spontaneous increases in the intracellular free calcium concentration. Acquired or inherited abnormalities in the properties of the SR calcium release channels or SR calcium-binding proteins underlie these spontaneous calcium release events.

Rapid mobilization of Ca^{2+} from the SR into the cytosol is mediated by the synchronous opening of ryanodine-sensitive Ca^{2+} release channels (ryanodine receptors, RyRs). The cardiac RyR is composed of four equivalent subunits (homotetramer), each encoded by the RYR2 gene. During cardiac systole, the small influx of calcium ions through L-type Cav channels triggers a massive release of Ca^{2+} from the SR via synchronous opening of RyR2 channels, a process called Ca^{2+} -induced Ca^{2+} release (see Chapter 21). During diastole, RyR2 channels close and Ca^{2+} is recycled into the SR via calcium pumps, thereby refilling SR Ca^{2+} stores for the next release cycle. The duration and amplitude of Ca^{2+} efflux from the SR are therefore tightly controlled by the gating of RyR2 channels. RyR2 interacts with a number of accessory proteins to form a macromolecular Ca^{2+} release complex (see Fig. e33-6). Proteins interact with RyR2 at multiple sites within the cytosolic domains of RyR2 (e.g., protein phosphatases) or at the SR level (e.g., calsequestrin, the major calcium-binding protein in the SR lumen). Among the cytosolic ligands, FKBP-12.6 (calstabin 2) has been implicated in stabilizing the closed state of the RyR2 channel and thus preventing diastolic Ca^{2+} leakage (Fig. e33-8).⁷²

Mutations in the human RYR2 gene and in the gene CASQ2, which encodes calsequestrin (see Fig. e33-6), have been linked to CPVT. Experimental studies have revealed that the RYR2 and CASQ2 mutations that underlie CPVT cause an increase in the sensitivity of the RyR2 channel to luminal Ca^{2+} activation on adrenergic stimulation (e.g., from emotional or physical stress) and enhance the propensity for spontaneous, diastolic Ca^{2+} release from the SR and subsequent DAD-triggered arrhythmias (see later).^{27,73-75} It is also possible that CPVT mutants exhibit reduced affinity for binding of the regulatory protein FKBP-12.6, thereby resulting in diastolic Ca^{2+} leakage from the SR.⁷⁶ Reduced FKBP-12.6 binding caused by protein kinase A-mediated hyperphosphorylation has been implicated in cardiac arrhythmogenesis associated with heart failure.⁷⁷ Polymorphic

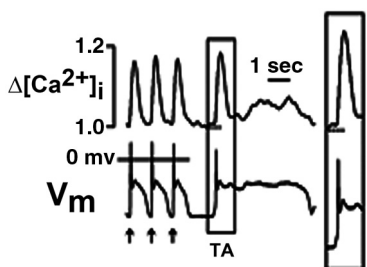


FIGURE e33-7 Arrhythmic spontaneous Ca^{2+} elevations in a Purkinje myocyte isolated from a mouse heterozygous for a gain-of-function mutation in the *RYR2* gene. Changes in intracellular free calcium ($\Delta[\text{Ca}^{2+}]_i$, upper trace) and transmembrane action potential (V_m) were simultaneously recorded in a mutant Purkinje myocyte during electrical field stimulation (arrows) and during a spontaneous elevation in Ca^{2+} (triggered action potential, TA). Note that the action potential upstroke is preceded by a low-amplitude elevation in Ca^{2+} , followed by a suprathreshold membrane depolarization that triggers a markedly prolonged action potential. (From Kang G, Giovanone SF, Liu N, et al: Purkinje cells from *RyR2* mutant mice are highly arrhythmic but responsive to targeted therapy. *Circ Res* 107:512, 2010.)

VIDEO 33-2

Trigger of whole-cell Ca^{2+} waves by subsarcolemmal Ca^{2+} events. Images were taken from a Purkinje cell region covering sarcolemma, subsarcolemmal space, and a small area of the cell-center. The cell was loaded with the calcium-sensitive dye fluo-4. Changes in $[\text{Ca}^{2+}]$, were color-coded, with red and white indicating high and low $[\text{Ca}^{2+}]$, levels, respectively. Two types of Ca^{2+} events are demonstrated: spontaneous elevations that are confined to a ~6-mm wide region under the outer membrane (wavelet), and wavelets that initiate waves that propagate to the cell-center. (From Stuyvers BD, Dun W, Matkovich S, et al: Ca^{2+} sparks and waves in canine Purkinje cells. *Circ Res* 97:35, 2005.)

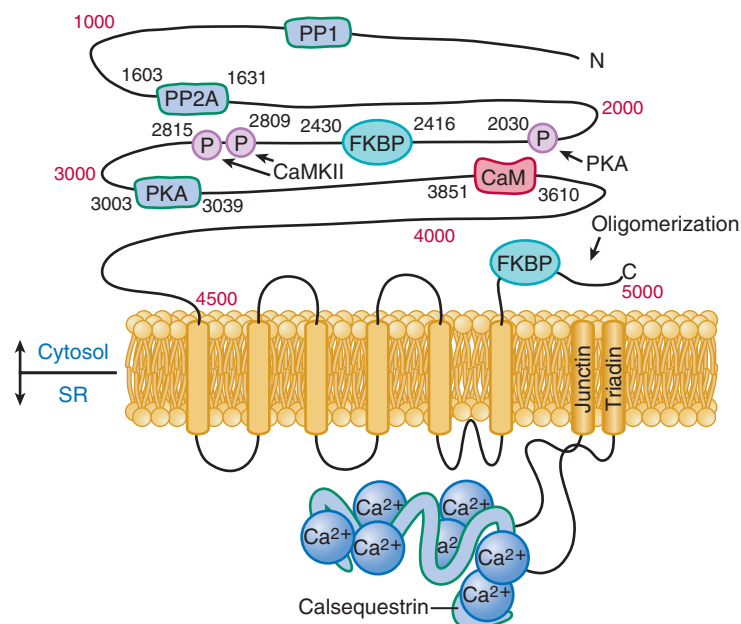


FIGURE e33-8 Structure of the cardiac ryanodine receptor monomer subunit RyR2 delineating the sites of interaction with auxiliary proteins and the phosphorylation sites (P). CaM = calmodulin; CaMKII = calmodulin-dependent kinase II; FKBP = FK506 binding protein 12.6; PKA = protein kinase A; PP = protein phosphatase. Calsequestrin, junctin, and triadin are proteins that interact with RyR2 in the SR. (From Bers DM: Macromolecular complexes regulating cardiac ryanodine receptor function. *J Mol Cell Cardiol* 37:417, 2004.)

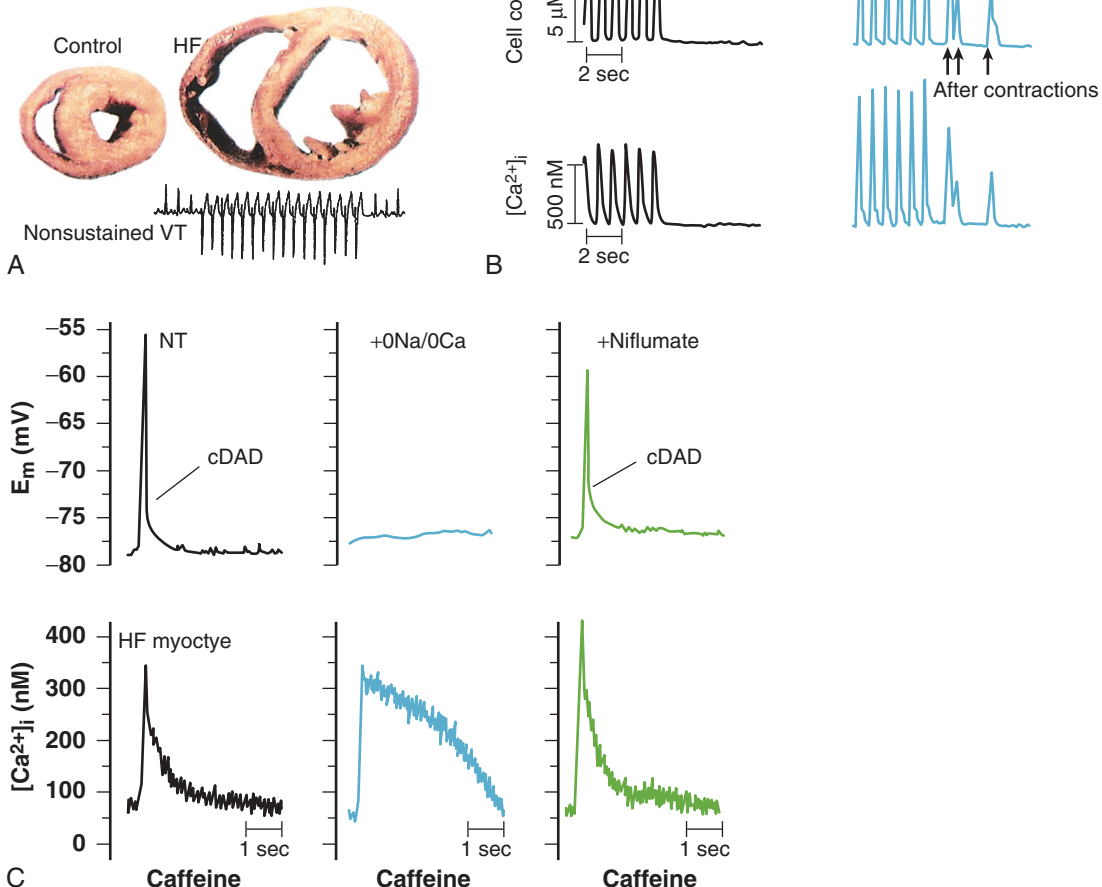


FIGURE 33-20 Ventricular arrhythmia in an animal model of heart failure (aortic constriction-insufficiency in the rabbit). **A**, Cross sections of a control and failing heart (HF) and Holter recording of nonsustained ventricular tachycardia (VT) seen in a failing heart. **B**, Spontaneous aftercontractions and increases in $[Ca^{2+}]_i$ in a failing cardiomyocyte after exposure to isoproterenol. **C**, Induction of a DAD by the application of caffeine (cDAD) in a cardiomyocyte isolated from a failing rabbit heart. In normal Tyrode (NT) solution, caffeine causes rapid release of Ca^{2+} from the SR, thereby leading to increases in the intracellular free calcium concentration (bottom tracing), which in turn causes membrane depolarization. Blocking of the Na^+/Ca^{2+} exchange current in Na^+ -free and Ca^{2+} -free solution (0Na/0Ca) abolished DADs despite a similar increase in $[Ca^{2+}]_i$, whereas blocking of the Ca^{2+} -activated Cl^- current with niflumate did not prevent DADs. E_m = membrane voltage. (From Pogwizd SM, Schlotthauer K, Li L, et al: Arrhythmogenesis and contractile dysfunction in heart failure. *Circ Res* 88:1159, 2001. By permission of the American Heart Association.)

ventricular tachycardia develops in FKBP-12.6-deficient mice on adrenergic stimulation.⁷⁸ Treatment with the 1,4-benzothiazepine derivatives JTV519 and S107, which restore FKBP-12.6 affinity for RyR2, has been shown to suppress catecholamine-induced polymorphic ventricular tachycardia in FKBP-12.6-deficient mice.^{27,79}

The IP₃ receptor (IP₃R) is another Ca^{2+} release channel in cardiomyocytes that is activated by binding of the second messenger IP₃ and cytosolic Ca^{2+} . IP₃R exists as a homotetramer or heterotetramer, each encoded by the *ITPR1*, *ITPR2*, or *ITPR3* gene (Fig. e33-9). The type 2 IP₃R is the predominant subtype in atrial myocytes, where they are located near RyR2 channels at the SR Ca^{2+} release sites and contribute to altered excitation-contraction coupling and arrhythmogenesis in the atria.⁸⁰ In Purkinje myocytes, type 1 IP₃Rs colocalize with type 3 RyR in the subsarcolemmal space to form a functional dyad that critically determines electrical excitability.^{68,81} IP₃-dependent Ca^{2+} signaling has been implicated in cardiac arrhythmias attributable to ischemia and reperfusion injury, inflammatory processes, and developing cardiac failure.⁸² IP₃Rs are upregulated in heart failure and AF.⁸³ In atrial and Purkinje myocytes, IP₃ causes spontaneous $[Ca^{2+}]_i$ transients, Ca^{2+} waves, and Ca^{2+} alternans and facilitates the generation of afterdepolarizations.⁸²

The cascade of events linking cellular Ca^{2+} -handling abnormalities to cardiac arrhythmias is illustrated in Figure 33-21. Ca^{2+} leaking through SR Ca^{2+} release channels during diastole gives rise to localized increases in the cytosolic calcium level in a single cardiomyocyte. The

focally elevated Ca^{2+} then causes a propagating Ca^{2+} wave that depolarizes the cardiomyocyte membrane and triggers a DAD via transient activation of the inward Na^+/Ca^{2+} exchange current ($I_{Na/Ca}$).⁵² Inhibition of calmodulin kinase eliminates transient inward $I_{Na/Ca}$ in isolated rabbit ventricular myocytes, thus indicating that activation of this enzyme plays an important role in cardiac arrhythmogenesis. In addition, drugs that reduce I_{Na} also reduce the transient inward current, relieve Ca^{2+} overload, and can abolish DADs. DADs most likely play a causative role in arrhythmogenesis in the failing heart, where upregulation of $I_{Na/Ca}$ in combination with downregulation of the inward rectifier K^+ current I_{K1} , facilitates DAD generation (see Fig. 33-20).⁵²

Although a causal role of spontaneous SR Ca^{2+} release events in triggering DADs in isolated cardiomyocytes is generally accepted, little is known about whether or how calcium waves within the heart actually produce arrhythmogenic membrane depolarizations. A study using simultaneous optical mapping of changes in $[Ca^{2+}]_i$ and membrane potential with cellular resolution in the intact, isolated perfused rat heart demonstrated that the occurrence of triggered activity requires the synchronous appearance of Ca^{2+} waves in multiple, adjacent cardiomyocytes. In contrast, sporadic Ca^{2+} waves in individual cardiomyocytes never gave rise to triggered activity (Fig. e33-10).⁸⁴

A recent dual-voltage (V_m) and Ca^{2+} optical mapping study similarly investigated the mechanism by which Ca^{2+} -induced DADs are synchronized in the myocardium in response to beta-adrenergic receptor

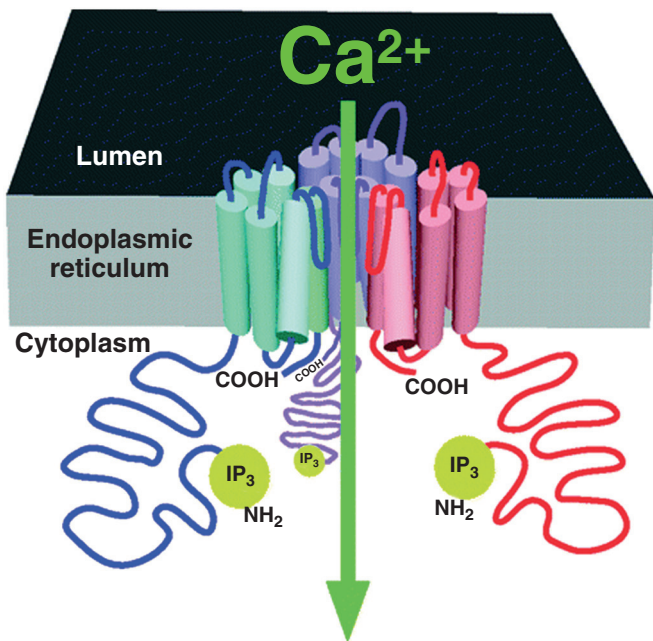


FIGURE e33-9 Structure of the IP_3 receptor (IP_3R). IP_3Rs are intracellular membrane proteins that exist as homotetramers or heterotetramers. The Ca^{2+} conducting pore is believed to be created at the central axis of the tetrameric structure. The cartoon depicts three of four IP_3 molecules (in different colors) in a single tetrameric channel structure. Part of the luminal loop (i.e., the loop facing the SR lumen) connecting transmembrane helices 5 and 6 of each monomer dips into the fourfold symmetrical axis and creates the pathway for efflux of Ca^{2+} from the SR lumen. (From Foskett JK, White C, Cheung KH, et al: Inositol trisphosphate receptor Ca^{2+} release channels. *Physiol Rev* 87:593, 2007.)

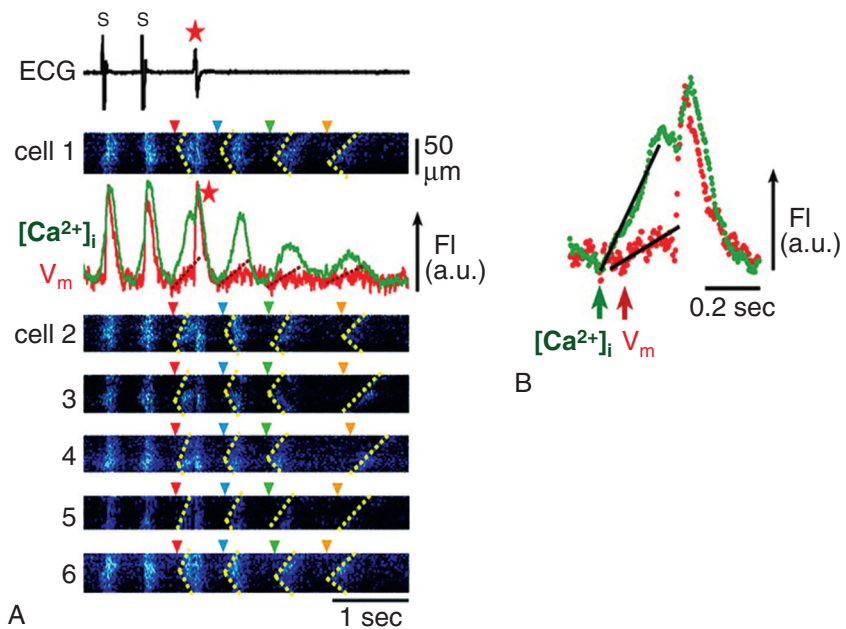


FIGURE e33-10 Triggered activity mediated by Ca^{2+} waves in an intact rat heart. **A**, Synchronous emergence of Ca^{2+} waves (dotted lines) in individual cells (1 through 6) accompanies a single event of triggered activity (red asterisk), followed by Ca^{2+} oscillations (green trace), with concomitant membrane fluctuations (red trace) showing a gradual reduction in amplitude. Only the first Ca^{2+} wave (red arrowhead), not the following three, triggers a propagating impulse. Fluorescence intensities of the calcium- and voltage-sensitive dyes fluo-4 and RH237, respectively, were measured in adjacent subepicardial ventricular myocytes within a Langendorff-perfused rat heart with dual-view, rapid scanning confocal microscopy. The triggered activity was induced by 2-Hz pacing under low K^+ (2.4 mmol/L) perfusion and isoproterenol (3 nmol/L). **B**, Simultaneous V_m and intracellular Ca^{2+} recordings during the triggered beat demarcated by the red arrowhead in **A** at an expanded time scale demonstrate that the increase in $[\text{Ca}^{2+}]_i$ precedes membrane depolarization. Fl = fluorescence intensity. (Modified from Fujiwara K, Tanaka H, Mani H, et al: Burst emergence of intracellular Ca^{2+} waves evokes arrhythmicogenic oscillatory depolarization via the $\text{Na}^+-\text{Ca}^{2+}$ exchanger. *Circ Res* 103:509, 2008. With permission from the American Heart Association.)

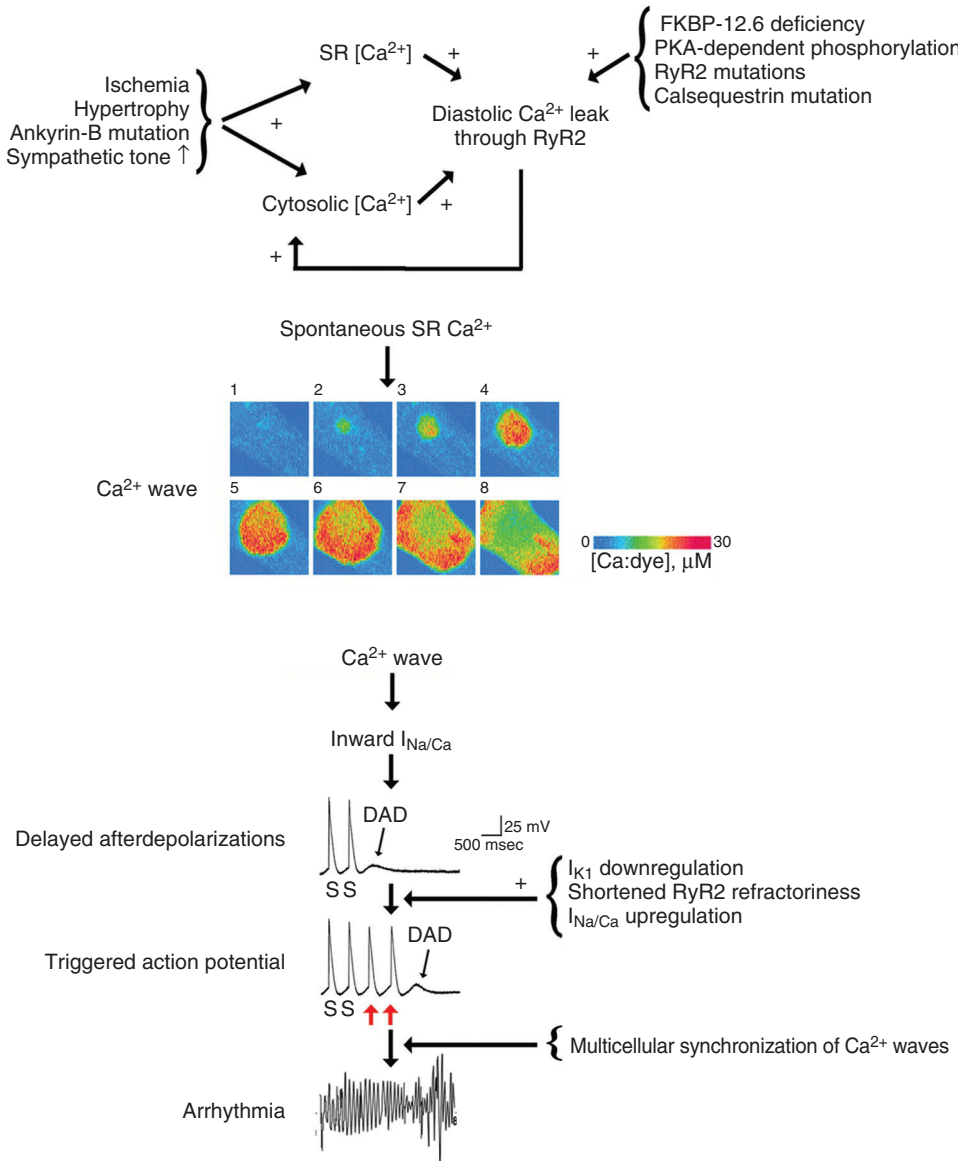


FIGURE 33-21 Proposed scheme of events leading to DADs and triggered tachyarrhythmia. **Top panel,** Congenital (e.g., gain-of-function mutations in the *RYR2* or *CASQ2* genes) or acquired factors (e.g., ischemia, hypertrophy, increased sympathetic tone, heart failure) will cause a diastolic Ca^{2+} leak through RyR2 that results in localized and transient increases in $[Ca^{2+}]$ in cardiomyocytes. **Middle panel,** Representative series of images showing changes in $[Ca^{2+}]$ during a Ca^{2+} wave in a single cardiomyocyte loaded with a Ca^{2+} -sensitive fluorescent dye. Images were obtained at 117-millisecond intervals. Focally elevated Ca^{2+} (2) diffuses to the adjacent junctional SR, where it initiates more Ca^{2+} release events that result in a propagating Ca^{2+} wave (3 to 8). **Bottom panel,** The Ca^{2+} wave, through activation of inward $I_{Na/Ca}$, will depolarize the cardiomyocyte (DAD). If of sufficient magnitude to overcome the source-sink mismatch, the DAD will depolarize the cardiomyocyte above threshold and result in a single or repetitive premature heartbeat (red arrows), which can trigger an arrhythmia. Downregulation of the inwardly rectifying potassium current (I_{K1}), upregulation of $I_{Na/Ca}$, and shortened Ca^{2+} signaling refractoriness because of ryanodine receptor phosphorylation and/or oxidation can promote the generation of DAD-triggered action potentials. S = stimulus. (Modified from Rubart M, Zipes DP: Mechanisms of sudden cardiac death. *J Clin Invest* 115:2305, 2005. With permission from the Journal of Clinical Investigation.)

stimulation to overcome the source-sink mismatch and generate focal arrhythmias.⁸⁵ In this study, local intramyocardial injection of the sympathetic neurotransmitter norepinephrine was used to induce triggered arrhythmias. Spatial patterns of V_m - Ca^{2+} delay during norepinephrine-induced PVCs were compared with sinus rhythm, ventricular pacing, and normal Tyrode solution-induced PVCs, as shown in Figure e33-11.

Another study involving isolated left ventricular cardiomyocytes from failing canine hearts suggested shortened Ca^{2+} signaling refractoriness because of altered post-translational modification of the ryanodine receptor Ca^{2+} release channel as a mechanism responsible for the increased incidence of diastolic Ca^{2+} waves associated with this disease and could provide an additional substrate for synchronization of arrhythmogenic events at the tissue level in hearts prone to VF.⁸⁶

Short coupling intervals and pacing at rates more rapid than the triggered activity rate (overdrive pacing) increase the amplitude and shorten the cycle length of the DAD after cessation of pacing (overdrive acceleration) rather than suppressing and delaying the escape rate of the afterdepolarization, as in normal automatic mechanisms. Premature stimulation exerts a similar effect: the shorter the premature interval, the larger the amplitude and the shorter the escape interval of the triggered event.

The clinical implication might be that tachyarrhythmias caused by DAD-triggered activity may not be suppressed easily or indeed may be precipitated by rapid rates, either spontaneously (such as with sinus tachycardia) or induced by pacing. Finally, because a single premature stimulus can both initiate and terminate triggered activity, differentiation from reentry (see later) becomes difficult. The response to overdrive pacing may help separate triggered arrhythmias from reentrant arrhythmias.

Early Afterdepolarizations

Various interventions, each of which results in an increase in intracellular positivity, can cause EADs. EADs may be responsible for the lengthened repolarization time and ventricular tachyarrhythmias seen in several clinical situations, such as the acquired and congenital forms of LQTS (see Fig. 33-19; see Chapter 37).⁸⁷ Left ansa subclavian stimulation increases the amplitude of cesium-induced EADs in dogs and the prevalence of ventricular tachyarrhythmias more than right ansa subclavian stimulation does, possibly because of a greater quantitative effect of the left than of the right stellate ganglion on the left ventricle.

Long-QT Syndrome

Patients with heritable LQTS have an abnormally prolonged cardiac action potential duration and are at increased risk for sudden cardiac death from ventricular tachyarrhythmias (see Chapters 32 and 37). The genesis of LQTS-associated ventricular tachycardia or fibrillation is uncertain. Evidence

is mounting that an increased intracellular Ca^{2+} concentration related to spontaneous release of Ca^{2+} from the SR in cardiomyocytes, coupled with dispersion of repolarization, plays a causative role in LQTS-associated cardiac arrhythmia and sudden cardiac death. Action potential prolongation may increase influx of Ca^{2+} through L-type Ca^{2+} channels during a cardiac cycle and cause excessive accumulation of Ca^{2+} in the SR and spontaneous release of Ca^{2+} from the SR. The ensuing elevation of intracellular free calcium can depolarize cardiomyocyte membrane potential by activation of Ca^{2+} -dependent chloride currents, the electrogenic Na^+/Ca^{2+} exchange current, or both, thereby evoking EADs. EADs can trigger a propagated response and thus elicit an extra beat, which can potentially launch a tachycardia.

Genetically modified mice have been used extensively to model congenital arrhythmogenic disorders, including LQTS. However, the

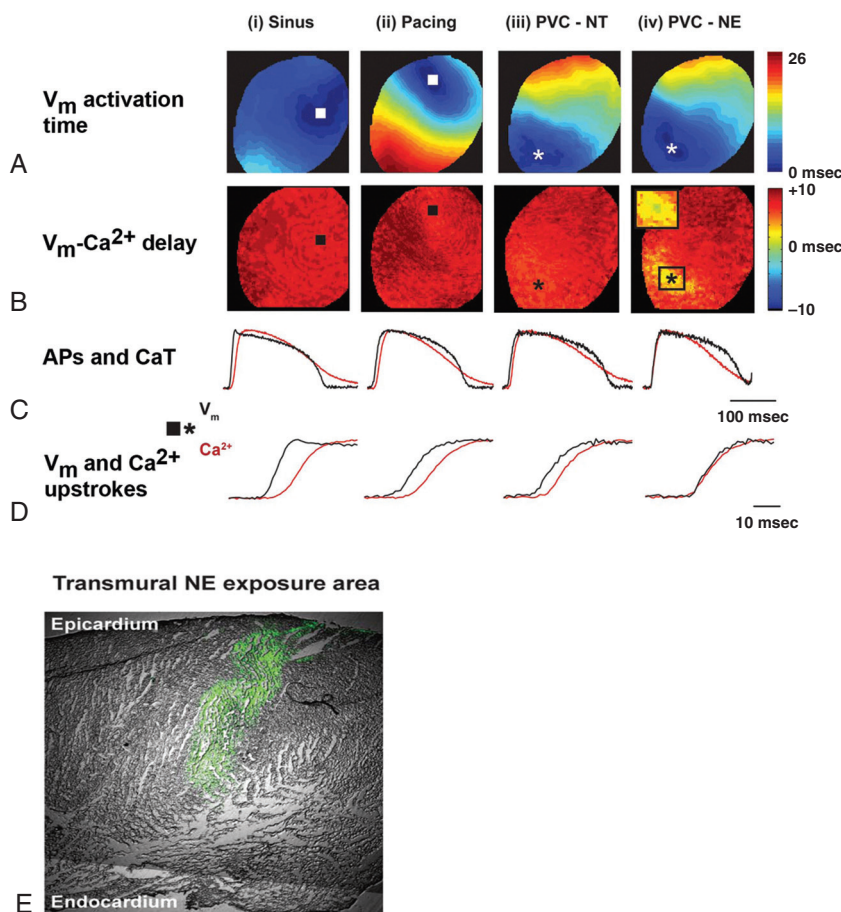


FIGURE e33-11 Ca^{2+} -induced triggered activity in the rabbit heart. **A, B**, Color-coded isochrone maps of transmembrane voltage (V_m) activation (**A**) and delay between V_m and Ca^{2+} upstroke ($V_m\text{-Ca}^{2+}$ delay; **B**) in an isolated perfused rabbit heart during (i) sinus rhythm, (ii) ventricular pacing, (iii) normal Tyrode solution (NT)-induced PVC, and (iv) norepinephrine (NE)-induced PVC. Color codes are shown on the right. During sinus rhythm, ventricular pacing, and NT-induced PVCs, Ca^{2+} activation followed V_m with a relatively uniform delay across the epicardial surface (**B**, i-iii); however, during NE-induced PVCs, areas of abnormally short $V_m\text{-Ca}^{2+}$ delays (iv) were seen at the site of earliest V_m activation, thus suggesting that beta-adrenergically mediated SR Ca^{2+} release events were of sufficient magnitude to cause a propagating action potential via activation of the Na/Ca exchanger. **C**, Optical action potentials (APs; black) and Ca^{2+} transients (CaTs; red) from the earliest activated sites. **D**, V_m and Ca^{2+} upstrokes from the earliest activated sites. **E**, Transmural section of the left ventricle showing the area of NE distribution (green) following its direct intracardiac injection. (From Myles RC, Wang L, Kang C, et al: Local α -adrenergic stimulation overcomes source-sink mismatch to generate focal arrhythmia. *Circ Res* 110:1454, 2012.)

usefulness of this approach is limited because of the profound differences in electrophysiologic properties between the murine and human heart. The ability to generate patient-specific human iPSCs offers a new paradigm for modeling human disease. Recently, several research groups have independently reported successful derivation of functional cardiomyocytes from LQTS patient-specific human iPSC lines. Electrophysiologic evaluation of LQTS cardiomyocytes demonstrated that they recapitulate the disease phenotype *in vitro*, including marked action potential prolongation and increased susceptibility to spontaneous or pharmacologically induced triggered activity.^{88,89} An example of such a study in cardiomyocytes derived from LQTS patient-specific iPSCs is summarized in **Figure e33-12**.



Large-scale production of human iPSC-derived cardiomyocytes has made it possible to generate sufficient numbers of uniform cardiac monolayers that can be used for the study of arrhythmia mechanisms *in vitro*.⁹⁰ Collectively, pluripotent stem cell technology now offers a unique platform to evaluate patient-specific arrhythmia mechanisms and to optimize patient therapy.

Experimental observations have also suggested an important role of transmural or longitudinal heterogeneity of repolarization. Marked transmural dispersion of repolarization can create a vulnerable window for the development of reentry. Direct experimental evidence of the existence of transmural dispersion in the action potential has been provided for the human heart.⁹¹ Optical voltage mapping of arterially perfused wedges from human hearts revealed significant transmural action potential gradients in the nonfailing heart ranging from a mean of 383 milliseconds (action potential duration at 80% repolarization) in the subepicardium to a mean of 494 milliseconds in the endocardium. Three of five hearts studied showed midmyocardial islands of cells that had distinctly long action potential durations averaging 537 milliseconds and a steep local action potential duration gradient of 27 msec/mm. In contrast, failing hearts were observed to have a significantly reduced transmural gradient averaging 29 milliseconds and to lack islands of cells with delayed repolarization. The ionic mechanisms underlying transmural dispersion of repolarization in the human heart are currently unknown but may involve spatial variations in expression of the transient outward potassium current I_{to} and the delayed rectifying potassium current I_{Ks} (see **Table 33-3**).

Sympathetic stimulation, primarily left, can increase the EAD amplitude to provoke ventricular tachyarrhythmias. Alpha-adrenoceptor stimulation also increases the amplitude of cesium-induced EADs and the prevalence of ventricular tachyarrhythmias, both of which are suppressed by magnesium.

In patients with acquired LQTS and torsades de pointes from drugs such as quinidine, *N*-acetylprocainamide, cisapride, erythromycin, and some class III antiarrhythmic agents, EADs can also be responsible (see **Chapters 9 and 35**). Such drugs easily elicit EADs experimentally and clinically, whereas magnesium suppresses them. It is possible that multiple drugs can cause summation effects to provoke EADs and torsades de pointes in patients. Activators of ATP-dependent potassium channels, such as pinacidil and nicorandil, can eliminate EADs.

Parasystole

Classically, parasystole has been likened to the function of a fixed-rate, asynchronously discharging pacemaker—its timing is not altered by the dominant rhythm, it produces depolarization when the myocardium is excitable, and the intervals between discharges are multiples of a basic interval (see **Chapters 36 and 37**). Complete entrance block, constant or intermittent, insulates and protects the parasystolic focus from surrounding electrical events and accounts for such behavior. On occasion, the focus can exhibit exit block, during which it may fail to depolarize excitable myocardium. In fact, the dominant cardiac rhythm may modulate parasystolic discharge to speed up or to slow down its rate. Brief subthreshold depolarizations induced during the first half of the cardiac cycle of a spontaneously discharging pacemaker delay the subsequent discharge, whereas similar depolarizations induced in the second half of the cardiac cycle accelerate it (**Fig. e33-13**).



Disorders of Impulse Conduction

Conduction delay and block can result in bradycardias or tachyarrhythmias. Bradycardias occur when the propagating impulse is blocked and is followed by asystole or a slow escape rhythm; tachyarrhythmias occur when the delay and block produce reentrant excitation (see later). Various factors involving both active and passive membrane properties determine the conduction velocity of an impulse and whether conduction is successful. Among these factors are the stimulating efficacy of the propagating impulse, which is related to the amplitude and rate of rise of phase 0; the excitability of the tissue into which the impulse is conducted; and the geometry of the tissue.

Deceleration-Dependent Block

Diastolic depolarization has been suggested as a cause of conduction block at slow rates, so-called bradycardia- or deceleration-dependent block (see **Chapter 37**). However, excitability and the speed of impulse propagation *increase* as the membrane depolarizes until approximately -70 mV despite a reduction in action potential amplitude and \dot{V}_{max} (supernormal conduction). Experiments in Purkinje fiber bundles have demonstrated that diastolic (phase 4) depolarization is not a necessary condition for the occurrence of deceleration-dependent block.⁹² Evidently, depolarization-induced inactivation of fast Na^+ channels is offset by other factors, such as a reduction in the difference between membrane potential and threshold potential and an increase in membrane excitability.

Tachycardia-Dependent Block

More commonly, impulses are blocked at rapid rates or short cycle lengths as a result of incomplete recovery of refractoriness (postrepolarization refractoriness) caused by incomplete time- or voltage-dependent recovery of excitability.⁹³ For example, such incomplete recovery is the usual mechanism responsible for a nonconducted premature P wave or one that conducts with a functional bundle branch block.

Decremental Conduction

Decremental conduction is a term used commonly in the clinical literature but is often misapplied to describe any Wenckebach-like conduction block, that is, responses similar to a block in the AV node during which progressive conduction delay precedes the nonconducted impulse. Correctly used, decremental conduction refers to a situation in which the properties of the fiber change along its length such that the action potential loses its efficacy as a stimulus to excite the fiber ahead of it. Thus the stimulating efficacy of the propagating action potential diminishes progressively, possibly as a result of its decreasing amplitude and decreasing V_{max} .

Reentry

Electrical activity during each normal cardiac cycle begins in the sinoatrial node and continues until the entire heart has been activated. Each cell becomes activated in turn, and the cardiac impulse dies out when all fibers have been discharged and are completely refractory. During this absolute refractory period, the cardiac impulse has “no place to go.” It must be extinguished and restarted by the next sinus impulse. If, however, a group of fibers not activated during the initial wave of depolarization recovers excitability in time to be discharged before the impulse dies out, the fibers may serve as a link to reexcite areas that were just discharged and have now recovered from the initial depolarization. Such a process has been given various names—reentry, reentrant excitation, circus movement, reciprocal or echo beat, or reciprocating tachycardia—all meaning approximately the same thing.

Entrainment

Entrainment of the tachycardia (i.e., increasing the rate of the tachycardia by pacing), with resumption of the intrinsic rate of the tachycardia when pacing is stopped, establishes the presence of reentry (**Fig. 33-22A**). Entrainment represents capture or continuous resetting of the reentrant circuit of the tachycardia by the pacing-induced

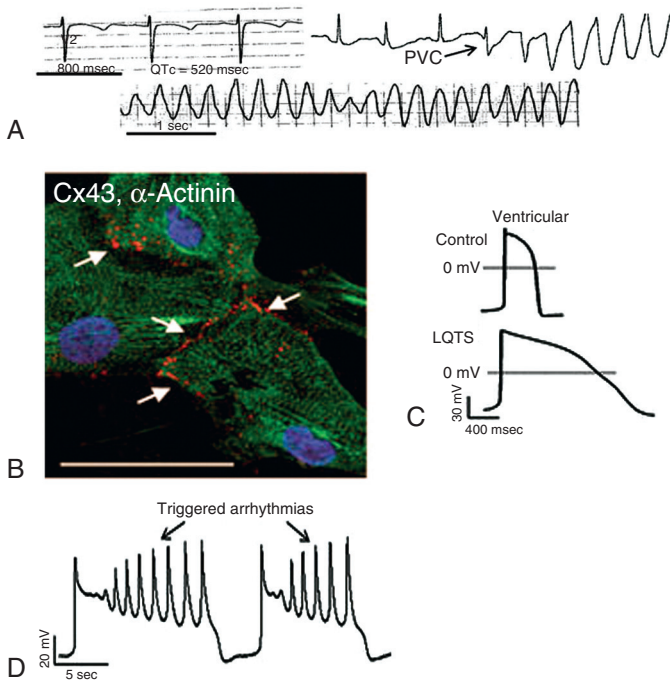


FIGURE e33-12 Recapitulation of LQTS via iPST technology. **A**, Surface electrocardiogram from a 28-year-old woman with familial type-2 LQTS as a result of a loss-of-function mutation in the *KCNH2* gene, which encodes the pore-forming subunit of the HERG potassium channel (see Table 33-3). Tracings were recorded during sinus rhythm (**upper left panel**; the QT interval corrected for heart rate is 520 milliseconds) and during initiation (**upper right panel**) and sustainment of torsades de pointes. **B**, iPSC-derived cardiomyocytes in culture express structural markers of the cardiac lineage. Dermal fibroblasts were obtained from the LQTS patient above and were reprogrammed to generate LQTS patient-specific human iPSCs via transduction with a cocktail of transcription factors. These iPSCs were then induced to differentiate into cardiomyocytes. Immunocytochemistry revealed expression of sarcomeric alpha-actinin (green) and the gap junction protein connexin 43 (red; arrows) in LQTS cardiomyocytes. **C**, Transmembrane action potential recordings from LQTS ventricular cardiomyocytes revealed a markedly prolonged action potential duration relative to recordings obtained from healthy control patient iPSC-derived myocytes, consistent with a reduction in KCNH2-encoded I_Kr in the LQTS patient. **D**, Spontaneous development of repetitive EADs in LQTS cardiomyocytes. (From Itzhaki I, Maizels L, Huber I, et al: Modeling the long QT syndrome with induced pluripotent stem cells. *Nature* 471:225, 2011.)

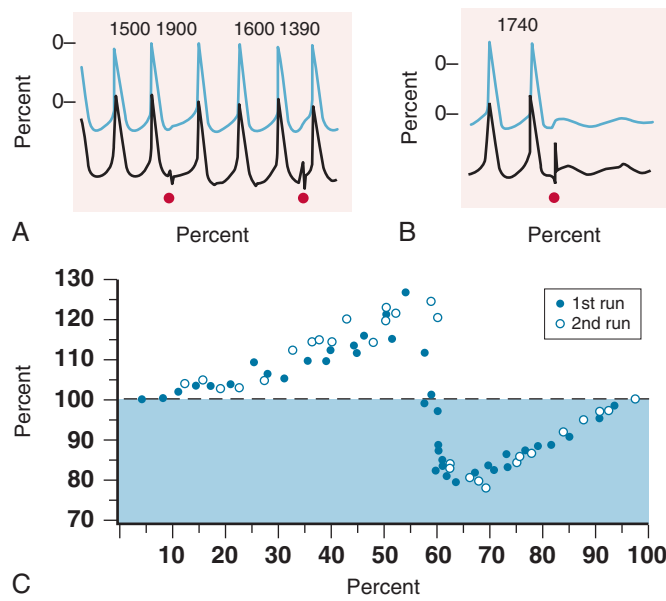


FIGURE e33-13 Modulation of pacemaker activity by subthreshold current pulses in diseased human ventricle. **A**, Two recording sites along the same trabecula in a spontaneously active preparation. Current pulses (indicated by the red dots) of 30 milliseconds in duration were injected through the lower microelectrode at various times. The interval between the spontaneous action potentials is given in milliseconds above each cycle. Injection of a subthreshold current pulse through the lower microelectrode relatively early in the spontaneous cycle (\approx 680 msec after initiation of the rapid portion of the preceding action potential upstroke) produced a subthreshold depolarization in the upper recording and delayed the next spontaneous discharge by 400 to 1900 milliseconds. This response curve would fall in the first half of the curve indicated in **C**. A current pulse of the same intensity and duration delivered later in the spontaneous cycle (950 msec after the preceding upstroke) accelerated the next discharge by 210 to 1390 milliseconds relative to the previous two action potentials. The response to this current injection falls in the second half of the graph depicted in **C**. **B**, A stimulus at a precise interval in the cardiac cycle (called the singular point; in this example, 930 msec after the preceding action potential upstroke) abolishes pacemaker activity. **C**, Phase-response curves from experimental data obtained in canine Purkinje fibers in a manner similar to that in the human experiment shown in **A** and **B**. Two different runs are shown. The ordinate in this graph is the percent age increase or decrease in spontaneous cycle length of the “parasystolic focus” (control cycle length equals 100%); the abscissa is the percentage of the “parasystolic focus” spontaneous cycle length during which stimulation was performed. The spontaneous cycle length was maximally prolonged (by 26%) or shortened (by 20%) by subthreshold depolarizations that entered the parasystolic focus after approximately 50% and 60% of the cycle had elapsed, respectively. Very similar curves can be plotted for patients with paroxysm (e.g., see Figs. 9 and 10 in Zipes DP: Plenary lecture. Cardiac electrophysiology: Promises and contributions. *J Am Coll Cardiol* 13:1329, 1989). (**A, B**, From Gilmour RF Jr, Heger JJ, Prystowsky EN, et al: Cellular electrophysiological abnormalities of diseased human ventricular myocardium. *Am J Cardiol* 51:137, 1983; **C**, from Jalife J, Moe GK: Effect of electronic potentials on pacemaker activity of canine Purkinje fibers and relation to paroxysm. *Circ Res* 39:801, 1976. With permission from the American Heart Association.)

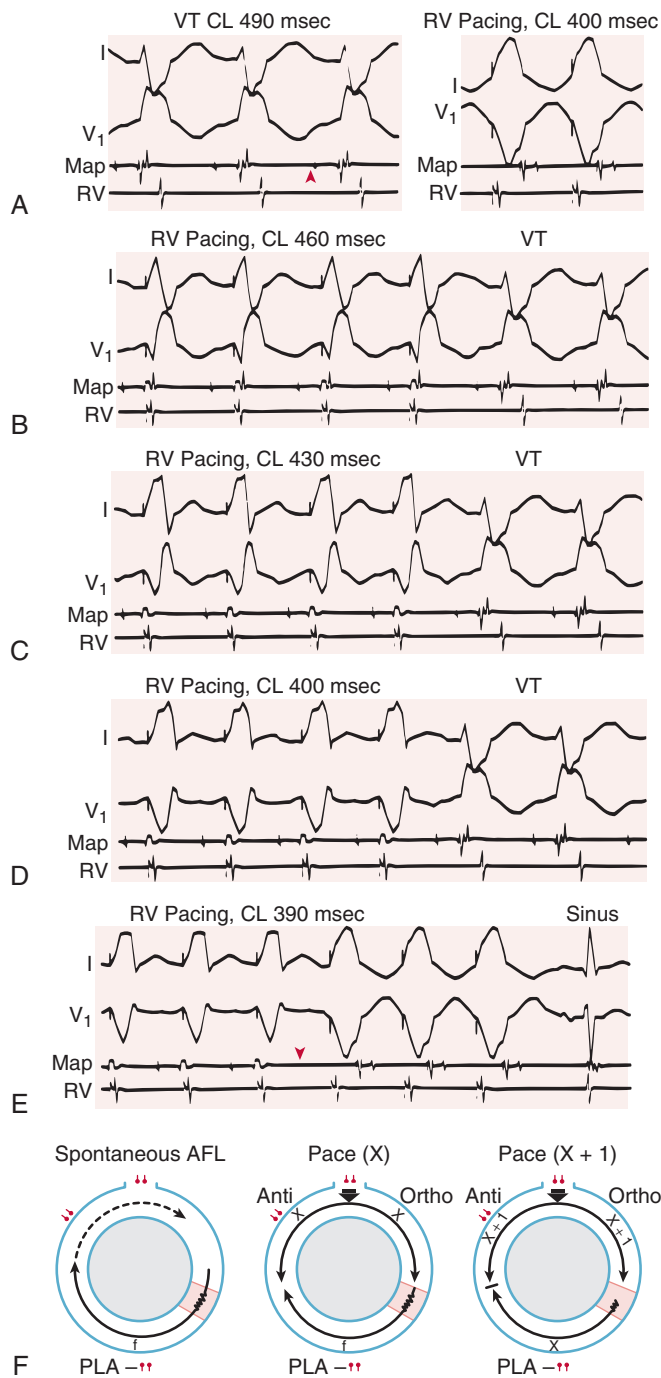


FIGURE 33-22 A-E. Criteria for entrainment exemplified in a case of postinfarction ventricular tachycardia (VT). **A, left,** Two leads of the electrocardiogram of a VT and intracardiac recordings from a mapping catheter (Map) at a left ventricular site critical for VT continuation, as well as from the right ventricular apex (RV). Note the diastolic potential (red arrowhead) during VT. Recordings are similarly arranged in all subsequent panels. **A, right,** RV pacing in the setting of sinus rhythm. **B, RV Pacing, CL 400 msec**, **C, RV Pacing, CL 460 msec**, **D, RV Pacing, CL 430 msec**, **E, RV Pacing, CL 400 msec**. RV pacing at a cycle length (CL) slightly shorter than VT produces a QRS complex that is a blend between fully VT and fully paced ("fusion") complexes. All recordings are accelerated to the paced CL, and after pacing ceases, the same VT resumes. Each fused QRS complex is identical and the last beat is entrained, but surface fusion is absent. **C, D,** The same phenomena, but at shorter paced CLs. Note that the fused QRS complex appears to be more similar to pacing than it does to VT as the pacing CL shortens. **B-D**, Progressive degrees of fusion on the electrocardiogram. The Map recording of **B** through **D** also shows a progression of fusion, with both the morphology and timing of a portion of the electrogram changing with faster pacing. **E**, Finally, a still shorter paced CL results in a sudden change in both the Map electrogram (block in the small diastolic potential, red arrowhead) and the surface electrocardiogram, which is now fully paced. When pacing ceases, VT has been interrupted. **F**, Diagrammatic representation of the reentrant circuit during spontaneous atrial flutter (AFL) and transient entrainment of the AFL. **Left,** The reentrant circuit during spontaneous type I AFL. f = circulating wave front of the AFL. **Center,** Introduction of the first pacing impulse (X) during rapid pacing from a high atrial site during AFL. The large arrow indicates entry of the pacing impulse into the reentrant circuit, whereupon it is conducted orthodromically (Ortho) and antidromically (Anti). The antidiromic wave front of the pacing impulse (X) collides with the previous beat, in this case the circulating wave front of the spontaneous AFL (f), which results in an atrial fusion beat and, in effect, terminates the AFL. However, the orthodromic wave front from the pacing impulse (X) continues the tachycardia and resets it to the pacing rate. **Right,** Introduction of the next pacing impulse (X + 1) during rapid pacing from the same high atrial site. The large arrow again indicates entry of the pacing impulse into the reentrant circuit, whereupon it is conducted orthodromically and antidromically. Once again, the antidiromic wave front from the pacing impulse (X + 1) collides with the orthodromic wave front of the previous beat. In this case it is the orthodromic wave front of the previous paced beat (X), and an atrial fusion beat results. The orthodromic wave front from the pacing impulse (X + 1) continues the tachycardia and resets it to the pacing rate. In all three parts, arrows indicate the direction of spread of the impulses; the serpentine line indicates slow conduction through a presumed area of slow conduction (stippled region) in the reentrant circuit; and the red dots with tails indicate bipolar electrodes at the high atrial pacing site, the posteroinferior portion of the left atrium (PLA), and another atrial site. **(A-E)**, From Zipes DP. A century of cardiac arrhythmia: In search of Jason's golden fleece. *J Am Coll Cardiol* 34:959, 1999. **F**, from Waldo AL: Atrial flutter. Entrainment characteristics. *J Cardiovasc Electrophysiol* 8:337, 1997.

activation. Each pacing stimulus creates a wave front that travels in an anterograde direction (orthodromic) and resets the tachycardia to the pacing rate. A wave front propagating retrogradely in the opposite direction (antidromic) collides with the orthodromic wave front of the previous beat (Fig. 33-22B). These wave front interactions create electrocardiographic and electrophysiologic features that can be explained only by reentry. Therefore the criteria of entrainment can be used to prove the reentrant mechanism of a clinical tachycardia and form the basis for localizing the pathway traveled by the tachycardia wave front. Such localization is essential for ablation therapy.

Anatomic Reentry

Studies on reentry have used models with anatomically defined separate pathways in which it could be shown that they had an area of unidirectional block and recirculation of the impulse to its point of

origin. An example using AV nodal reentry is illustrated in Figure 33-23. Because the two pathways have different electrophysiologic properties (e.g., shorter refractory period and slower conduction in one pathway versus a longer refractory period and faster conduction of the other), the impulse is first blocked in one pathway with a longer refractory period (green area in Fig. 33-23) and then propagates slowly in the adjacent pathway whose refractory period is shorter (red area in Fig. 33-23A, right panel). If conduction in this alternative route is sufficiently depressed, the slowly propagating impulse excites tissue beyond the blocked pathway (see Fig. 33-23A, right panel, dashed yellow arrow) and returns in a reversed direction along the pathway initially blocked to reexcite tissue proximal to the site of block. A clinical arrhythmia caused by anatomic reentry is most likely to have a monomorphic contour (Video 33-3).¹¹

For reentry of this type to occur, the time for conduction within the depressed but unblocked area and for excitation of the distal segments must exceed the refractory period of the initially blocked pathway (Fig. 33-24A; also see Fig. 33-23 and Video 33-4, which shows electrical reentry in the infarct border zone) and the tissue proximal to the site of block. Stated another way, continuous reentry requires the anatomic length of the circuit traveled to equal or exceed the reentrant wavelength. The latter is equal to the mean conduction velocity of the impulse multiplied by the longest refractory period of the elements in the circuit. Both values can be different at different points along the reentry pathway, and thus the wavelength value is somewhat contrived.

Conditions for Reentry

The length of the pathway is fixed and determined by the anatomy. Conditions that depress conduction velocity or abbreviate the refractory period promote the development of reentry in this model, whereas prolonging refractoriness and speeding conduction velocity

**VIDEO 33-3**

Simulation of fast-slow reentry using an electroanatomical model. Responses to S1 and S2 stimuli are shown. S1-S2 interval is 96 ms. The preparation was stimulated at the His bundle as shown by the stimulating electrodes. There is a flash and click coincident with each stimulus. (From Li J, Greener ID, Inada S, et al: Computer three-dimensional reconstruction of the atrioventricular node. *Circ Res* 102:975, 2008.)

VIDEO 33-4

Simulation of electrical reentry in a three-dimensional model of the infarct border zone. The model was paced with a stimulus train at a basic cycle length of 300 ms (S_1) and the coupling interval (S_1S_2) was progressively reduced until block occurred. The subepicardial pacing site is marked by a red sphere in sequence 1 and 2. Activation sequences 1 and 2 were obtained during subepicardial pacing at a coupling interval of 157 ms. Propagation of beat 1 is blocked within the subepicardial border zone, but not across the junction of the border zone and the midwall or at the network boundary (green line), which connects the subepicardial and subendocardial border zones, although at reduced propagation speed. Paced beat 2 fails to propagate from the border zone to the midwall (unidirectional block) and stable re-entrant activation occurs. (From Rutherford SL, Trew ML, Sands GB, et al: High-Resolution 3-Dimensional Reconstruction of the Infarct Border Zone. *Circ Res* 2012 Jun 19.)

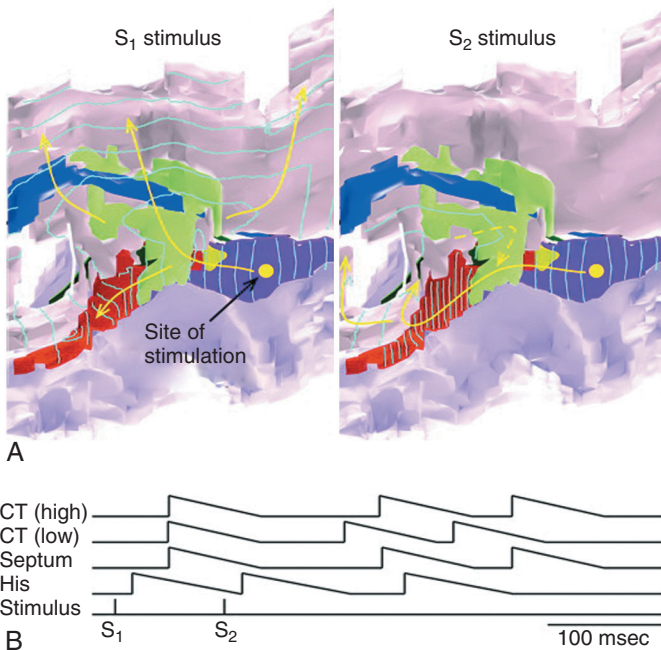


FIGURE 33-23 Simulation of reentry in a model of the AV node. **A**, Electrical stimuli are applied to the His bundle (yellow point) by using an S₁-S₂ protocol (S₁-S₂ interval, 96 milliseconds). The activation sequences (shown as isochrones in 5-millisecond intervals) in response to S₁ and S₂ stimuli are shown. Arrows highlight the conduction pathways. Two stimuli are delivered. The S₁ action potential exits into the atrial muscle via the transitional tissue (green area), the putative fast pathway. The premature S₂ action potential fails to exit via the transitional tissue because the S₁-S₂ interval is shorter than the refractory period of the transitional tissue. Instead, the S₂ action potential exits into atrial muscle via the inferior nodal extension (INE, the putative slow pathway; red area) because the refractory period of the INE is shorter. The conduction velocity within the INE is low, as indicated by the isochrone crowding within the red area. The action potential then propagates anterogradely along the fast pathway (transitional tissue is no longer refractory) back into the His bundle. **B**, Simulated action potentials (at the high and low crista terminalis, interatrial septum, and His bundle) at different time points on the reentry circuit during S₁-S₂ stimulation. The S₂ action potential retrogradely excites atrial tissue (the action potential at the low crista terminalis appears first) and then anterogradely the His bundle, thereby completing one reentry cycle. The reentry beat propagates along the INE and out into the atrial muscle once more but then fails to anterogradely reexcite the His bundle. Color coding of the various tissue types is the same as in Figure 33-7. (From Li J, Greener ID, Inada S, et al: Computer three-dimensional reconstruction of the atrioventricular node. Circ Res 102:975, 2008. By permission of the American Heart Association.)

can hinder it. For example, if conduction velocity (0.30 m/sec) and refractoriness (350 milliseconds) for ventricular muscle were normal, a pathway of 105 mm ($0.30 \text{ m/sec} \times 0.35 \text{ sec}$) would be necessary for reentry to occur. However, under certain conditions, conduction velocity in ventricular muscle and Purkinje fibers can be very slow (0.03 m/sec), and if refractoriness is not greatly prolonged (600 milliseconds), a pathway of only 18 mm ($0.03 \text{ m/sec} \times 0.60 \text{ sec}$) may be necessary. Such reentry frequently exhibits an excitable gap, that is, a time interval between the end of refractoriness from one cycle and the beginning of depolarization in the next, when tissue in the circuit is excitable. This condition results because the wavelength of the reentrant circuit is less than the length of the pathway. Electrical stimulation during this period can invade the reentrant circuit and reset its timing or terminate the tachycardia. Although "microanatomic" reentry (confinement of the reentrant circuit to a few adjacent myocytes) has been postulated to occur in fibrotic myocardium,⁹³ its occurrence in intact heart muscle has not been demonstrated directly. This difficulty results from the inability to unambiguously distinguish microreentry from triggered activity with currently available techniques.

Rapid pacing can entrain the tachycardia, that is, continuously reset it by entering the circuit and propagating around it in the same way as the reentrant impulse, which increases the tachycardia rate to the pacing rate without terminating the tachycardia (see

Fig. 33-22). In reentrant circuits with an excitable gap, conduction velocity determines the revolution time of the impulse around the circuit and therefore the rate of the tachycardia. Prolongation of refractoriness, unless it is long enough to eliminate the excitable gap and make the impulse propagate in relatively refractory tissue, does not influence the revolution time around the circuit or the rate of the tachycardia. Anatomic reentry occurs in patients with Wolff-Parkinson-White syndrome, in AV nodal reentry, in some atrial flutters, in some ventricular tachycardias, and in VF. For example, mapping studies in isolated ovine atria have demonstrated key roles of anatomic structures (e.g., fibrotic patches) in the maintenance of reentry during fibrillation.⁹⁴

Functional Reentry

Functional reentry lacks confining anatomic boundaries and can occur in contiguous fibers that exhibit functionally different electrophysiologic properties caused by local differences in transmembrane action potential (e.g., Purkinje-myocyte transition). Dispersion of excitability, refractoriness, or both, as well as anisotropic distributions of intercellular resistance, permit initiation and maintenance of reentry. Functional heterogeneity in the electrophysiologic properties of the myocardium has been shown to contribute to the generation and maintenance of tachycardia and fibrillation. These heterogeneities can be fixed, as in the case of spatial redistribution of gap junctions in the failing heart⁴⁹ or infarct border zone or in the case of spatial gradients in the magnitude of the background K⁺ current I_{K1} (see Fig. 33-24B).⁹⁵ They can also change dynamically, as in an acutely ischemic myocardium⁹⁶ or in the presence of repolarization-prolonging agents.⁹⁷ A very important determinant of the dynamically induced component of heterogeneity has been identified as electrical restitution, or variation of the action potential duration and conduction velocity with the diastolic interval.⁹⁸ It has been proposed that the breakup of periodic waves is precipitated by oscillations in the action potential duration (so-called action potential duration alternans) of sufficiently large amplitude to cause conduction block along a spiral wave front (see Fig. 33-27).

Tachycardias Caused by Reentry

Reentry is probably the cause of many tachyarrhythmias, including various types of supraventricular and ventricular tachycardias, flutter, and fibrillation (see Chapter 37).

Atrial Flutter

Reentry is the most likely cause of the usual form of atrial flutter, with the reentrant circuit being confined to the right atrium in typical atrial flutter, where it usually travels counterclockwise in a caudocranial direction in the interatrial septum and in a craniocaudal direction in the right atrial free wall. An area of slow conduction is present in the posterolateral to posteromedial inferior area of the right atrium, along with a central area of block that can include an anatomic (inferior vena cava) and functional component. This area of slow conduction is rather constant and represents the site of successful ablation of atrial flutter. Ablation results are consistent with a macroreentry circuit.

Different reentrant circuits exist in patients with other types of atrial flutter, such as those that occur after surgery or ablation or are associated with an atrial septal defect (see Chapter 62).

Atrial Fibrillation

Spatiotemporal Organization and Focal Discharge

According to the multiple-wavelet hypothesis, AF is characterized by fragmentation of the wave front into multiple daughter wavelets (see Chapter 38). They wander randomly throughout the atrium and give rise to new wavelets that collide with each other and are mutually annihilated or that give rise to new wavelets in a perpetual activity.

The randomness of the irregular electrical activity during AF has been disputed on the basis of both statistical methods and

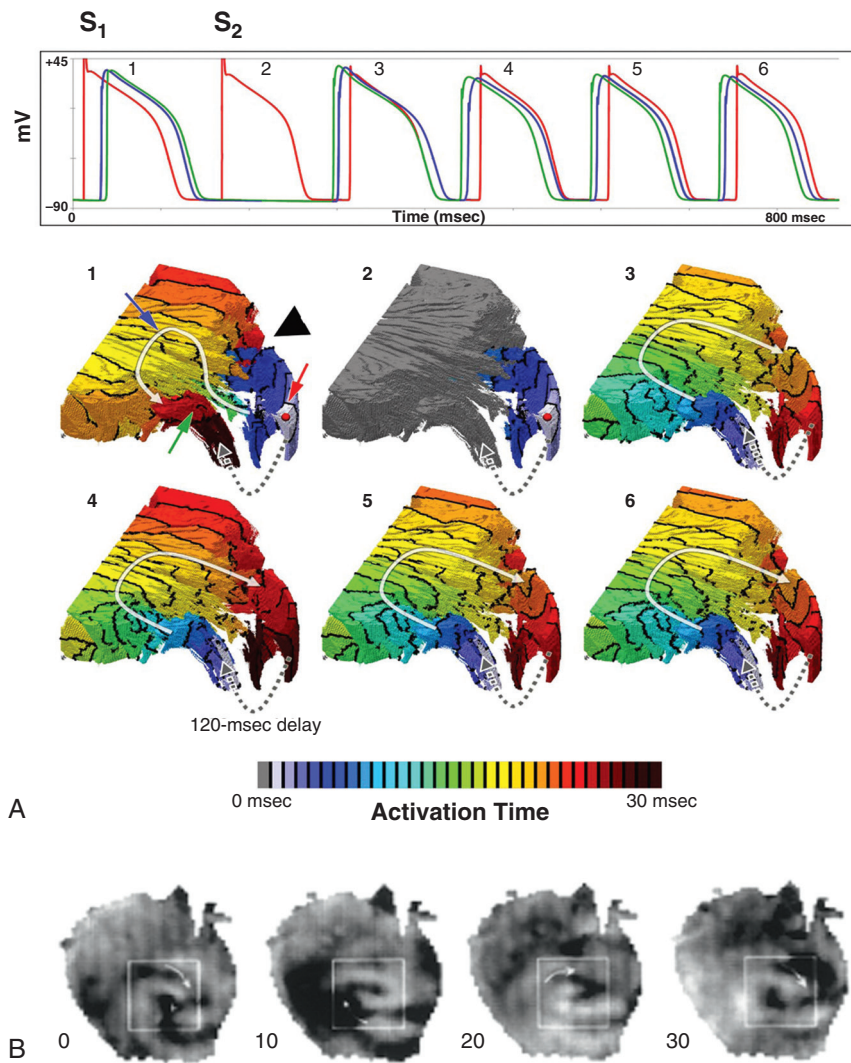


FIGURE 33-24 Models of reentry. **A**, Simulation of electrical reentry in the infarct border zone. Panels 1 through 6 show three-dimensional reconstructions of voltage activation in a high-resolution model of the infarct border zone during electrical stimulation at the subepicardial border zone (red sphere in panels 1 and 2) and during sustained electrical reentry (panels 3 through 6). The model was paced with a stimulus train at a basic cycle length of 300 milliseconds (S_1), and the coupling interval between S_1 and S_2 was progressively reduced until block occurred. The upper panel shows action potential traces at the subepicardial border zone (red), midwall (green), and subendocardial border zone (blue) sites indicated by arrows in panel 1. Numbers above the action potential trace correspond to the voltage activation sequences of beats 1 to 6. Beats 1 and 2 are paced with a coupling interval (S_1-S_2) of 157 milliseconds. Propagation of beat 1 is blocked within the subepicardial border zone (arrowhead) but not at the junction of the border zone and the midwall (solid white line) or at the network boundary (dashed line), although conduction along these paths is slow. Beat 2 fails to propagate from the border zone to the midmyocardium (unidirectional block), and sustained reentrant activation occurs in beats 3 to 6. (For more on the activation time series, see Video 33-4.) **B**, Spiral wave model. Recording of spiral wave reentry during VF in a Langendorff-perfused guinea pig heart using a potentiometric fluorophore. Shown are the distributions of membrane potentials at four different times during one rotation on the left ventricular epicardial surface, with white and black being the most positive and most negative membrane potentials, respectively. Numbers are time in milliseconds. Arrows denote the direction of wave front propagation. (**A**, From Rutherford SL, Trew ML, Sands GB, et al: High-resolution 3-dimensional reconstruction of the infarct border zone. *Circ Res* 111:301, 2012; **B**, from Samie FH, Berenfeld O, Anumonwo J, et al: Background potassium current. A determinant of rotor dynamics in ventricular fibrillation. *Circ Res* 89:1216, 2001. By permission of the American Heart Association.)

experimental studies. A combination of high-resolution video imaging, recordings of the electrocardiogram, and spectral analysis was used to demonstrate that reentry in anatomically or functionally determined circuits forms the basis of spatiotemporal periodicity during acute AF. The cycle length of the source in the left atrium determines the dominant peak in the frequency spectra. The underlying periodicity may stem from a repetitive focal source of activity propagated from an individual pulmonary vein or left atrial site to the remainder of the atrium as fibrillating waves. If a single repetitive focal source of activity that undergoes fractionation underlies the maintenance of AF, ablation of this focal source should interrupt AF. Indeed, delivery of radiofrequency energy to discrete sites in the distal pulmonary veins in humans has been shown to eliminate or reduce recurrence of AF. In a large animal model of inducible AF associated with heart failure, it was recently demonstrated that AF dynamics is characterized by rapid repetitive activation (resulting from either microanatomic reentry or triggered activity) revolving around fibrotic obstacles in the posterior

left atrium or pulmonary vein ostia. Furthermore, fibrillatory activity was maintained by intramural reentry centered on fibrotic patches and appeared as endocardial breakthroughs at the posterior left atrium (endocardial breakthroughs are considered sudden and unexpected appearances of localized electrical activity not related to activation or slow conduction in the surrounding regions). In atria with heart failure, AF waves changed the origin and direction of propagation on a beat-to-beat basis, whereas in normal left atria, the breakthrough sites and direction of activation of AF wave fronts were highly recurrent from one AF wave to the next (Fig. e33-14 and Video 33-5). Interestingly, numeric simulations of AF dynamics best recapitulated the experimental observations in this study when cardiomyocytes were assumed to be electrotonically coupled to myofibroblasts, thus supporting a role of heterocellular electrical coupling in atrial arrhythmogenesis.⁹⁴

Several experimental models have been used to study the structural and basic electrophysiologic properties of pulmonary veins that

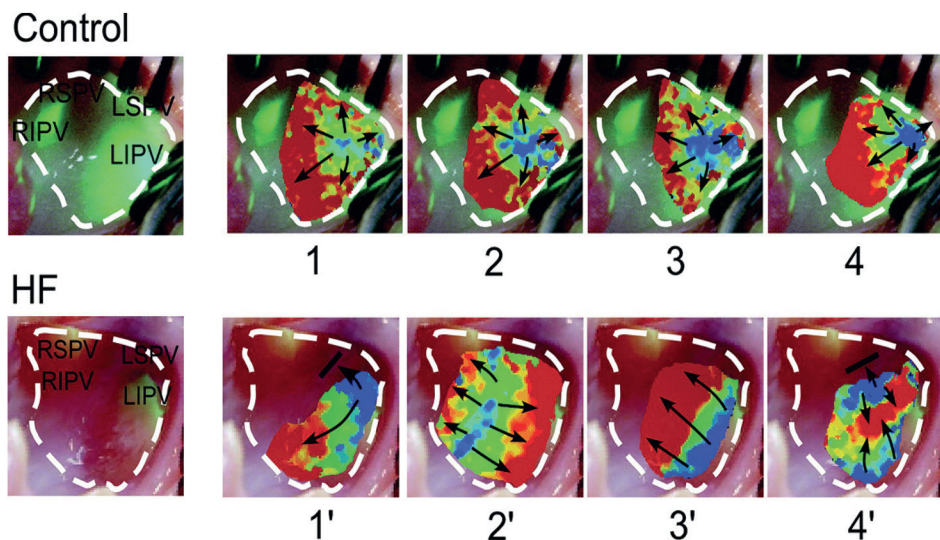


FIGURE e33-14 Left atrial activation maps of four consecutive AF waves at the posterior aspect of the left atrium from a control animal and an animal with experimentally induced heart failure. Activation times are color-coded, with the earliest and latest activation encoded in blue and red, respectively. The activation maps were superimposed on a color picture of the preparation. The patterns of propagation are highly recurrent in the control in comparison to the heart failure (HF) atrium. LIPV = left inferior pulmonary vein; LSPV = left superior pulmonary vein; RIPV = right inferior pulmonary vein; RSPV = right superior pulmonary vein. (From Tanaka K, Zlochiver S, Vikstrom KL, et al: Spatial distribution of fibrosis governs fibrillation wave dynamics in the posterior left atrium during heart failure. *Circ Res* 101:839, 2007.)

VIDEO 33-5

Phase movie of posterior left atrial activation during atrial fibrillation in an ovine heart with experimentally induced congestive heart failure, showing changing and peripherally located endocardial breakthroughs. The wavefront is depicted in blue-purple and the wavetail is shown in yellow. The phase movie was generated using the delay embedding method. (From Tanaka K, Zlochiver S, Vikstrom KL, et al: Spatial distribution of fibrosis governs fibrillation wave dynamics in the posterior left atrium during heart failure. *Circ Res* 101:839, 2007.)

are thought to play a role in initiation and maintenance of AF. Morphologic studies have demonstrated the presence of complex anatomic structures and phenotypically different cardiomyocytes in pulmonary veins.^{99,100} Electrophysiologic studies have shown that a combination of reentrant and nonreentrant mechanisms (automaticity and triggered activity) is the underlying arrhythmic mechanism for initiation of AF from the pulmonary veins.^{100,101} Abnormal intracellular calcium handling probably plays a pivotal role in the pulmonary vein electrical activity. Dual mapping of cardiomyocyte membrane potential and intracellular free calcium has demonstrated the appearance of spontaneous calcium release events resulting in focal discharge.⁹⁰ The role of dysfunction of calcium-handling proteins (e.g., Na⁺/Ca²⁺ exchanger, ryanodine receptor calcium release channels) in AF awaits further investigation.

Ion Channel Abnormalities in Atrial Fibrillation

Monogenic (Familial) Atrial Fibrillation. Although familial forms of AF are relatively rare, identification of mutations in AF kindreds has provided valuable insight into the molecular pathways underlying the arrhythmia.¹⁰² Most mutations linked to familial AF have been located in genes that encode sodium or potassium channel subunits. Functional analyses of these mutations have revealed either gain-of-function or loss-of-function effects. Mutations in genes encoding pore-forming alpha or auxiliary beta subunits of the delayed rectifier potassium channel and the voltage-gated sodium channel (I_{K_s} and I_{Na_p} , respectively; see Table 33-3) have been reported in familial AF. The mechanisms by which these mutations cause AF are not clearly understood. Gain-of-function mutations in I_{K_s} give rise to increased repolarizing currents, which then shorten the action potential duration and atrial refractoriness, thereby facilitating fibrillatory activity. An augmented inward sodium current can induce triggered activity. Conversely, a reduced inward sodium current promotes reentry by abbreviating the action potential duration/refractoriness and thus the reentry wavelength. Other potassium channel mutations associated with AF have been localized to the *KCNJ2* and *KCNA5* genes, which encode the inward rectifier and ultrarapid delayed rectifier potassium current, respectively (see Table 33-3). Finally, mutations in the *GJA5* gene, which encodes the gap junction channel subunit connexin 40, have been linked to familial AF. Functionally, abnormal intercellular electrical coupling can result in conduction heterogeneity and facilitate reentry.

Genome-Wide Association Studies for Lone Atrial Fibrillation. Genome-wide association studies have identified variations in multiple genomic regions that are associated with lone AF.^{103,104} These regions encode ion channels (e.g., the calcium-activated potassium channel gene *KCNN3* and the HCN channel gene *HCN4*), transcription factors related to cardiopulmonary development (e.g., the homeodomain transcription factor *PRRX1*), and cell-signaling molecules (e.g., CAV1, a cellular membrane protein involved in signal transduction). The mechanistic links between these genetic variations and susceptibility to AF remain to be determined.

A number of experimental studies have probed the primary role of abnormalities in ion channel expression or properties in causing AF. Rapid pacing-induced AF in dogs causes a decrease in binding of FKBP-12.6 to the ryanodine receptor Ca²⁺ release channel (see Fig. e33-5), thereby resulting in diastolic SR Ca²⁺ leakage, which in turn, through activation of Ca²⁺-sensitive currents, can initiate electrical instability and contribute to AF.¹⁰⁵ Mice with a genetic gain-of-function defect in the gene encoding the type 2 ryanodine receptor exhibit increased susceptibility to inducible AF. AF induction in this animal model may involve triggered activity arising from EADs, whereas maintenance of AF requires reentrant activity.⁸³ Cav1.3 Ca²⁺ channel-deficient mice exhibit increased susceptibility to inducible atrial flutter and AF.¹⁰⁶ Mice in which the gene encoding KCNE1, an auxiliary subunit of the pore-forming K⁺ channel alpha subunit KCNQ1, has been knocked out display frequent spontaneous episodes of AF.¹⁰⁷

Electrical Remodeling of the Atria

Electrical remodeling of the atria appears to be a key determinant for maintenance of AF. Prolonged rapid atrial rates cause electrophysiologic alterations in the atria, including shortening and loss of the physiologic rate adaptation of refractoriness and a decrease in conduction velocity. Because abbreviation of the atrial refractory period is disproportionately larger than the reduction in conduction velocity, the wavelength of the reentrant wavelets shortens and thereby promotes reentrant activity.

The ionic basis of shortening of the refractory period and slowing of conduction may be a significant reduction in the density of the L-type Ca²⁺ and the fast Na⁺ currents. The electrophysiologic changes are paralleled by similar decreases in messenger RNA levels of Ca²⁺ and Na⁺ channel genes, which suggests alterations in gene expression as the underlying molecular mechanisms of atrial electrical remodeling. Changes in the density, spatial distribution, or both of various connexin types may also cause alterations in atrial impulse propagation. In addition, autonomic remodeling appears to play a key role in both triggering and maintaining AF. Long-term selective vagal denervation of the atria and sinoatrial and AV nodes prevents induction of AF. Heterogeneous sympathetic denervation of the atria favors the development of sustained AF.

Sinus Reentry

The sinoatrial node shares with the AV node electrophysiologic features such as the potential for dissociation of conduction, that is, an impulse can be conducted in some nodal fibers but not in others, thereby permitting reentry to occur (see Chapter 37). The reentrant circuit can be located entirely within the sinoatrial node or involve both the sinoatrial node and atrium. Supraventricular tachycardias caused by sinus node reentry are generally less symptomatic than other supraventricular tachycardias because of slower rates. Ablation of the sinoatrial node may occasionally be necessary for refractory tachycardia.

Atrial Reentry

Reentry within the atrium, unrelated to the sinoatrial node, can be a cause of supraventricular tachycardia in humans. Distinguishing atrial tachycardia caused by automaticity or afterdepolarizations from atrial tachycardia sustained by reentry over small areas (i.e., microanatomic reentry) is difficult.

Atrioventricular Nodal Reentry

Differences in the electrical properties of the various tissue types that contribute to the AV node are responsible for AV nodal reentrant tachycardia (AVNRT; see Figs. 33-7 and 33-23). Optical mapping of AV nodal transmembrane action potentials during echo beats reveals the reentrant pathways underlying the various types of AVNRT (Fig. 33-25; see also Fig. 33-7 for nomenclature of the AV nodal regions). The reentrant pathway of the slow-fast type starts counterclockwise with a block in the fast pathway (the transitional zone; see the light green area in Fig. 33-7), delay in conduction across the slow pathway (the inferior nodal extension; see the red area in Fig. 33-7) to the compact AV node (triangular-shaped, colored area to the left of black dot 4 in Fig. 33-7), exit from the AV node to the fast pathway, and rapid return to the slow pathway through atrial tissue located at the base of the triangle of Koch. The reentrant circuit of the fast-slow type is clockwise. In the slow-slow type, anterograde conduction is over the intermediate pathway and retrograde conduction is over the slow pathway. Because slow-pathway conduction is involved in each type of AVNRT, ablation of the slow pathway is effective for all types of AVNRT. These results also demonstrate that atrial tissue surrounding the triangle of Koch is clearly involved in all three types of AV nodal reentry in these examples.

Preeexcitation Syndrome

In most patients who have reciprocating tachycardias associated with Wolff-Parkinson-White syndrome, the accessory pathway conducts more rapidly than the normal AV node but takes a longer time to recover excitability; that is, the anterograde refractory period of the accessory pathway exceeds that of the AV node at long cycles. Consequently, a premature atrial complex that occurs sufficiently early is blocked anterogradely in the accessory pathway and continues to the ventricle over the normal AV node and His bundle. After the ventricles have been excited, the impulse is able to enter the accessory pathway retrogradely and return to the atrium. A continuous conduction loop of this type establishes the circuit for the tachycardia. The usual (orthodromic) activation wave during such a reciprocating tachycardia in a patient with an accessory pathway occurs anterogradely over the normal AV node-His-Purkinje system

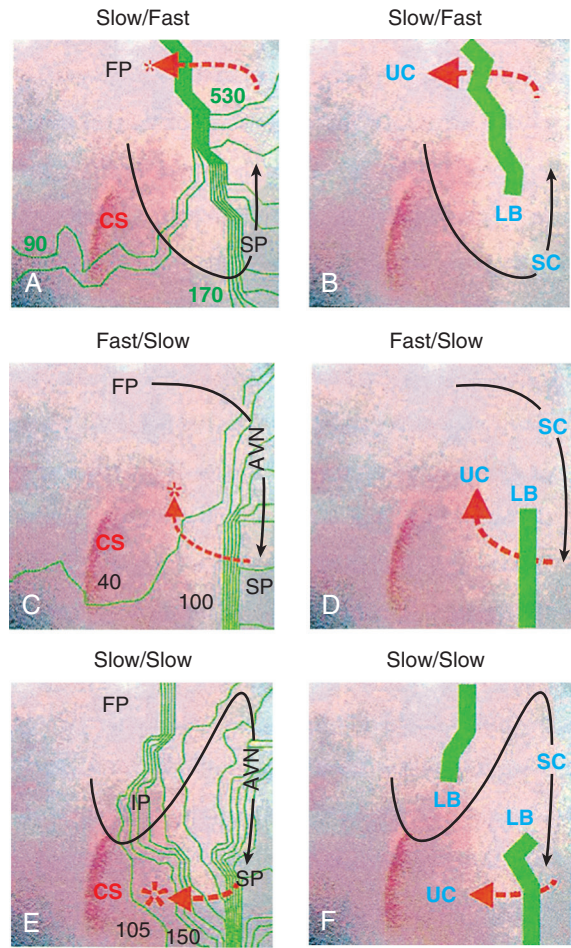


FIGURE 33-25 Reentrant circuits of different types of AVNRT. Pictures of the optical activation maps of A_2 obtained from three different experiments at A_2 coupling intervals of 190, 220, and 190 milliseconds, respectively, were merged with the pictures of the mapping area to show the initiation of echo beats in **A** (Slow/Fast), **C** (Fast/Slow), and **E** (Slow/Slow). The numbers on the maps indicate the activation times in reference to the A_2 stimulus. The black arrow indicates anterograde conduction, and the asterisk and the dashed red arrow represent the site of earliest retrograde atrial activation. The corresponding locations of the lines of block (LB, green), slow anterograde conduction (SC, black arrow), and unidirectional conduction (UC, red) are shown in **B**, **D**, and **F**, respectively. CS = coronary sinus; FP = fast pathway; IP = intermediate pathway; SP = slow pathway. (From Wu J, Zipes DP: Mechanisms underlying atrioventricular nodal reentrant tachycardia using optical mapping. *J Cardiovasc Electrophysiol* 13:831, 2002.)

and retrogradely over the accessory pathway, which results in a normal QRS complex (**Fig. 33-26**).

Because the circuit requires both atria and ventricles, the term *supraventricular tachycardia* is not precisely correct, and the tachycardia is more accurately termed *atrioventricular reciprocating tachycardia* (AVRT). The reentrant loop can be interrupted by ablation of the normal AV node–His bundle pathway or the accessory pathway. On occasion, the activation wave travels in a reverse (antidromic) direction to the ventricles over the accessory pathway and to the atria retrogradely up the AV node. Two accessory pathways can form the circuit in some patients with antidromic AVRT. In some patients the accessory pathway may be capable of only retrograde conduction (“concealed”), but the circuit and mechanism of AVRT remain the same. Less commonly, the accessory pathway can conduct only anterogradely. The pathway can be localized by analysis of the scalar electrocardiogram. Patients can have AF as well as AVRT. Developmental studies in mice have demonstrated that myocardium-specific inactivation of T-box 2, a transcription factor essential for AV canal patterning, leads to the formation of fast-conducting accessory path-

ways, malformation of the annulus fibrosus, and ventricular preexcitation in mice (**Fig. e33-15**).¹⁰⁸

Unusual accessory pathways with AV node-like electrophysiologic properties, that is, nodofascicular or nodoventricular fibers, can constitute the circuit for reciprocating tachycardias in patients who have some form of Wolff-Parkinson-White syndrome. Tachycardia in patients with nodoventricular fibers can be caused by reentry, with these fibers being used as the anterograde pathway and the His-Purkinje fibers and a portion of the AV node being used retrogradely. In the putative Lown-Ganong-Levine syndrome (short PR interval and normal QRS complex), conduction over a James fiber that connects the atrium to the distal portion of the AV node and His bundle has been proposed, although little functional evidence exists to support the presence of this entity.

Ventricular Tachycardia Caused by Reentry

Reentry in the ventricle, both anatomic and functional, as a cause of sustained ventricular tachycardia has been supported by many animal and clinical studies (see **Fig. 33-24** and **Chapter 37**). Reentry in ventricular muscle, with or without contributions from specialized tissue, is responsible for many or most ventricular tachycardias in patients with ischemic heart disease. The area of microreentry appears to be small, and less commonly a macroreentry is found around the infarct scar. Surviving myocardial tissue separated by connective tissue provides serpentine routes of activation traversing infarcted areas that can establish reentry pathways. Bundle branch reentry can cause sustained ventricular tachycardia, particularly in patients with dilated cardiomyopathy.

Both figure-of-8 and single-circle reentrant loops have been described as circulating around an area of functional block in a manner consistent with the leading circle hypothesis or as conducting slowly across an apparent area of block created by anisotropy.¹⁰⁹ When intramural myocardium survives, it can form part of the reentrant loop. Structural discontinuities that separate muscle bundles—as a result of naturally occurring myocardial fiber orientation and anisotropic conduction, for example, as well as collagen matrices formed from the fibrosis after a myocardial infarction—establish the basis for slowed conduction, fragmented electrograms, and continuous electrical activity, which can lead to reentry. After the infarction, the surviving epicardial border zone undergoes substantial electrical remodeling,¹¹⁰ including reduced conduction velocity and increased anisotropy associated with the occurrence of reentrant circuits and ventricular tachycardia.⁴³ Slowing of conduction arises from alterations in the spatial distribution and electrophysiologic properties of connexin 43 gap junctions,⁴³ as well as from reduced voltage-gated sodium current. Whether myocyte depolarization secondary to electrotonic coupling to adjacent myofibroblasts (which typically have a much more depolarized potential) plays a role in electrical remodeling in postinfarction border zone myocardium remains to be seen.⁶⁶ During acute ischemia, various factors, including elevated $[K]_o$ and reduced pH, combine to create depressed action potentials in ischemic cells that retard conduction and can lead to reentry. Indeed, optical mapping studies in arterially perfused canine wedge preparations during global no-flow ischemia have demonstrated initiation of reentry during initial ischemia and subsequent reperfusion caused by the unidirectional block of conduction resulting from the spatiotemporal dispersion in tissue responses to stimulation.⁹⁷ The rapidly changing combination of transmural dispersion in response to endocardial pacing stimuli and the velocity of conduction creates a dynamic substrate in which reentry can be initiated and sustained. The results of this study are compatible with previous observations that fibrillation during reperfusion can be caused by intramural reentry. Interestingly, transmural reentry under these experimental conditions could be triggered by epicardial but not by endocardial stimulation at a time when there was an epicardial conduction delay or block with preserved endocardial conduction because of the increased susceptibility of the epicardium to the effects of ischemia. Clinically, this might facilitate induction of tachycardia by a PVC arising in the epicardium but not in the endocardium.

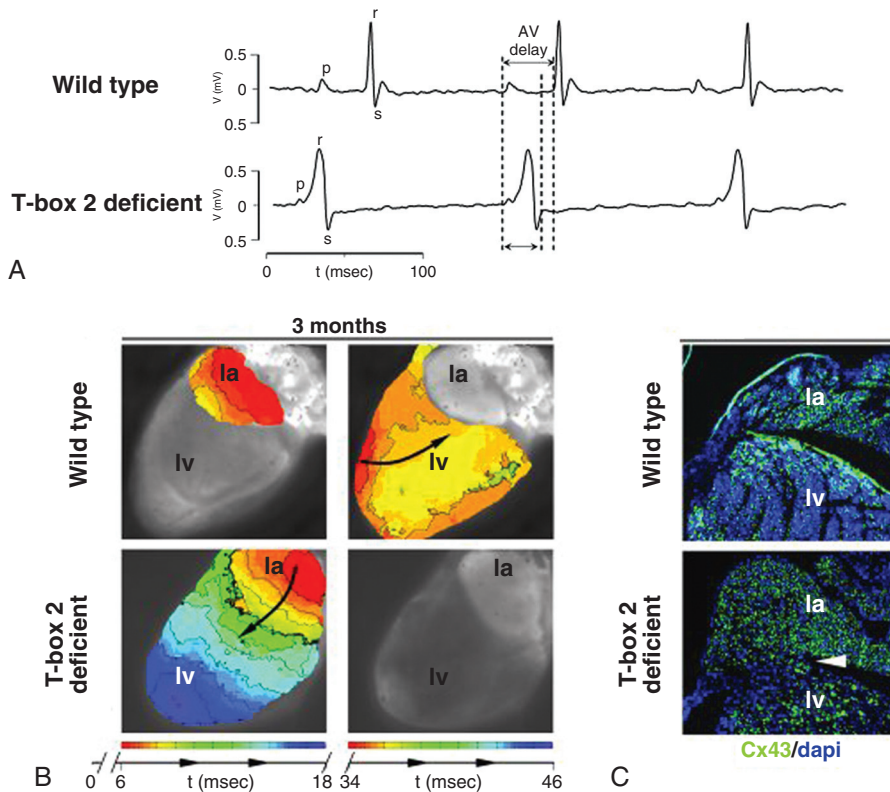


FIGURE e33-15 Accessory pathway formation in a mouse model of ventricular preexcitation. **A**, Surface electrocardiograms from an adult wild-type mouse and mouse with cardiomyocyte-specific inactivation of T-box 2, a transcription factor essential for AV canal patterning during development. Myocardial T-box 2 deficiency resulted in a severely shortened PR interval with a broadened QRS complex and initial slurring consistent with ventricular preexcitation. The total activation time of the atria and ventricles with preexcitation is less than the normal AV delay, thus indicating that the AV node is not used to activate (part of) the ventricle. Hence, these QRS complexes are not a representation of fusion of normal activation and preexcitation via the accessory pathway. **B**, Isochrone activation maps in an adult wild-type and T-box 2-deficient heart. In the wild-type heart, after an AV delay of 34 milliseconds, the ventricle is activated from the apex to the base. In the T-box 2-deficient heart, the ventricle is activated from the base to the apex after an AV delay of 9 milliseconds. **C**, Immunohistochemical analyses revealed connexin 43 expression (Cx43; green) in accessory myocardial connections between the left atrium (la) and the left ventricular (lv) base in the T-box 2-deficient heart (blue: nuclei). (From Aanhaanen WT, Boukens BJ, Sizarov A, et al: Defective *Tbx2*-dependent patterning of the atrioventricular canal myocardium causes accessory pathway formation in mice. *J Clin Invest* 121:534, 2011.)

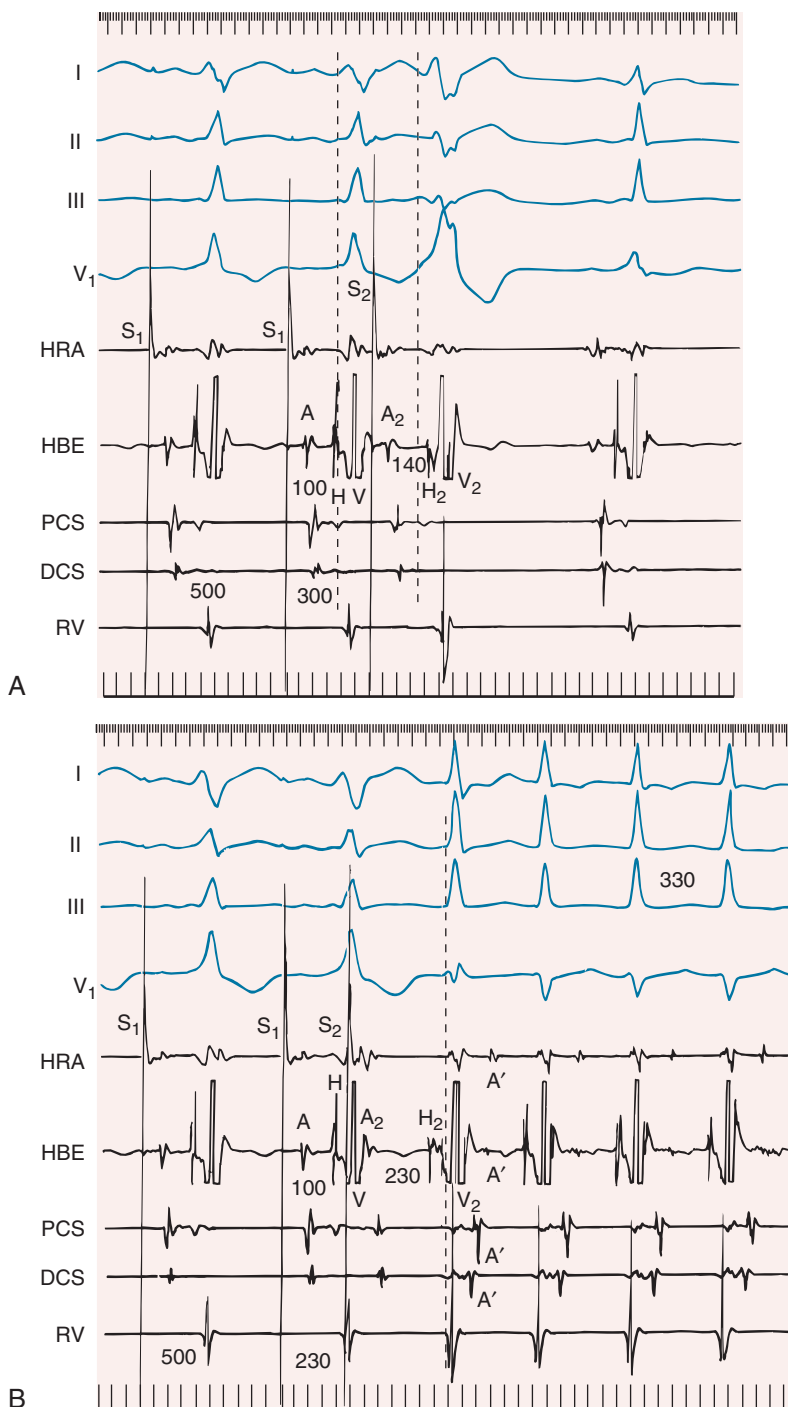


FIGURE 33-26 **A,** Wolff-Parkinson-White syndrome. Following high right atrial pacing at a cycle length of 500 milliseconds (S_1-S_1), premature stimulation at a coupling interval of 300 milliseconds (S_1-S_2) produces physiologic delay in AV nodal conduction, which results in an increase in the A-H interval from 100 to 140 milliseconds but no delay in the AV interval. Consequently, activation of the His bundle follows activation of the QRS complex (second interrupted line), and the QRS complex becomes more anomalous in appearance because of increased ventricular activation over the accessory pathway. **B,** Induction of reciprocating AV tachycardia. Premature stimulation at a coupling interval of 230 milliseconds prolongs the A-H interval to 230 milliseconds and results in anterograde block in the accessory pathway and normalization of the QRS complex (a slight functional aberrancy in the nature of incomplete right bundle branch block occurs). Note that H_2 precedes onset of the QRS complex (interrupted line). Following V_2 , the atria are excited retrogradely (A') beginning in the distal coronary sinus, followed by atrial activation in leads recording from the proximal coronary sinus, His bundle, and high right atrium. A supraventricular tachycardia is initiated at a cycle length of 330 milliseconds. I, II, III, and V₁ indicate scalar electrocardiographic leads. A = H-V, atrial, His bundle, and ventricular activation during the drive train; A₂ = H₂, V₂, atrial, His bundle, and ventricular activation during the premature stimulus; DCS = distal coronary sinus electrogram; HBE = His bundle electrogram; HRA = high right atrium; PCS = proximal coronary sinus electrogram; RV = right ventricular electrogram. Time lines are in 50- and 10-millisecond intervals. S_1 = stimulus of the drive train; S_2 = premature stimulus. (From Zipes DP, Mahomed Y, King RD, et al: Wolff-Parkinson-White syndrome: Cryosurgical treatment. Indiana Med 89:432, 1986.)

Brugada Syndrome

Phase 2 reentry has been implicated in the genesis of ventricular tachycardia-fibrillation associated with the inheritable Brugada syndrome,¹¹¹ which is characterized by ST-segment elevation (unrelated to ischemia, electrolyte abnormalities, or structural heart disease) in

the right precordial (V₁ to V₃) leads of the electrocardiogram, often but not always accompanied by an apparent right bundle branch block. The hereditary nature of the syndrome is well established. Brugada syndrome has been linked to loss-of-function mutations in SCN5A, which encodes the pore-forming cardiac sodium channel

alpha subunit Nav1.5, and mutations in *SCN1B*, which encodes the function-modifying sodium channel beta₁ subunit (see Chapter 32).^{112,113} Although Na⁺ channel mutations are most common, mutations in the alpha and beta subunits of the Ca²⁺ channel gene have been found in some patients with Brugada syndrome, as have mutations in the glycerol-3-phosphate dehydrogenase 1-like gene (*GPD1L*) on chromosome 3p22-25 (BS2), which reduce the Na⁺ current I_{Na}. Brugada syndrome-associated gene defects cause a reduction or loss of sodium or calcium current in combination with altered functional properties of voltage-gated sodium channels. Alterations in the sodium channel current cause heterogeneous loss of the action potential dome during the plateau phase (phase 2) in the right ventricular epicardium, which leads to a marked dispersion of repolarization and refractoriness and the potential for phase 2 reentry.¹¹⁴ Ablation of right ventricular epicardium eliminated ventricular arrhythmias in an animal model of pharmacologically induced Brugada syndrome.¹¹¹

Catecholaminergic Polymorphic Ventricular Tachycardia

CPVT is an inherited arrhythmogenic disease characterized by stress-induced, adrenergically mediated polymorphic ventricular tachycardia occurring in structurally normal hearts. Heterozygous missense mutations in the gene encoding the RyR2 have been reported in most patients with CPVT, although mutations in the calsequestrin gene can also cause CPVT.¹¹⁵ A common mechanism underlying RyR2-associated CPVT is increased leakage of Ca²⁺ from the SR during diastole leading to intracellular Ca²⁺ waves and triggered activity.^{76,116} Carvedilol, a beta blocker used for prevention of ventricular tachyarrhythmias in heart failure, and flecainide, a blocker of voltage-gated sodium channels, have recently been shown to suppress CPVT via direct inhibition of cardiac ryanodine receptor-mediated Ca²⁺ release, thus indicating that these agents possess hitherto unknown pharmacologic properties that can be exploited for the treatment of Ca²⁺-dependent arrhythmias in the clinical setting.^{117,118}

Arrhythmogenic Right Ventricular Cardiomyopathy

Arrhythmogenic right ventricular cardiomyopathy (ARVC) is also an inherited disease characterized by sustained monomorphic ventricular tachycardia and sudden death. Previous studies have linked ARVC with mutations in proteins of the cardiac desmosome, a component of the intercalated disc essential for mechanical coupling between cardiomyocytes. Mutations in multiple genes, including desmoplakin, desmoglein 2, desmocollin 2, plakophilin 2, plakoglobin (JUP, also called gamma-catenin), ryanodine receptor 2, laminin receptor 1, and transforming growth factor-beta 3, have been identified in patients with ARVC. Approximately 70% of the mutations linked to inherited ARVC are in the gene encoding plakophilin 2 (*PKP2*), which interacts with other cytoskeletal proteins to stabilize the desmosome. In vitro studies have demonstrated that loss of *PKP2* expression reduces the voltage-gated sodium current and connexin 43 expression at the intercalated disc and thus results in slowed action potential propagation. Cardiomyocyte-specific inactivation of JUP in mice has recently been shown to recapitulate many aspects of the human ARVC phenotype, including ventricular dilation, cardiac fibrosis, ventricular dysfunction, and tachyarrhythmias.¹¹⁹

Ventricular Fibrillation: Initiation and Maintenance

Previous experimental and simulation investigations have suggested that VF is maintained solely by reentry (see Chapter 37). This reentry was thought to be unstable and to be maintained by wandering wavelets of activation following constantly changing paths of activation and exhibiting frequent conduction block caused by nonuniform dispersion of refractoriness. More recent investigations have suggested other mechanisms of maintenance of VF and have introduced the concepts of restitution kinetics, wave front, wave break, focal discharge, and rotor as replacement for the classic reentry theory.¹²⁰ (For a demonstration of wave front dynamics during fibrillation, see Video 33-6.)

The hallmark of cardiac fibrillation is ongoing wave break (or wave splitting).¹²¹ Wave break is caused by a conduction block occurring at a specific site along the wave front while the remaining portions of

the front continue to propagate. This localized block, wave break, causes splitting of the mother wave front into two daughter wavelets. Two hypotheses exist in regard to the genesis of wave breaks during fibrillation. The mother rotor hypothesis states that VF is maintained by a single, stationary, intramural stable reentrant circuit (i.e., the mother rotor) in a dominant domain, which has the shortest refractory period from which activations propagate into the more slowly activating domains with longer refractory periods. Wave breaks result from Wenckebach-like conduction as high-frequency impulses emanating from the dominant domain are unable to sustain 1:1 conduction through heterogeneous tissue. In this case the fastest activating (i.e., dominating) rotor rather than ongoing wave break is the engine driving cardiac fibrillation, and wave break occurs only secondarily.^{120,122} Evidence supporting this concept is that frequency analyses have shown (1) single, stable (both in space and time), dominant frequencies in the power spectra of membrane voltage signals obtained from various regions of the heart; (2) correlation of dominant frequencies and the frequency of reentry; (3) relative infrequency of reentry on the surface of the heart during fibrillation, with an intramural location of the mother rotor being favored, such as the Purkinje network; and (4) Wenckebach-like conduction at the borders between different dominant frequency domains. These borders can result from preexisting structural or functional heterogeneities. For example, high-resolution electrical mapping has suggested that fast activation during VF is driven by Purkinje fibers. Spatial heterogeneity in the magnitude of ionic currents has been implicated in the generation of spatial gradients in activation rates and in maintaining rotor stability in the fastest activating regions. For example, the magnitude of the inward rectifying K⁺ current I_{K1} (see Table 33-3) was larger in the rapidly activating left ventricular myocytes than in the slower activating right ventricular myocytes.⁷⁸ Furthermore, regions with larger I_{K1} had faster activation rates and more stable rotors than did regions with smaller I_{K1}.⁷⁷

In contrast to the stable mother rotor theory, other experimental evidence has supported the idea that dynamic wave break plays a fundamental role in the initiation and maintenance of short-duration VF (wandering wavelet hypothesis).^{120,121,123,124} According to this hypothesis, VF is maintained by wandering wavelets with constantly changing, evanescent, reentrant circuits. Experimental evidence favoring the multiple-wavelet hypothesis includes (1) an inability to detect a single dominant frequency in the power spectra of mapping data from fibrillating hearts; (2) spatiotemporal instability of frequency domain distributions during VF, with the exception of anatomic borders, such as the Purkinje-myocyte transition; (3) failure to demonstrate stable intramural reentry at higher frequencies than at the surface; and (4) boundaries dynamically generated by wavelet behavior rather than by anatomic conduction block. To reproduce the dynamic spatiotemporal instability of dominant frequency domains, a combination of dynamically changing and fixed tissue heterogeneity is required.⁹⁹ The most important determinant of the dynamically induced component of heterogeneity has been identified as electrical restitution, or variation of the action potential duration and conduction velocity with the diastolic interval. For example, it has been proposed that the breakup of periodic waves is precipitated by oscillations in the action potential duration (so-called action potential duration alternans [APD alternans]) that are sufficiently large to cause a conduction block along the spiral wave front. Simulations (Fig. 33-27) have shown that a reentrant rotor becomes unstable and breaks down into multiple rotors when the slope of the restitution curve for the action potential duration versus the diastolic interval is greater than 1. Pharmacologic blockade of the L-type calcium current can terminate VF by reducing the action potential duration restitution slope (see Fig. 33-27).¹²⁵ If it is occurring in a spatially discordant pattern, alternans is considered a key arrhythmogenic factor predisposing the heart to reentry and fibrillation.¹²⁶ At the cellular level, the origin of APD alternans appears to be determined primarily by alternations in cardiomyocyte calcium transient amplitude or duration (calcium alternans).

During spatially discordant alternans, the action potential duration alternates out of phase in different regions of the heart, thereby increasing dispersion of refractoriness so that ectopic beats have a high probability of inducing reentry. This mechanism is illustrated in Figure 33-28; some regions of the heart alternate in a long-short-long pattern, whereas other regions at the same time alternate in a short-long-short pattern. These out-of-phase regions are separated by a nodal line in which no alternans is present, but spatial gradients in the action potential duration are steepest along this line. Thus spatially discordant alternans creates gradients in tissue refractoriness,

VIDEO 33-6

Recording of spiral wave reentry during ventricular fibrillation in a Langendorff-perfused guinea pig heart using a potentiometric dye. Shown are the spatiotemporal dynamics of membrane potential changes on the left ventricular surface, with white and black being the most positive and most negative membrane potentials, respectively. (From Samie FH, Berenfeld O, Anumonwo J, et al: Background potassium current. A determinant of rotor dynamics in ventricular fibrillation. Circ Res 89:1216, 2001.)

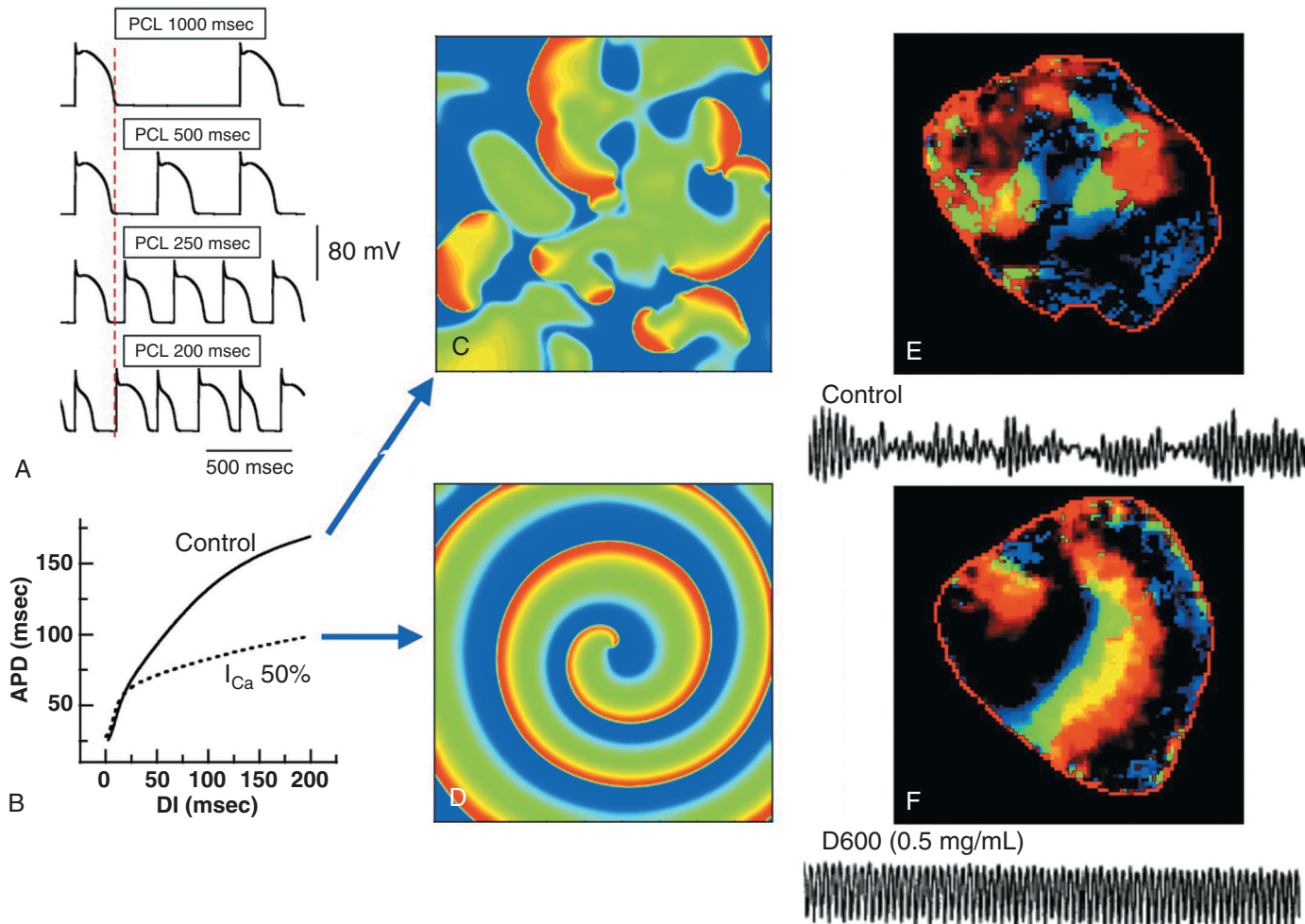


FIGURE 33-27 Action potential duration (APD) restitution slope and rotor stability. **A**, APD shortening and APD alternans as the pacing cycle length (PCL) decreases (computer simulations). **B**, APD restitution curves with a slope greater than 1 (solid line) or less than 1 (dashed line, obtained with 50% block of the calcium current). **C, D**, Spiral wave behavior several seconds after initiating a rotor in homogeneous two-dimensional tissue. All myocytes are assumed to be identical, with either a steep (**C**) or shallow (**D**) APD restitution slope. **E, F**, Conversion of multiple-wavelet VF to mother rotor VF. Optically measured surface voltage maps were obtained from an intact Langendorff-perfused rabbit heart before (**E**) and after (**F**) partially blocking the L-type calcium current to flatten the APD restitution slope to less than 1. In **E**, multiple wave fronts move in a complex VF pattern. In **F**, VF has converted to ventricular tachycardia, manifested as a stable rotor. Black tracings below the color panels in **E** and **F** are corresponding electrograms. DI = diastolic interval. (From Weiss JN, Qu Z, Chen PS, et al: The dynamics of cardiac fibrillation. *Circulation* 112:1232, 2005. By permission of the American Heart Association.)

which in turn favor the development of reentry by a premature beat (Fig. 33-28B). At the cellular level, the steepness of the action potential duration restitution curve and intracellular calcium level ($[Ca^{2+}]_i$) dynamics cause the action potential duration and $[Ca^{2+}]_i$ transient to alternate. Given the bidirectional coupling between changes in $[Ca^{2+}]_i$ and membrane potential—for example, the membrane potential determines the activity of L-type Cav channels, and conversely, the $[Ca^{2+}]_i$ transient amplitude strongly modulates the action potential duration through its effects on Ca^{2+} -sensitive currents (e.g., $I_{Na/Ca}$) during the action potential plateau—an alteration in $[Ca^{2+}]_i$ transient amplitude can cause a secondary alternation in the action potential duration. Indeed, experimental evidence has strongly suggested that the onset of APD alternans is primarily attributable to instabilities in $[Ca^{2+}]_i$ cycling dynamics, thus defining a causal role of intracellular Ca^{2+} -handling abnormalities in initiating electrical instability. At the tissue level, alternans combines with instabilities in conduction velocity to cause alternans to become spatially discordant. T wave alternans is the electrocardiographic manifestation of action potential duration $[Ca^{2+}]_i$ alternans and thus is a clinical predictor of future arrhythmic events.

In addition to a role of Purkinje fibers in the initiation of VF, other studies have suggested involvement of Purkinje fibers in the maintenance of VF, either as part of a reentrant circuit or as a source of focal activation. Their role appears to be more important during later (>1 minute) than during earlier stages of VF.¹⁰⁰

Ventricular Tachycardias Caused by Nonreentrant Mechanisms

In some cases of ventricular tachycardia related to coronary artery disease, especially in patients without coronary artery disease, nonreentrant mechanisms are important causes of ventricular tachycardias. However, in many patients the mechanism of the ventricular tachycardia remains unknown.

Triggered Activity

A group of probably nonreentrant ventricular tachycardias occurring in the absence of structural heart disease can be initiated and terminated by programmed stimulation. They are catecholamine dependent and can be terminated by the Valsalva maneuver, adenosine, and verapamil. These ventricular tachycardias are generally but not exclusively located in the right ventricular outflow tract and may be caused by triggered activity, possibly DADs that are cAMP dependent.⁵⁹ EADs have been recorded in this tachycardia as well. Left ventricular fascicular tachycardias can be suppressed by verapamil but not generally by adenosine, and some may be caused by triggered activity and others by reentry. EADs and triggered activity may be responsible for torsades de pointes.

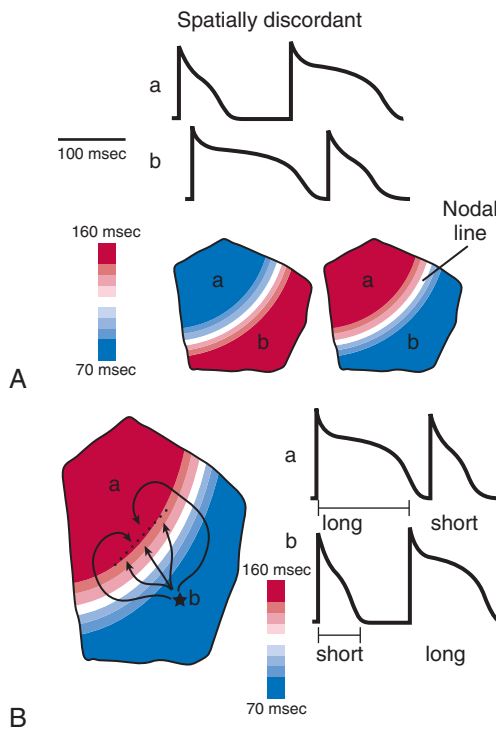


FIGURE 33-28 Initiation of reentry by a premature beat during spatially discordant alternans. **A, upper panel.** At rapid rates, action potentials at site a alternate short-long, whereas at the same time, action potentials at site b alternate long-short, thereby creating a steep gradient of action potential duration (APD) distribution with a nodal line that has no APD alternation separating the out-of-phase regions a and b (**lower panel**). **B,** A premature beat (asterisk) occurring in region b blocks (dotted line) as it propagates across the nodal line into the region with a long APD (a). The premature beat propagates laterally along the nodal line while waiting for the long APD region to repolarize and then reenters the blocked region to initiate figure-of-8 reentry. (From Weiss JN, Karma A, Shiferaw Y, et al: From pulsus to pulseless: The saga of cardiac alternans. *Circ Res* 98:1244, 2006. By permission of the American Heart Association.)

Automaticity

Automatic discharge can be responsible for some ventricular tachycardias and does not appear to be suppressed by adenosine. Unless invasive studies are undertaken, mechanisms of ventricular tachycardia can only be conjectured.

References

Anatomy of the Cardiac Conduction System

- Maltsev VA, Vinogradova TM, Lakatta EG: The emergence of a general theory of the initiation and strength of the heartbeat. *J Pharmacol Sci* 100:338, 2006.
- Chandler NJ, Greener ID, Tellez JO, et al: Molecular architecture of the human sinus node. *Circulation* 119:1562, 2009.
- Larsson HP: How is the heart rate regulated in the sinoatrial node? Another piece to the puzzle. *Gen Physiol* 136:237, 2010.
- Lakatta EG, DiFrancesco D: What keeps us ticking: A funny current, a calcium clock, or both? *J Mol Cell Cardiol* 47:157, 2009.
- Boyett MR, Inada S, Yoo S, et al: Connexins in the sinoatrial and atrioventricular nodes. *Adv Cardiol* 42:175, 2006.
- Fedorov VV, Schuessler RB, Hemill M, et al: Structural and functional evidence for discrete exit pathways that connect the canine sinoatrial node and atria. *Circ Res* 104:915, 2009.
- Boink GJ, Rosen MR: Regenerative therapies in electrophysiology and pacing: Introducing the next steps. *J Interv Card Electrophysiol* 31:3, 2011.
- Schwartz PJ, Zipes DP: Autonomic modulation of cardiac arrhythmias. In Zipes DP, Jalife J (eds): *Cardiac Electrophysiology: From Cell to Bedside*. 3rd ed. Philadelphia, WB Saunders, 1999, pp 300-314.
- Barbuti A, Terragni B, Brioschi C, et al: Localization of f-channels to caveolae mediates specific β_2 -adrenergic receptor modulation of rate in sinoatrial myocytes. *J Mol Cell Cardiol* 42:71, 2007.
- Ko Y, Yeh H, Ko Y, et al: Three-dimensional reconstruction of the rabbit atrioventricular conduction axis by combining histological, desmin, and connexin mapping data. *Circulation* 109:1172, 2004.
- Li J, Greener ID, Inada S, et al: Computer three dimensional reconstruction of the atrioventricular node. *Circ Res* 102:975, 2008.
- Di Maio A, Ter Keurs HE, Franzini-Armstrong C: T-tubule profiles in Purkinje fibres of mammalian myocardium. *J Muscle Res Cell Motil* 28:115, 2007.
- Rohr S, Kucera JP, Fast VG, et al: Paradoxical improvement of impulse conduction in cardiac tissue by partial uncoupling. *Science* 275:841, 1997.
- Ieda M, Kanazawa H, Kimura K, et al: Sema3a maintains normal heart rhythm through sympathetic innervation patterning. *Nat Med* 13:604, 2007.
- Hucker WJ, Nikolski VP, Efimov IR: Autonomic control and innervation of the atrioventricular junctional pacemaker. *Heart Rhythm* 4:1326, 2007.
- Kimura K, Ieda M, Fukuda K: Development, maturation, and transdifferentiation of cardiac sympathetic nerves. *Circ Res* 110:325, 2012.
- Mantravadi R, Gabris B, Liu T, et al: Autonomic nerve stimulation reverses ventricular repolarization sequence in rabbit hearts. *Circ Res* 100:e72, 2007.
- Vaseghi M, Lux RL, Mahajan A, et al: Sympathetic stimulation increases dispersion of repolarization in humans with myocardial infarction. *Am J Physiol Heart Circ Physiol* 302:H1838, 2012.
- Jacques D, Abdel-Samad D: Neuropeptide Y (NPY) and NPY receptors in the cardiovascular system: Implication in the regulation of intracellular calcium. *Can J Physiol Pharmacol* 85:43, 2007.
- Oh YS, Jong AY, Kim DT, et al: Spatial distribution of nerve sprouting after myocardial infarction in mice. *Heart Rhythm* 3:728, 2006.
- Zhou S, Jung BC, Tan AY, et al: Spontaneous stellate ganglion nerve activity and ventricular arrhythmias in a canine model of sudden death. *Heart Rhythm* 5:131, 2008.
- Liu Y, Lee Y, Pak H, et al: Effects of simvastatin on cardiac neural and electrophysiologic remodeling in rabbits with hypercholesterolemia. *Heart Rhythm* 6:69, 2009.
- Kanazawa H, Ieda M, Kimura K, et al: Heart failure causes cholinergic transdifferentiation of cardiac sympathetic nerves via gp130-signaling cytokines in rodents. *J Clin Invest* 120:408, 2010.
- Clarke GL, Bhattacharjee A, Tague SE, et al: β -Adrenoceptor blockers increase cardiac sympathetic innervation by inhibiting autoreceptor suppression of axon growth. *J Neurosci* 30:12446, 2010.
- Tan AY, Chen PS: Autonomic nerves in pulmonary veins. *Heart Rhythm* 4:S57, 2007.
- Pokushalov E, Romanov A, Shugayev P, et al: Selective ganglionated plexi ablation for paroxysmal atrial fibrillation. *Heart Rhythm* 6:1257, 2009.
- Scanaevaca M, Pisani C, Hachul D, et al: Selective atrial vagal denervation guided by evoked vagal reflex to treat patients with paroxysmal atrial fibrillation. *Circulation* 114:876, 2006.
- Lehnart SE, Mongillo M, Belinger A, et al: Leaky Ca^{2+} release channel/ryanodine receptor 2 causes seizures and sudden cardiac death in mice. *J Clin Invest* 118:2230, 2008.
- Scornik FS, Desai M, Brugada R, et al: Functional expression of "cardiac-type" Nav1.5 sodium channel in canine intracardiac ganglia. *Heart Rhythm* 3:842, 2006.
- Wilde AA, Bhuiyan ZA, Crotti L, et al: Left cardiac sympathetic denervation for catecholaminergic polymorphic ventricular tachycardia. *N Engl J Med* 358:2024, 2008.
- Kapa S, Venkatachalam KL, Asirvatham SJ: The autonomic nervous system in cardiac electrophysiology: An elegant interaction and emerging concepts. *Cardiol Rev* 18:275, 2010.
- Basic Electrophysiologic Principles**
- Song Y, Shryock JC, Belardinelli L, et al: A slowly-inactivating sodium current contributes to spontaneous diastolic depolarization of atrial myocytes. *Am J Physiol Heart Circ Physiol* 297:H1254, 2009.
- Song Y, Shryock JC, Belardinelli L: An increase of late sodium current induces delayed after-depolarizations and sustained triggered activity in atrial myocytes. *Am J Physiol Heart Circ Physiol* 294:H2031, 2008.
- Wagner S, Dybkova N, Rasenack ENL, et al: Ca^{2+} /calmodulin-dependent protein kinase II regulates cardiac sodium channels. *J Clin Invest* 116:3127, 2006.
- Kass RS, Moss AJ: Long QT syndrome: Novel insights into the mechanisms of cardiac arrhythmias. *J Clin Invest* 112:810, 2003.
- Shah M, Akar FG, Tomaselli GF: Molecular basis of arrhythmias. *Circulation* 112:2517, 2005.
- Zipes DP, Tomaselli GF: What causes sudden death in heart failure? *Circ Res* 95:754, 2004.
- Kleber A, Rudy Y: Basic mechanisms of cardiac impulse propagation and associated arrhythmias. *Physiol Rev* 84:431, 2004.
- Kanapitis G, Mese G, Valunienė L, et al: Gap junction channels exhibit connexin-specific permeability to cyclic nucleotides. *J Gen Physiol* 131:293, 2008.
- Li J, Patel VV, Kostetskii I, et al: Cardiac-specific loss of N-cadherin leads to alteration in connexins with conduction slowing and arrhythmogenesis. *Circ Res* 97:474, 2005.
- Kreuzberg MM, Söhl G, Kin J: Functional properties of mouse connexin30.2 expressed in the conduction system of the heart. *Circ Res* 96:1169, 2005.
- Akar FG, Spragg DD, Tunin RS, et al: Mechanisms underlying conduction slowing and arrhythmogenesis in nonischemic dilated cardiomyopathy. *Circ Res* 95:717, 2004.
- Kieken F, Mutsaers N, Dolmatova E, et al: Structural and molecular mechanisms of gap junction remodeling in epicardial border zone myocytes following myocardial infarction. *Circ Res* 104:1103, 2009.
- Danik SB, Liu F, Zhang F, et al: Modulation of cardiac gap junction expression and arrhythmic susceptibility. *Circ Res* 95:1035, 2004.
- Morley GE, Danik SB, Bernstein S, et al: Reduced intercellular coupling leads to paradoxical propagation across the Purkinje-ventricular junction and aberrant myocardial activation. *Proc Natl Acad Sci U S A* 102:4126, 2005.
- Yao JA, Gutstein DE, Liu F, et al: Cell coupling between ventricular myocyte pairs from connexin43-deficient murine hearts. *Circ Res* 93:736, 2003.
- Firouzi M, Ramanna H, Kok B, et al: Association of human connexin40 gene polymorphisms with atrial vulnerability as a risk factor for idiopathic atrial fibrillation. *Circ Res* 95:e29, 2004.
- Gard JJ, Yamada K, Green KG, et al: Remodeling of gap junctions and slow conduction in a mouse model of desmin-related cardiomyopathy. *Cardiovasc Res* 67:539, 2005.
- Kaplan SR, Gard JJ, Carvalho-Huerta L, et al: Structural and molecular pathology of the heart in Carvalho syndrome. *Cardiovasc Pathol* 13:26, 2004.
- Kaplan SR, Gard JJ, Protonotarios N, et al: Remodeling of gap junctions in arrhythmogenic right ventricular cardiomyopathy due to a deletion in plakophilin (Naxos disease). *Heart Rhythm* 1:3, 2004.
- Oxford EM, Musa H, Maass K, et al: Connexin43 remodeling caused by inhibition of plakophilin-2 expression in cardiac cells. *Circ Res* 101:703, 2007.
- Rubart M, Zipes DP: Mechanisms of sudden cardiac death. *J Clin Invest* 115:2305, 2005.
- Reuter H, Henderson SA, Han T, et al: The Na^+ - Ca^{2+} exchanger is essential for the action of cardiac glycosides. *Circ Res* 90:305, 2002.
- Lei M, Jones SA, Liu J, et al: Requirement of neuronal- and cardiac-type sodium channels for murine sinoatrial node pacemaking. *J Physiol* 559:835, 2004.
- Baruscotti M, Bucci A, DiFrancesco D: Physiology and pharmacology of the cardiac pacemaker ("funny") current. *Pharmacol Ther* 107:59, 2005.
- Verkerk AO, den Ruijter HM, Bourier J, et al: Dietary fish oil reduces pacemaker current and heart rate in rabbit. *Heart Rhythm* 6:1485, 2009.
- Costantini DL, Arruda EP, Agarwal P, et al: The homeodomain transcription factor Irx5 establishes the mouse cardiac ventricular repolarization gradient. *Cell* 123:347, 2005.
- Cooper PJ, Soeller C, Cannell MB: Excitation-contraction coupling in human heart failure examined by action potential clamp in rat cardiac myocytes. *J Mol Cell Cardiol* 49:911, 2010.
- Zygmunt AC, Goodrow RJ, Weigel CM: $I_{Na,Ca}$ and $I_{Ca,Ca}$ contribute to isoproterenol-induced delayed afterdepolarizations in midmyocardial cells. *Am J Physiol* 275:H1979, 1998.
- Bers DM, Ginsburg KS: Na:Ca stoichiometry and cytosolic Ca-dependent activation of NCX in intact cardiomyocytes. *Ann NY Acad Sci* 1099:326, 2007.

Molecular Composition of Ion Channels

Voltage-Gated Na⁺ Channels

Voltage-gated Na⁺ (Nav) channel pore-forming (alpha) subunits have four homologous domains (I to IV), each of which contains six transmembrane-spanning regions, and these four domains come together to form the Na⁺ permeable pore (see Fig. 33-11).¹ Among the multiple Nav alpha subunits, Nav1.5 (which is encoded by the *SCN5A* gene) is the prominent Nav alpha subunit expressed in mammalian myocardium. The name of the voltage-gated sodium channel consists of the chemical symbol of the principal permeating ion (Na) and v, which indicates its principal physiologic regulator (voltage). The number following v indicates the gene subfamily (Nav1), and the number following the decimal point identifies the specific channel isoform (e.g., Nav1.1). An identical nomenclature applies to voltage-gated calcium and potassium channels. Mutations in the sequence linking domains III and IV in *SCN5A*, which are associated with LQT3 syndrome, disrupt Nav channel inactivation and thereby give rise to a sustained inward Na⁺ current during the plateau phase of the action potential and to prolongation of the action potential. Cases of sudden infant death syndrome in black Americans have been linked to a polymorphism in the *SCN5A* gene, which encodes a variant cardiac sodium channel with diminished channel inactivation in the presence of lowered intracellular pH.² Mutations in *SCN5A* are also linked to Brugada syndrome. Brugada syndrome mutations result in reduced Nav current amplitude, which leads to slowing of phase 0 action potential upstroke, reduced action potential amplitude, and altered phase 1 repolarization.

Nav1.5 pore-forming alpha subunits coassemble with one to two auxiliary Nav beta subunits to form functional cell surface Nav channels in cardiomyocytes. Nav beta subunits appear to play an important role in anchoring ion channel proteins to the outer cell membrane.

Voltage-Gated Ca²⁺ Channels

Like Nav channels, cardiac voltage-gated Ca²⁺ (Cav) channels are assemblies of a pore-forming alpha subunit and auxiliary Cav beta or Cav alpha₂-delta subunits (see Fig. 33-11). Among the various alpha subunits, Cav1.2, encoded by the *CACNA1C* gene, is the prominent Cav alpha subunit expressed in mammalian myocardium. Cav1.2 channels exhibit many of the time- and voltage-dependent properties and pharmacologic sensitivities of cardiac L-type Ca²⁺ currents (see Table 33-3). Accessory subunits modulate the functional properties of Cav channels.

Cav3.1/alpha₁G alpha subunits form a Ca²⁺-selective channel with time- and voltage-dependent characteristics and pharmacologic sensitivities that resemble those of the low-voltage activated T-type Ca²⁺ channel. Disruption of the gene encoding Cav3.1/alpha₁G alpha subunits (*CACNA1G*) in mice has been demonstrated to slow the sinus node rate and AV conduction, consistent with its role in sinoatrial and AV node function.³

Voltage-Gated K⁺ Channels

Voltage-gated K⁺ channels (Kv) are composed of four separate pore-forming (alpha) subunits, each containing six regions (S₁ through S₆) of hydrophobic amino acids that are thought to form membrane-spanning domains (see Fig. 33-11).¹ Kv alpha subunits expressed in the human heart include members of the Kv1, Kv4, hERG, and KvLQT subfamilies. In addition, Kv channel alpha subunit proteins interact with Kv channel accessory subunits, including minK, KiChIP2, and MiRP1 (see Table 33-3), to form functional cell surface channels with distinct time- and voltage-dependent properties. Coassembly of the Kv4.3 alpha subunits and the accessory subunit KChIP2 gives rise to the cardiac transient outward Kv channel I_{to}. ERG1 alpha subunits, together with MiRP1 accessory subunits, contribute to the generation of functional cardiac I_{Kr} channels. Mutations in the gene encoding ERG1 (*KCNH2*) have been shown to underlie congenital LQT2

syndrome. These LQT2 syndrome mutations are loss-of-function mutations that lead to reduced functional I_{Kr} channel expression or to alterations in channel processing or trafficking.⁴

KvLQT1 alpha subunits associate with minK accessory subunits to form functional channels that resemble slowly activating, noninactivating K⁺ currents, referred to as I_{Ks}, in human myocardium. Mutations in the minK-encoding gene *KCNE1* are associated with LQT5 syndrome. Mutations in the gene encoding KvLQT1 alpha subunits, *KCNQ1*, have been linked to LQT1 syndrome. These mutations are all loss-of-function mutations that result in reduced expression of functional I_{Ks} channels in the outer membrane. Two single-site mutations that cause familial AF are located on adjacent amino acid residues in the first membrane-spanning segment of KCNQ1 and lead to altered physical interactions with the KCNE1 subunits, which ultimately results in slowing of deactivation of I_{Ks} channels.⁵

Kv1.5 alpha subunits contribute to K⁺-selective channels with time- and voltage-dependent characteristics that resemble the rapidly activating and slowly inactivating I_{Kur} in human atrial myocytes. I_{Kur} densities are markedly downregulated in the atria of patients with chronic AF.

Small-conductance, Ca²⁺-sensitive K⁺ channels are tetrameric assemblies of SK alpha subunits and underlie a Ca²⁺-activated K⁺ current, I_{K,Ca}, in human cardiomyocytes.⁶

Inwardly Rectifying Cardiac K⁺ (Kir) Channels

Kir channels in cardiac myocytes, as in other cells, conduct inward current at membrane potentials negative to E_K and smaller outward currents at membrane potentials positive to E_K. The activity of Kir channels is a function of both membrane potential and the extracellular K⁺ concentration ([K⁺]_o). As [K⁺]_o changes, the channel conducts inward current at potentials negative to the new E_K, whereas a small outward current within a certain potential range positive to the new E_K remains. Inwardly rectifying K⁺ channels are formed by inward rectifier K⁺ channel pore-forming alpha subunits (see Fig. 33-11). In contrast to Kv alpha subunits, Kir alpha subunits have only two (not six) transmembrane domains (see Fig. 33-11). Molecular studies have provided direct evidence that the alpha subunits of the Kir2 subfamily (Kir2.1 and Kir2.2) encode the strongly inwardly rectifying Kir channel I_{Ki} in cardiomyocytes.

In cardiomyocytes, Kir6.2 alpha subunits assemble with sulfonylurea receptor proteins to form K⁺-selective sarcolemmal I_{K,ATP} channels. I_{K,ATP} channels are thought to play a pivotal role in myocardial ischemia and preconditioning. For example, opening of cardiac sarcolemmal I_{K,ATP} channels underlies electrocardiographic ST-segment elevation during acute myocardial ischemia. Drugs such as nicorandil and diazoxide open adenosine triphosphate (ATP)-sensitive K⁺ channels, whereas sulfonylurea compounds (such as glibenclamide) inhibit the activity of I_{K,ATP}.

The molecular basis of the acetylcholine-activated K⁺ channel I_{K,Ach} is a heteromultimer of two inwardly rectifying potassium channel subunits, Kir3.1 and Kir3.4. Stimulation of I_{K,Ach} by vagally secreted acetylcholine decreases spontaneous depolarization in the sinoatrial node and slows the velocity of conduction in the AV node. Adenosine, through type 1 purinergic receptor-mediated G protein activation, also increases I_{K,Ach} activity in atrial, sinoatrial node, and AV node cells, thus making this compound a treatment of choice for AV reentry tachycardia.

Cardiac Pacemaker Channel

Channels underlying the pacemaker (“funny”) current I_f of sinoatrial myocytes are encoded by the HCN channel gene family. Of the four known HCN pore-forming alpha subunits, HCN4 is the most highly expressed in the mammalian myocardium. A mutation in the human HCN4 gene has been linked to familial sinus bradycardia.⁷



61. Yeh S, Chang H, Shieh R: Electrostatics in the cytoplasmic pore produce intrinsic inward rectification in the Kir2.1 channels. *J Gen Physiol* 126:551, 2005.
62. Li N, Timofeyev V, Tuteja D, et al: Ablation of a Ca^{2+} -activated K^+ channel (SK2 channel) results in action potential prolongation in atrial myocytes and atrial fibrillation. *J Physiol* 587:1087, 2009.
63. Lakatta EG, Maltsev VA, Vinogradova TM: A coupled SYSTEM of intracellular Ca^{2+} clocks and surface membrane voltage clocks controls the timekeeping mechanism of the heart's pacemaker. *Circ Res* 106:659, 2010.
64. Liao Z, Lockhead D, Larson ED, et al: Phosphorylation and modulation of hyperpolarization-activated HCN4 channels by protein kinase A in the mouse sinoatrial node. *J Gen Physiol* 136:247, 2010.
65. Joung B, Tang L, Maruyama M, et al: Intracellular calcium dynamics and acceleration of sinus rhythm by β -adrenergic stimulation. *Circulation* 119:788, 2009.
66. Miragoli M, Salvarami N, Rohr S: Myofibroblasts induce ectopic activity in cardiac tissue. *Circ Res* 101:755, 2007.
67. Kang G, Giovannone SF, Liu N, et al: Purkinje cells from RyR2 mutant mice are highly arrhythmicogenic but responsive to targeted therapy. *Circ Res* 107:512, 2010.
68. Stuyvers BD, Dun W, Matkovich S, et al: Ca^{2+} sparks and waves in canine Purkinje cells: A triple layered system of Ca^{2+} activation. *Circ Res* 97:35, 2005.
- Mechanisms of Arrhythmogenesis**
69. Patterson E, Po SS, Scherlag BJ, et al: Triggered firing in pulmonary veins initiated by in vitro autonomic nerve stimulation. *Heart Rhythm* 2:624, 2005.
70. Mohler PJ, Schott J, Gramolini AO, et al: Ankyrin-B mutation causes type 4 long-QT cardiac arrhythmia and sudden cardiac death. *Nature* 421:634, 2003.
71. Farzaneh-Far A, Lerman BB: Idiopathic ventricular outflow tract tachycardia. *Heart* 91:136, 2005.
72. Andersson DC, Marks AR: Fixing ryanodine receptor Ca leak—a novel therapeutic strategy for contractile failure in heart and skeletal muscle. *Drug Discov Today Dis Mech* 7:e151, 2010.
73. Cerrone MM, Colombi B, Santoro M, et al: Bidirectional ventricular tachycardia and fibrillation elicited in a knock-in mouse model carrier of a mutation in the cardiac ryanodine receptor. *Circ Res* 96:77, 2005.
74. Terentyev D, Nori A, Santoro M, et al: Abnormal interactions of calsequestrin with the ryanodine receptor calcium release channel complex linked to exercise-induced sudden cardiac death. *Circ Res* 98:1151, 2006.
75. Chelu MG, Sarma S, Sood S, et al: Calmodulin kinase II-mediated sarcoplasmic reticulum Ca^{2+} leak promotes atrial fibrillation in mice. *J Clin Invest* 119:1940, 2009.
76. Lehnart SE, Mongillo M, Belinger A, et al: Leaky Ca^{2+} release channel/ryanodine receptor 2 causes seizures and sudden cardiac death in mice. *J Clin Invest* 118:2230, 2008.
77. Yano M, Ikeda Y, Matsuzaki M: Altered intracellular Ca^{2+} handling in heart failure. *J Clin Invest* 115:556, 2005.
78. Wehrens XH, Lehnart SE, Reiken SR, et al: Protection from cardiac arrhythmia through ryanodine receptor-stabilizing protein calstabin2. *Science* 304:292, 2004.
79. Lehnart SE, Terrenoire C, Reiken S, et al: Stabilization of cardiac ryanodine receptor prevents intracellular calcium leak and arrhythmias. *Proc Natl Acad Sci USA* 103:7906, 2006.
80. Li X, Zima AV, Sheikh F, et al: Endothelin-1-induced arrhythmogenic Ca^{2+} signaling is abolished in atrial myocytes of inositol-1,4,5-trisphosphate(IP3)-receptor type 2-deficient mice. *Circ Res* 96:1274, 2005.
81. Hirose M, Stuyvers BD, Dun W, et al: Wide long lasting perinuclear calcium release events generated by an interaction between ryanodine and IP3 receptors in canine Purkinje cell. *J Mol Cell Cardiol* 45:176, 2008.
82. Zima AV, Blatter LA: Inositol-1,4,5-trisphosphate-dependent Ca^{2+} signalling in cat atrial excitation-contraction coupling and arrhythmias. *J Physiol* 555:607, 2004.
83. Zhao ZH, Zhang HC, Xu Y: Inositol-1,4,5-trisphosphate and ryanodine-dependent Ca^{2+} signaling in a chronic dog model of atrial fibrillation. *Cardiology* 107:269, 2007.
84. Fujiwara K, Tanaka H, Mani H, et al: Burst emergence of intracellular Ca^{2+} waves evokes arrhythmogenic oscillatory depolarization via the $\text{Na}^+-\text{Ca}^{2+}$ exchanger. *Circ Res* 103:509, 2008.
85. Myles RC, Wang L, Kang C, et al: Local β -adrenergic stimulation overcomes source-sink mismatch to generate focal arrhythmia. *Circ Res* 110:1454, 2012.
86. Belevych AE, Terentyev D, Terentyeva R, et al: Shortened Ca^{2+} signaling refractoriness underlies cellular arrhythmogenesis in a postinfarction model of sudden cardiac death. *Circ Res* 110:569, 2012.
87. Kass RS, Moss AJ: Long QT syndrome: Novel insights into the mechanisms of cardiac arrhythmias. *J Clin Invest* 112:810, 2003.
88. Itzhaki I, Maizels L, Huber I, et al: Modelling the long QT syndrome with induced pluripotent stem cells. *Nature* 471:225, 2011.
89. Moretti A, Bellin M, Welling A, et al: Patient-specific induced pluripotent stem-cell models for long-QT syndrome. *N Engl J Med* 363:1397, 2010.
90. Lee P, Klos M, Bollensdorff C, et al: Simultaneous voltage and calcium mapping of genetically purified human induced pluripotent stem cell-derived cardiac myocyte monolayers. *Circ Res* 110:1556, 2012.
91. Glukhov AV, Fedorov VV, Lou Q, et al: Transmural dispersion of repolarization in failing and nonfailing human ventricle. *Circ Res* 106:981, 2010.
92. El-Sherif N, Jalife J: Paroxysmal atrioventricular block: Are phase 3 and phase 4 block mechanisms or misnomers? *Heart Rhythm* 6:1514, 2009.
93. Spach M: Mounting evidence that fibrosis generates a major mechanism for atrial fibrillation. *Circ Res* 101:743, 2007.
94. Tanaka K, Zlochiver S, Vikstrom KL, et al: Spatial distribution of fibrosis governs fibrillation wave dynamics in the posterior left atrium during heart failure. *Circ Res* 101:839, 2007.
95. Muñoz V, Grzeda KR, Desplantez T, et al: Adenoviral expression of I_{Ks} contributes to wave-break and fibrillatory conduction in neonatal rat ventricular cardiomyocyte monolayers. *Circ Res* 101:475, 2007.
96. Wu J, Zipes DP: Transmural reentry triggered by epicardial stimulation during acute ischemia in canine ventricular muscle. *Am J Physiol Heart Circ Physiol* 283:H2004, 2002.
97. Ueda N, Zipes DP, Wu J: Functional and transmural modulation of M cell behavior in canine ventricular wall. *Am J Physiol Heart Circ Physiol* 287:H2569, 2004.
98. Weiss JN, Qu Z, Chen PS, et al: The dynamics of cardiac fibrillation. *Circulation* 112:1232, 2005.
99. Chen Y, Chen S: Electrophysiology of pulmonary veins. *J Cardiovasc Electrophysiol* 17:220, 2006.
100. Chou CC, Nihei M, Zhou S, et al: Intracellular calcium dynamics and anisotropic reentry in isolated canine pulmonary veins and left atrium. *Circulation* 111:2889, 2005.
101. Chou CC, Zhou S, Tan AY, et al: High-density mapping of pulmonary veins and left atrium during ibutilide administration in a canine model of sustained atrial fibrillation. *Am J Physiol Heart Circ Physiol* 289:H2704, 2005.
102. Mahida S, Lubitz SA, Rienstra M, et al: Monogenic atrial fibrillation as pathophysiological paradigms. *Cardiovasc Res* 89:692, 2011.
103. Ellinor PT, Lunetta KL, Glazer NL, et al: Common variants in KCNN3 are associated with lone atrial fibrillation. *Nat Genet* 42:240, 2010.
104. Ellinor PT, Lunetta KL, Albert CM, et al: Meta-analysis identifies six new susceptibility loci for atrial fibrillation. *Nat Genet* 44:670, 2012.
105. Vest JA, Wehrens XH, Reiken SR, et al: Defective cardiac ryanodine receptor regulation during atrial fibrillation. *Circulation* 111:2025, 2005.
106. Zhang Z, He Y, Tuteja D, et al: Functional roles of Cav1.3($\alpha 1D$) calcium channels in atria: Insights gained from gene-targeted null mutant mice. *Circulation* 112:1936, 2005.
107. Temple J, Fries P, Rottman J, et al: Atrial fibrillation in KCNE1-null mice. *Circ Res* 97:62, 2005.
108. Aanhaugen WT, Boukens BJ, Sizarov A, et al: Defective Tbx2-dependent patterning of the atrioventricular canal myocardium causes accessory pathway formation in mice. *J Clin Invest* 121:1534, 2011.
109. Ciaccio EJ, Ashikaga H, Kaba RA, et al: Model of reentrant ventricular tachycardia based upon infarct border zone geometry predicts reentrant circuit features as determined by activation mapping. *Heart Rhythm* 4:1034, 2007.
110. Cabo C, Boyden PA: Heterogeneous gap junction remodeling stabilizes reentrant circuits in the epicardial border zone of the healing canine infarct: A computational study. *Am J Physiol Heart Circ Physiol* 291:H2606, 2006.
111. Morita H, Zipes DP, Morita ST, et al: Epicardial ablation eliminates ventricular arrhythmias in an experimental model of Brugada syndrome. *Heart Rhythm* 6:665, 2009.
112. Watanabe H, Koopmann TT, Scourneau SL, et al: Sodium channel $\beta 1$ subunit mutations associated with Brugada syndrome and cardiac conduction disease in humans. *J Clin Invest* 118:2260, 2008.
113. Cerrone M, Priori SG: Genetics of sudden death: Focus on inherited channelopathies. *Eur Heart J* 32:2109, 2011.
114. Morita H, Zipes DP, Wu J: Brugada syndrome: Insights of ST elevation, arrhythmogenicity, and risk stratification from experimental observations. *Heart Rhythm* 6:S34, 2009.
115. ter Keurs HEDJ, Boyden PA: Calcium and arrhythmogenesis. *Physiol Rev* 87:457, 2007.
116. Fernandez-Velasco M, Rueda A, Rizzi N, et al: Increased Ca^{2+} sensitivity of the ryanodine receptor mutant RyR2R4496C underlies catecholaminergic polymorphic ventricular tachycardia. *Circ Res* 104:201, 2009.
117. Zhou Q, Xiao J, Jiang D, et al: Carvedilol and its new analogs suppress arrhythmogenic store overload-induced Ca^{2+} release. *Nat Med* 17:1003, 2011.
118. Watanabe H, Chopra N, Laver D, et al: Flecainide prevents catecholaminergic polymorphic ventricular tachycardia in mice and humans. *Nat Med* 15:380, 2009.
119. Li D, Liu Y, Maruyama M, et al: Restrictive loss of plakoglobin in cardiomyocytes leads to arrhythmogenic cardiomyopathy. *Hum Mol Genet* 20:4582, 2011.
120. Tabereaux PB, Dossdal DJ, Ideker RE, et al: Mechanisms of VF maintenance: Wandering wavelets, mother rotors, or focus. *Heart Rhythm* 6:405, 2009.
121. Ten Tusscher KH, Hren R, Panfilov AV: Organization of ventricular fibrillation in the human heart. *Circ Res* 100:e87, 2007.
122. Newton JC, Smith WM, Ideker RE: Estimated global transmural distribution of activation rate and conduction block during porcine and canine ventricular fibrillation. *Circ Res* 94:836, 2004.
123. Choi B, Nho W, Liu T, et al: Life span of ventricular fibrillation frequencies. *Circ Res* 91:339, 2002.
124. Roger JM, Huang J, Melnick SB, et al: Sustained reentry in the left ventricle of fibrillating pig hearts. *Circ Res* 92:539, 2003.
125. Weiss JN, Qu Z, Chen PS, et al: The dynamics of cardiac fibrillation. *Circulation* 112:1232, 2005.
126. Weiss JN, Karma A, Shiferaw Y, et al: From pulsus to pulseless: The saga of cardiac alternans. *Circ Res* 98:1244, 2006.



References

1. Nerbonne JM, Kass RS: Molecular physiology of cardiac repolarization. *Physiol Rev* 85:1205, 2005.
2. Plant LD, Bowers PN, Liu Q, et al: A common cardiac sodium channel variant associated with sudden infant death in African Americans, SCN5A S1103Y. *J Clin Invest* 116:430, 2006.
3. Mangoni ME, Traboulsee A, Leoni AL, et al: Bradycardia and slowing of the atrioventricular conduction in mice lacking CaV3.1/alpha1G T-type calcium channels. *Circ Res* 98:1422, 2006.
4. Anderson CL, Delisle BP, Anson BD, et al: Most LQT2 mutations reduce Kv11.1 (hERG) current by a class 2 (trafficking-deficient) mechanism. *Circulation* 113:365, 2006.
5. Chan PJ, Osteen JD, Xiong D, et al: Characterization of KCNQ1 atrial fibrillation mutations reveals distinct dependence on KCNE1. *J Gen Physiol* 139:135, 2012.
6. Li N, Timofeyev V, Tuteja D, et al: Ablation of a Ca²⁺-activated K⁺ channel (SK2 channel) results in action potential prolongation in atrial myocytes and atrial fibrillation. *J Physiol* 587:1087, 2009.
7. Baruscotti M, Bucci A, DiFrancesco D: Physiology and pharmacology of the cardiac pacemaker ("funny") current. *Pharmacol Ther* 107:59, 2005.